



KAPITAŁ LUDZKI  
NARODOWA STRATEGIA SPÓJNOŚCI



Politechnika Wrocławska

UNIA EUROPEJSKA  
EUROPEJSKI  
FUNDUSZ SPOŁECZNY



**ROZWÓJ POTENCJAŁU I OFERTY DYDAKTYCZNEJ POLITECHNIKI WROCŁAWSKIEJ**

Wrocław University of Technology

# Control in Electrical Power Engineering

Przemysław Janik, Tomasz Sikorski

## POWER QUALITY ASSESSMENT

Wrocław 2011

Projekt współfinansowany ze środków Unii Europejskiej w ramach  
Europejskiego Funduszu Społecznego

Wrocław University of Technology

# Control in Electrical Power Engineering

Przemysław Janik, Tomasz Sikorski

## **POWER QUALITY ASSESSMENT**

Wrocław 2011

Copyright © by Wrocław University of Technology  
Wrocław 2011

Reviewer: Zbigniew Leonowicz

ISBN 978-83-62098-64-4

Published by PRINTPAP Łódź, [www.printpap.pl](http://www.printpap.pl)

# Content

<b>1. INTRODUCTION</b>	<b>4</b>
<b>2. OVERVIEW OF DISTURBING PHENOMENA AND INDICES</b>	<b>6</b>
2.1. MOTIVATION FOR SYSTEMATICAL APPROACH	6
2.2. VOLTAGE SAG	7
2.3. BRIEF INTERRUPTIONS	8
2.4. VOLTAGE SWELLS	9
2.5. TRANSIENTS	10
2.6. UNBALANCE	10
2.7. HARMONIC DISTORTION	11
2.8. FLICKER	13
2.9. POWER QUALITY STANDARDS	14
2.10. LITERATURE	15
<b>3. RESONANCES</b>	<b>16</b>
3.1. PROBLEM FORMULATION	16
3.2. ASSESSMENT OF SERIES RESONANCE	18
3.3. ASSESSMENT OF PARALLEL RESONANCE	21
3.4. LITERATURE	26
<b>4. ANALOG FILTER DESIGN METHODOLOGY FOR HARMONIC CANCELATION</b>	<b>26</b>
4.1. PROBLEM FORMULATION	26
4.2. HIGHER ORDER HARMONICS ORIGINATING IN NONLINEAR LOADS	28
4.3. CURRENTS DRAWN BY A NON-SINUSOIDAL LOAD, GENERAL CHARACTERISTIC	29
4.4. BASIC DEPENDENCIES IN THE RESONANT CIRCUIT SELECTED FOR THE FILTER	32
4.5. PROPOSED DESIGN FOR EFFICIENT HARMONIC FILTRATION	35
4.6. COMPUTATION OF FILTRATION PARAMETERS	36
4.7. SIMULATION OF NONLINEAR LOAD WORKING WITH A FILTER	39
4.8. LITERATURE	42
<b>5. FOURIER TECHNIQUES FOR SPECTRAL ANALYSIS</b>	<b>42</b>
5.1. DISCRETE TIME FOURIER TRANSFORM DEFINITION	43
5.2. DISCRETE FOURIER TRANSFORM DEFINITION	45
5.3. DISCRETE FOURIER TRANSFORM EXPRESSED USING TRIGONOMETRIC FUNCTIONS	47
5.4. PROPERTIES OF DFT	56
5.5. SHIFTING THEOREM IN DFT	58

5.6.	INVERSE DISCRETE FOURIER TRANSFORM.....	62
5.7.	DFT LEAKAGE (AMBIGUITY) AND ITS MINIMIZATION .....	62
5.8.	WINDOWS TYPES AND THEIR PROPERTIES.....	70
5.9.	RESOLUTION OF THE DFT, FILLING WITH ZEROS, SAMPLING IN THE FREQUENCY DOMAIN .....	72
5.10.	LITERATURE .....	74
<b>6.</b>	<b>SYMMETRICAL COMPONENTS FOR CURRENT AND VOLTAGE UNBALANCE ASSESSMENT.....</b>	<b>75</b>
6.1.	MATHEMATICAL BACKGROUND .....	76
6.1.1.	<i>Complex transformation parameter a</i> .....	76
6.1.2.	<i>Symmetrical components definition</i> .....	77
6.1.3.	<i>Symmetrical components of voltage, current, impedance and admittance</i> .....	79
6.1.4.	<i>Basic properties of symmetrical components</i> .....	80
6.2.	OHM’S LOW FOR SYMMETRICAL COMPONENTS .....	81
6.3.	KIRCHHOFF’S CURRENT LOW AND VOLTAGE LOW FOR SYMMETRICAL COMPONENTS .....	83
6.4.	FILTERING OF SYMMETRICAL COMPONENTS .....	84
6.4.1.	<i>Zero sequence filtering</i> .....	85
6.4.2.	<i>Positive and negative sequence components filtering</i> .....	86
6.5.	DETERMINATION OF UNBALANCE WITH ACCORDANCE TO INTERNATIONAL STANDARDS .....	90
6.5.1.	<i>Unbalance factor</i> .....	90
6.5.2.	<i>Evaluation according to standards</i> .....	91
6.6.	LITERATURE .....	92
<b>7.</b>	<b>ADVANCED TOPIC. DETERMINATION OF TRANSIENT PARAMETERS IN WIND ENERGY CONVERSION</b>	
<b>SYSTEM</b>	<b>.....</b>	<b>92</b>
7.1.	MOTIVATION AND PROBLEM FORMULATION .....	92
7.2.	PRONY METHOD .....	93
7.3.	NONLINEAR REGRESSION METHOD.....	96
7.4.	WAVELET TRANSFORM.....	97
7.5.	SIMULATION OF INDUCTION GENERATOR WITH CAPACITORS.....	99
7.6.	PARAMETERS OF TRANSIENTS COMPUTED USING PRONY ALGORITHM AND NONLINEAR REGRESSION.....	100
7.7.	CONCLUDING REMARKS .....	105
7.8.	LITERATURE .....	105
<b>8.</b>	<b>COMPUTATIONAL APPLICATION OF POWER QUALITY ASSESSMENT: DIPS.....</b>	<b>107</b>
8.1.	METHODS OF VOLTAGE MAGNITUDE ESTIMATION .....	109
8.2.	APPLICATION OF RMS TREND CALCULATION IN MATLAB .....	113
8.3.	COMPARISON OF THE METHODS.....	119
8.4.	DIP DURATION .....	121
8.5.	PHASE-ANGLE JUMP .....	125

8.6.	MONITORING MODE IN VOLTAGE DIPS ASSESSMENT .....	128
8.7.	DIP TRANSFER IN POWER SYSTEMS .....	132
8.8.	LITERATURE .....	137
<b>9.</b>	<b>COMPUTATIONAL APPLICATION OF POWER QUALITY ASSESSMENT: HARMONICS .....</b>	<b>139</b>
9.1.	HARMONICS DISTORTION AND FOURIER SERIES PARAMETERIZATION .....	140
9.2.	INVESTIGATED PHENOMENA .....	143
9.3.	“LINEAR” SPECTRUM ESTIMATION USING FFT: .....	145
9.4.	HARMONICS AND SUBDIVISION INTO EVEN AND ODD HARMONICS .....	148
9.5.	GROUPS OF HARMONICS, INTERHARMONIC AND SUHARMONIC.....	150
9.6.	LITERATURE .....	155
<b>10.</b>	<b>ELEMENTS OF POWER QUALITY REPORT .....</b>	<b>156</b>
10.1.	POWER FREQUENCY ASSESSMENT .....	158
10.2.	SUPPLY VOLTAGE VARIATION .....	159
10.3.	FLICKER SEVERITY .....	160
10.4.	VOLTAGE UNBALANCE ASSESSMENT .....	161
10.5.	HARMONICS ASSESSMENT .....	162
10.6.	SUMMARY OF THE REPORT .....	165
10.7.	LITERATURE .....	165

## 1. Introduction

Power Quality (PQ) topics are of utmost importance in our world strictly dependent on continuous supply of electrical energy.

The field of Power Quality has no strictly defined borders as continuously more and more topics are being discussed in this area. A brief glance at headings of the international conferences justifies the presumption. *The International Conference on Harmonics and Quality of Power* (ICHQP) and *The International Conference on Renewable Energies and Power Quality* ICREPQ are two good examples reflecting the research activities across continents.

From the technical point of view we have a steady growing number of nonlinear loads, electronic controlled devices saving lamps etc., drawing highly non sinusoidal currents. On the other hand, computers, electronic control systems and protection devices are vulnerable and prone to power quality disturbances. The electrical network may be seen as an interconnection between the sinks and the sources of electrical disturbances. Standards and legal regulations help to find the “golden section” between allowed vulnerability of devices and allowed distortion levels in the electrical network.

The title of the book indicates strictly its purpose. In the vast area of PQ, it should give a student an inside look into the theoretical background of Power Quality assessment. So that reading and understanding of changing standards, procedures and technologies will be smooth and based on relatively solid foundations. It should help the students to focus on PQ problems in every day life of electrical engineer working in the deregulated environment.

After the Introduction, a brief overview of basic disturbing phenomena, their origin, effects and mitigation methods is given in Chapter 2.

In Chapter 3, the reader is given information about a common but dangerous phenomenon of resonances. The conditions for parallel and series resonance are given along with features and possible thread for the electrical components.

Chapter 4 presents an effective approach to an analog filter design helping to reduce harmonics. As the filter uses the idea of resonance, it is a natural consequence of the previous chapter. The theoretical presentation is rounded up with practical implementation and simulated filtration results.

Chapter 5 is a fulfillment or a logical consequence of the previous one. If we want to cancel or filter harmonics we should firstly assess their presence in the electrical grid. Fourier transform is a popular and powerful method in spectral analysis. However, appropriate computation of spectral components requires from the engineer at least basic knowledge of DFT properties and features.

Chapter 6 gives us the look into a three phase system. Previously presented topics can be usefully used for every phase of the three phase system separately, or for all of them together. Symmetrical components and symmetry as a global look at a three phase system are inevitable in the assessment of power quality for the results of non symmetry are disastrous.

Chapter 7 is an example of an advanced approach to signal parameters estimation in a system with a wind generator. The complete process has been shown. Starting with the introduction and motivation through methodology and algorithms up to the discussion of results.

Chapter 8 is dedicated to undervoltage event member, called voltage dips (or sags). A proper classification of this event requires an estimation of voltage magnitude as well as time duration during the dip. This chapter introduces mathematical backgrounds as well as a practical application of algorithms in Matlab environment with comparison and examples. In order to emphasize rules of the dips transfer in the power systems an example of a power system model is presented.

Chapter 9 is dedicated to application of Fast Fourier Transform for spectrum estimation. Selected issues of harmonics, interharmonics and harmonics group are introduced. Demonstration algorithms in Matlab and its results are presented on the basis of real measured signal of dc-arc furnace plant.

The aim of chapter 10 is to present an example of power quality report including the assessment of mentioned crucial parameters. Measurements were done in the main point of the supply of the factory which has an electronic assembly line including robots and power electronics.



## **2. Overview of disturbing phenomena and indices**

The overview of disturbing phenomena starts with a brief, systematized motivation formulation of the interest in power quality, generally. This text is mainly based on [2].

In the context of power quality, a disturbance is a temporary deviation from the steady state of waveform caused by faults of brief duration or by sudden changes in the power system. The disturbances considered by the International Electromagnetic Commission include voltage dips, brief interruptions, voltage increases, impulsive transients and oscillatory transients [2].

Nevertheless, waveform distortions (e.g. harmonics), unbalance, voltage fluctuation and flicker indicate clearly the deterioration of power quality. They are also mentioned in standards, and therefore will be introduced.

### **2.1.Motivation for systematical approach**

Before a detailed presentation of disturbances types is given, there is a need for justification of the systematic approach to Power Quality. The individual topics discussed in this field are rather not new. What is new is the system approach in the engineering, seeking interconnections and dependences between various, seemingly independent phenomena. A global assessment is needed to operate the electrical system safely and reliably. That is why disturbances have been grouped into classes which are simultaneously controlled and checked at various points of the electrical system.

Generally, there are four major reasons for the systematic approach and growing interest in Power Quality [1].

- Load equipment is more sensitive to power quality variations than equipment applied in the past. Many new load devices contain microprocessor based controls and power electronic devices that are sensitive to many types of disturbances.
- The increasing emphasis on overall power system efficiency has resulted in a continued growth in the application of devices such as high-efficiency, adjustable speed motor drives and shunt capacitors for power factor correction to reduce losses. This results in increased harmonic levels on power systems and has many people concerned about the future impact on system capabilities.

- Increased awareness of power quality issues by the end users. Utility customers are becoming better informed about such issues as interruptions, sags, and switching transients and challenge the utilities to improve the quality of power delivered.
- Many things are now interconnected in a network. Integrated processes mean that the failure of any component has much more important consequences.

Interestingly, the equipment installed to increase the productivity is also often the equipment that suffers the most from common power disruptions. And the equipment is sometimes the source of additional power quality problems.

## 2.2.Voltage sag

Voltage sag (sometimes called a dip) is defined as a sudden reduction of the voltage, ranging between 10% and 90% of the nominal voltage. The duration of a sag is from 0.5 cycle, up to several seconds. An example of a symmetrical voltage sag in a three phase system is shown in Figure 2.1.

Common sources of voltage sags are switching operations in the electrical network, changing transformer taps, changing configuration of the grid, switching heavy loads, especially electrical drives. Faults often affect a wide area causing sags lasting as long as the clearing of the fault. the simplified principle of the phenomenon is shown in Figure 2.2. The severity of a particular sag originating in a fault may be given by a simple formula

$$U_{sag} = \frac{Z_z}{Z_s + Z_z} \cdot E \quad (2.1)$$

The effect of voltage dips on equipment depends on both parameters of a sag, its duration and magnitude. Computer manufacturers developed a standard correlating the duration and severity of a sag with electronic equipment immunity, called CBEMA. The possible effect on equipment are extinction of discharge lamps, incorrect operation of control devices, speed variations and stopping of motors, tripping of contactors, computer miss operation [2]. And many more.

There is no simple and cheap protection against voltage sags. In case of small loads uninterrupted power supplies UPS are quite efficient. The use of power conditioners or even rebuilding of the electrical grid to reduce voltage losses on impedances are suggested for greater loads.

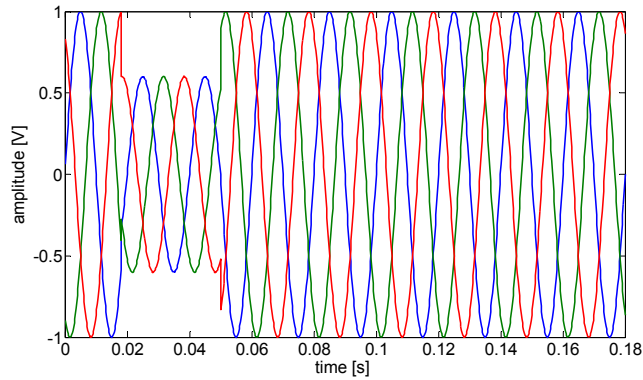


**Figure 2.1** Three phase voltage sag, symmetrical case

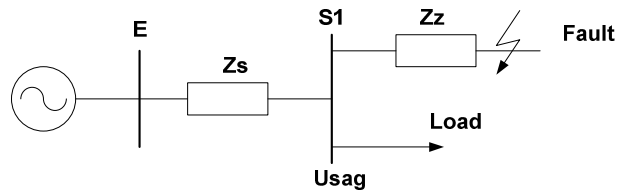


**Figure 2.2** Simplified model of a voltage divider representing the proliferation of sags

### 2.3. Brief Interruptions

No voltage at all may be considered as the most severe sag at all. The effects on equipment is an immediate shut-down and an unexpected stop of operation. Lost data and interrupted industrial processes may lead to huge financial losses.

An example of a three phase voltage interruption is shown in Figure 2.3.

The prime protection procedure against short interruptions is installation of uninterrupted power supplies.

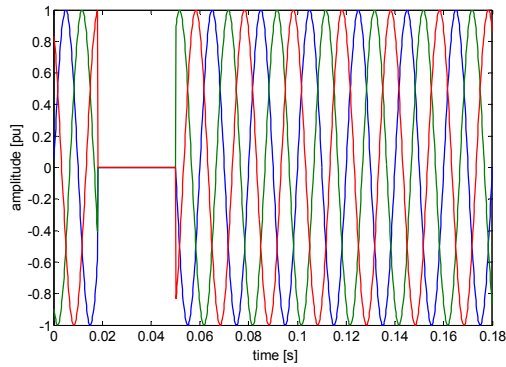


**Figure 2.3** Voltage interruption in a three phase system.

## 2.4.Voltage swells

Voltage swell is the opposite of a sag. A swell is defined as an increase to between 1.1 and 1.8 in pu for durations from 0.5 cycle to several seconds. Swells are also characterized by its magnitude and duration. A three phase case is shown in Figure 2.4. An unsymmetrical voltage swell is often present in un-faulted phases when a single phase fault occurs [2].

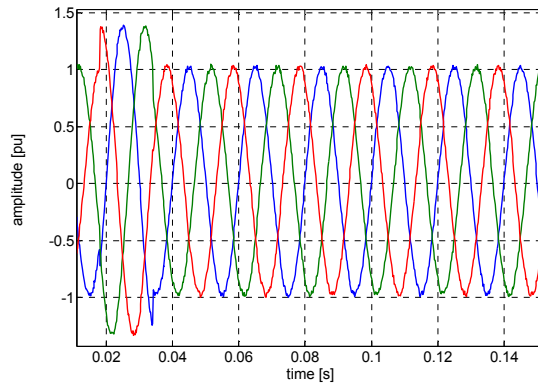


**Figure 2.4** Symmetrical voltage swell in a three phase system

Swells can upset electric controls and electric motor drives, which can trip because of their build in protection devices.

A possible solution to the problem is the application of uninterruptible power supplies and conditioners.

## 2.5.Transients

Voltage disturbances shorter than sags or swells are classified as transients and are caused by sudden changes in the power system. An example of a voltage sag is shown in Figure 2.5.

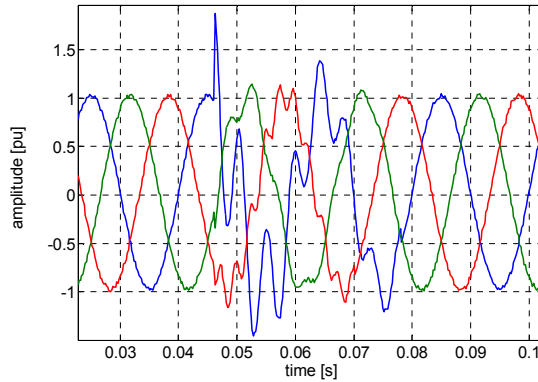


**Figure 2.5** Oscillatory transient in a three phase system

According to their duration, transient overvoltages can be divided into switching surge (duration in the range of milliseconds), and impulse spike (duration in the range of microseconds).

Surges are high energy pulses arising from power system switching disturbances, either directly or as a result of resonating circuits associated with switching devices. They also occur during step load changes.

Capacitor switching can cause resonant oscillations leading to an overvoltage some three to four times of the nominal rating, causing tripping or even damaging protective devices and equipment. Electronically based controls for industrial motors are particularly susceptible to these transients.

Protection against surges and impulses is normally achieved by surge-diverters and arc-gaps at high voltages and avalanche diodes at low voltages.

Faster transients in nanoseconds due to electrostatic discharges, an important category of EMC, are not normally discussed under power quality.

## 2.6.Unbalance

Unbalance describes a situation in which either the voltages of a three-phase voltage source are not identical in magnitude or the phase differences between them are not 120 electrical

degrees between them, or both. An example of unbalanced three phase voltages is shown in

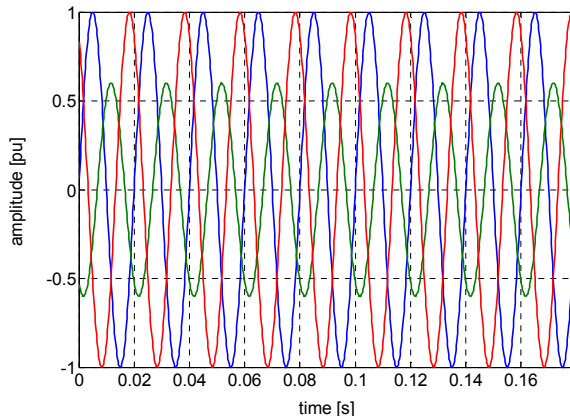


**Figure 2.6** Voltage unbalance

The degree of unbalance is usually defined by the proportion of negative and zero sequence components. This subject is discussed extensively in the chapter dedicated to unbalance.

The main causes of unbalance are single phase loads and un-transposed overhead transmission lines.

An electrical machine operating on an unbalanced supply will draw a current with a degree of unbalance several times that of the supply voltage. As a result, the three phase currents may differ considerably and a temperature rise will take place in the machine.

Motors and generators may be fitted with protection to detect extreme unbalance. If the supply unbalance is sufficient, the single phase protection may respond to the unbalanced currents and trip the machine.

## **2.7. Harmonic distortion**

Waveform distortion is generally discussed in terms of harmonics. This is a fast subject for which special books have been dedicated [3]. At this point only a general introduction will be given. Three phase signal distorted by harmonics is shown in Figure 2.7.

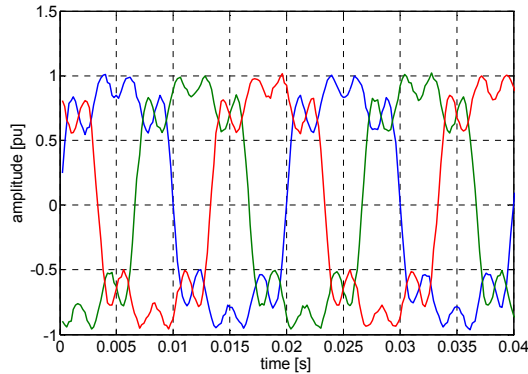


**Figure 2.7 Three phase signal distorted by harmonics**

Generally, any non-linear load is a source of current harmonics in the electrical system. The harmonic sources can be grouped into three categories according to their origin, size and predictability:

- small and predictable (domestic and residential appliances)
- large and random (arc furnaces, welders)
- large and predictable (static converters, HVDC transmission)

The main detrimental effects of harmonics are:

- maloperation of control devices, signaling systems, protective relays
- extra losses in capacitors, transformers and rotating machines
- additional noise from motors and other apparatus
- telephone interference
- the presence of power factor correction capacitors and cable capacitance is a potential reason for shunt and series resonances resulting in voltage amplification

To keep the harmonic voltage content within the recommended levels the main solutions are:

- the use of high pulse rectification (e.g. in HVDC transmission systems)
- passive filters, either tuned to individual frequencies or of the band pass type.
- active filters and conditioners

## 2.8.Flicker

Flicker has been described in [4] as:

“the impression of fluctuating luminance or color occurring when the frequency of the variation of the light stimulus lies between a few hertz and the fusion frequency of images. This is a very loose definition considering that “the fusion frequency of images” varies from person to person and depends on many factors.

Fluctuation of the system voltage (more specifically in the r.m.s. value) can cause perceptible (low frequency) light flicker depending on the magnitude and frequency of the variation. Power system engineers call this type of disturbance “voltage flicker” but often it is just shortened to “flicker”.

A simple flicker in a three phase system is shown in Figure 2.8. It represents a simple case of a voltage flicker, when the a.c. voltage is modulated (amplitude modulation) by a sine wave seen as the envelope of the voltage waveform.

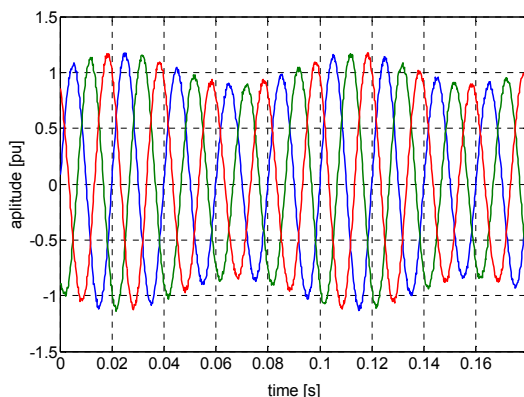


**Figure 2.8 Voltage flicker in a three phase system**

The general mathematical expression for a flicker is given by

$$v(t) = \left( \alpha_0 + \sum_{i=1}^M \left\{ \alpha_{fi} \sin(\beta_{fi} \omega_0 t + \varphi_{fi}) \right\} \right) \sin(\omega_0 t + \varphi_0) \quad (2.2)$$

and can be interpreted as modulation by a sine wave with relatively low frequency.

Non-periodic events can also cause a perceptible light flicker. Any potentially perceptible change in brightness should therefore be termed light flicker, broadening the given definition further by extending the lower frequency limit to non-periodic disturbances.

The main causes of flicker are loads drawing large and highly variable currents. Due to the impedance of the power system (generators, transformers and transmission lines) these



changes produce amplitude modulation of the voltage at the load bus and even at remote busses. Another common source of flicker is the starting of electric motors. Their operation in application that require an irregular torque is problematic. Motor applications range from household appliances up to more powerful appliances such as heat pumps or rolling mills. These flicker sources lead to electric lamp luminance fluctuations by means of amplitude modulation of the supply voltage.

The flickering of electric light causes annoyance to human observers. It reduces the life of electronic devices, incandescent and fluorescent devices, malfunction of phase-locked-loops and loss of synchronism in uninterruptible power supplies, maloperation of electronic controllers and protection devices.

## **2.9. Power Quality Standards**

The development of standards and guidelines is centered around the following objectives [5]:

- description and characterization of the phenomena
- major sources of power quality problems
- impact on other equipment and on the power system
- mathematical description of the phenomena using indices or statistical analysis to provide a quantitative assessment of its significance
- measurement techniques and guidelines
- emission limits for different types and classes of equipment
- immunity or tolerance level of different types of equipment
- testing methods and procedures for compliance with limits
- mitigation guidelines

The internationally recognized organization for standardization is the International Electrotechnical Commission which is based in Geneva. IEC has defined a series of standards, called Electrotechnical Capability, to deal with power quality issues. This series is published in separate parts according to the following structures.

1. General (IEC 61000-1-x) the general section introduces and provides fundamental principles on EMC issues and describes the various definitions and terminologies used in the standards

2. Environment (IEC 61000-2-x) this part describes and classifies the characteristics of the environment or surroundings where equipment will be used. It also provides guidelines on compatibility levels for various disturbances.
3. Limits (IEC 61000-3-x) this section defines the maximum levels of disturbances caused by equipment or appliances that can be tolerated within the power system. It also defines the immunity limits or equipment sensitive to EMC disturbances.
4. Testing and Measurement Techniques (IEC 61000-4-x) these provide guidelines on the design of equipment for measuring and monitoring of power quality disturbances. They also outline the equipment.
5. Installations and Mitigation Guidelines (IEC 61000-5-x) this section provides guidelines on the installation techniques to minimize emission and as well as to strengthening immunity against EMC disturbances. It also describes the use of various devices for solving power quality problems.
6. Generic Standards (IEC 61000-6-x) these include the standards specific to certain category of equipment or for certain environments. They contain both emission limits and immunity levels standards

Some of the other organizations who have developed their own standards are CENELEC, UIE, IEEE, ANSI, NEMA. These standards are usually very much application based on or specific to a certain environment.

The standard EN 50160 Voltage Characteristics in Public Distribution Systems is widely used in Europe and directly build-in into commercial power quality metering devices. This standard, or its parts is also included in legal regulations concerned with power quality.

## **2.10. Literature**

- [1] R. C. Dugan, M. F. McGranaghan, H. W. Beaty, Electric Power Systems Quality, McGraw-Hill, New York, 1996
- [2] J. Arrilaga, N. R. Watson, Power System Quality Assessment, John Wiley and Sons, Chichester, 2000
- [3] J. Arrilaga, N. R. Watson, Power System Harmonics, Wiley and Sons, Chichester, 2003
- [4] IEEE, Standard Dictionary of Electrical and Electronic Terms, Std.100, IEEE, 1984

[5] J. Arrillaga, D.A. Bradley, P.S. Bodger, Power System Harmonics, John Wiley & Sons, 1985

### 3. Resonances

Resonances are a common phenomenon in an electrical network. The occurrence of resonance is directly connected with other power quality issues. If there are unexpected harmonics, then the damage to system components may be high due to resonances. On the other hand, the resonance phenomenon is exploited in filtering devices, to short-circuit the unwanted harmonics. That's why the resonance issue comes first. The presentation and the problem formulation is directly based on [3].

#### 3.1. problem formulation

When the voltage applied to an electrical network containing resistance, inductance and capacitance is in phase with the resulting current, the circuit is said to be **resonant**. At resonance, the equivalent network impedance is purely resistive, since the supplied voltage and current are in phase. The power factor of a resonant network is unity [1].

Apart from power quality issues, the phenomenon of the resonance is of a great value in communication engineering. It enables small portions of the communication frequency spectrum to be selected for amplification independently of the remainder.

However, there is also a potential thread inherent in this phenomenon. If a voltage resonance or a current resonance is present in an electrical network, it may be dangerous for system components (damaged insulation, flash over, etc.).

Excess current or voltage may be dangerous for insulation of wires and components. Especially capacitors and transformers insulation is vulnerable to high voltages. Measuring transformers may also be damaged. Currents higher than allowed are responsible for additional mechanical stress put on all current leading elements. There is also additional heat accelerating the aging process of insulation. There is also a risk of saturation in transformers. Electrical apparatus, measuring transformers other devices malfunction can often be led back to unwanted resonances.

Special care is needed during the design process to avoid resonances for normal operation condition at 50 Hz. The situation becomes more complicated if harmonics and

interharmonics are present in current or voltage due to changes of capacitance and inductance along with frequency. That means, if there is a problem with harmonics, the risk of resonances is significantly higher. The common source of harmonics are nonlinear devices of any type, mostly power electronic. Special harmonic filters are designed for them. A slightly more difficult situation results from transient overvoltages and overcurrents. Lightning and capacitor switching are very typical examples. Capacitors are used to provide reactive power to correct the power factor, they are cheap and sufficient, but switching operations are quite frequent.

A wind generator equipped with compensating capacitors, as an example of a system component with variable consumption of reactive power is shown in Figure 3.1 [2]. Due to the variable consumption of reactive power, let us stress it again, the switching operations are frequent. The parameters of oscillatory transient vary with changing wind conditions and system parameters. An example of current time curve is shown in Figure 3.2.

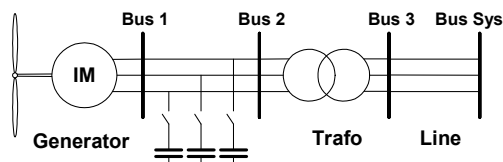


**Figure 3.1** Induction generator with compensating capacitors

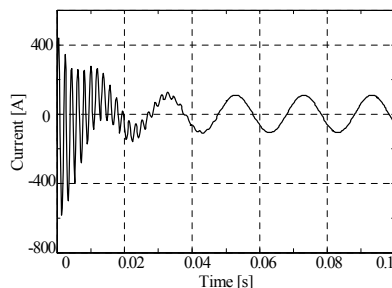


**Figure 3.2** Current resulting from capacitor bank switching in wind generator

There is no doubt about the necessity to avoid resonances in electrical networks. The systematic presentation of the phenomenon starts with the computation of conditions for series or parallel resonance. Then, follows the computation of the resonant frequency, determining the maximal voltage or current values.

Basic ideas for series resonance and parallel resonance will be shown below. All voltages and currents are complex, unless otherwise noticed.

### 3.2. Assessment of series resonance

Figure 3.3 shows a circuit comprising a coil of inductance  $L$ , resistance  $R$  and capacitance connected in series [3].

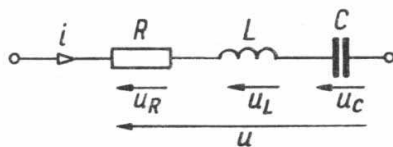


**Figure 3.3** R, L, C elements connected in series

The voltage across the series RLC circuit is given by

$$U = U_R + U_L + U_C \quad (3.1)$$

The circuit is at resonance, if  $U_L + U_C = 0$ , also

$$\left( \omega_0 L - \frac{1}{\omega_0 C} \right) I = 0 \quad (3.2)$$

Thus,

$$\omega = \frac{1}{\sqrt{LC}} \quad (3.3)$$

and the frequency at resonance

$$f = \frac{1}{2\pi\sqrt{LC}} \text{ Hz} \quad (3.4)$$

Figure 3.4 shows how the reactance and inductance and their algebraically added values vary with changing frequency.

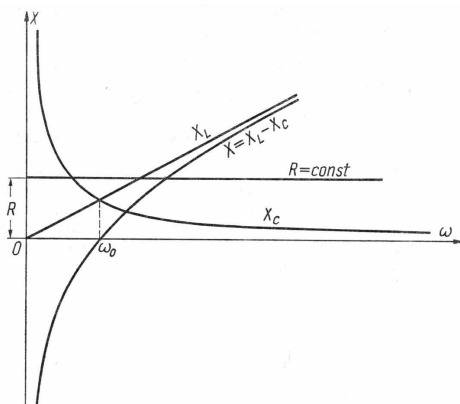


**Figure 3.4** Variations of  $R$ ,  $X_L$ ,  $X_C$  with the frequency

Since (3.2) is fulfilled at resonance, then the impedance  $Z = R = \text{constant}$ . This is the minimum possible value of impedance and the current reaches its maximum.

At frequencies less than  $f_0 (\omega_0)$ ,  $X_L < X_C$  the circuit is capacitive, at frequencies higher than  $f_0 (\omega_0)$ ,  $X_L > X_C$  the circuit is inductive.

The inductive reactance or capacitive reactance at resonance frequency is called *characteristic impedance (wave impedance)* and usually denoted with  $\rho$ .

$$\rho = \omega_0 L = \frac{1}{\omega_0 C} = \sqrt{\frac{L}{C}} \quad (3.5)$$

Quality factor or Q-factor [1] in series resonance is the ratio of characteristic impedance to the resistance

$$Q = \frac{\rho}{R} \quad (3.6)$$

Therefore the Q-factor of capacitor and inductive coil at resonance is equal to

$$Q_L = \frac{\omega_0 L}{R} = Q_C = \frac{1}{R\omega_0 C} \quad (3.7)$$

In other words, the Q-factor is a ratio of voltage across reactive element to the voltage across resistance. (3.8)

$$Q = \frac{U_L}{U_R} = \frac{U_C}{U_R} \quad (3.9)$$

Equation (3.9) indicates other name of Q - *circuit magnification factor*.

The Q-factor is defined in general using the energetic approach [4]. Let us multiply the numerator and denominator of (3.9) by  $\frac{1}{2}I_m^2$

$$Q = \omega_0 \frac{\frac{1}{2}I_m^2 L}{\frac{1}{2}I_m^2 R} = 2\pi \frac{\frac{1}{2}I_m^2 L}{RT \frac{1}{2}I_m^2} = 2\pi \frac{W_{L \max}}{W_R(T)} \quad (3.10)$$

where  $W_{L \max}$  is the maximal energy storied in the magnetic field of a coil and  $W_R(T)$  energy lost at resistance during one period T. The Q-factor is multiplied by  $2\pi$  ratio of maximal energy storied in an inductive coil to the energy lost in resistance over one period.

Let us assume that the voltage source frequency feeding RLC branch is variable. If the frequency is  $\omega_0$ , we say that the circuit is *tuned to resonance*. If the angular frequency  $\omega$  is

different from  $\omega_0$ , we say that the circuit is not tuned to resonance that there is a deviation from the resonant frequency.

In the impedances triangle for a RLC branch, the value of  $\operatorname{tg}(\varphi)$  is equal to the ratio  $X / L$ , which characterizes deviation from resonant frequency  $\xi$ .

$$\xi = \frac{X}{R} = \operatorname{tg}(\varphi) \quad \text{also} \quad \varphi = \operatorname{arctg}(\xi) \quad (3.11)$$

Therefore, impedance of RLC branch may be expressed as

$$Ze^{j\varphi} = R\sqrt{1+\xi^2}e^{j\varphi} \quad (3.12)$$

At resonance  $\xi = 0$  and  $Z=R$ , also

$$\frac{Z}{R} = \sqrt{1+\xi^2}e^{j\varphi} \quad (3.13)$$

Equation (3.11) is presented graphically for three chosen values of resistance: 5,10 and 20 Ohms (Figure 3.5).

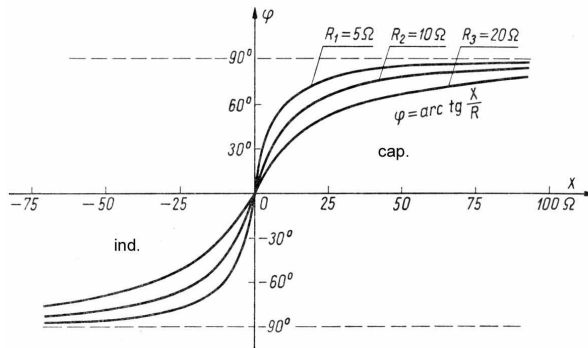


**Figure 3.5** Phase angle  $\varphi$  as a function of the deviation from resonant frequency.

Utilising (3.7) we can express the inductance and capacitance as a function of characteristic impedance

$$L = \frac{\rho}{\omega_0} \quad C = \frac{1}{\omega_0 \rho} \quad (3.14)$$

and substitute the values to the expression for RLC branch reactance we get

$$X = \omega L - \frac{1}{\omega C} = \left( \frac{\omega}{\omega_0} - \frac{\omega_0}{\omega} \right) \rho \quad (3.15)$$

Relative deviation from the resonant frequency  $\delta$  is given as a ratio of the reactance  $X$  and characteristic impedance  $\rho$ .

$$\delta = \frac{\omega}{\omega_0} - \frac{\omega_0}{\omega} = \frac{f}{f_0} - \frac{f_0}{f} \quad (3.16)$$

Substituting  $k = f / f_0$  we can rewrite (3.16) as

$$\delta = k - \frac{1}{k} \quad (3.17)$$

Deviation from the resonant frequency, relative deviation from the resonant frequency and Q-factor are dependent on each other

$$\xi = Q\delta \quad (3.18)$$

For frequencies near the resonant frequency, it is convenient to apply an approximated expression for  $\delta$ . The approximated expression is constructed under the assumption that  $\omega + \omega_0 \approx 2\omega$ , then  $\delta'$  is given as

$$\delta = \frac{\omega}{\omega_0} - \frac{\omega_0}{\omega} = \frac{\omega^2 - \omega_0^2}{\omega\omega_0} = \frac{\omega + \omega_0}{\omega_0} \approx 2 \frac{\omega - \omega_0}{\omega_0} = 2(k - 1) = \delta' \quad (3.19)$$

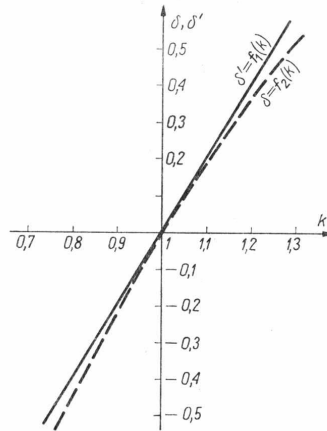


**Figure 3.6** relative deviation from the resonant frequency (true and approximated) as a function of relative frequency

### 3.3. Assessment of parallel resonance

Parallel resonance or current resonance may appear in a circuit with parallel GCL branches (Figure 3.7). For a given complex voltage  $U$ .



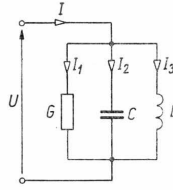


**Figure 3.7 Circuit with parallel branches for current resonance**

The currents across elements in the branches are given by

$$\left. \begin{aligned} I_R &= GU \\ I_C &= j\omega CU \\ I_L &= -j \frac{1}{\omega L} \end{aligned} \right\} \quad (3.20)$$

The current across capacitor is 90 degrees ahead of the voltage, the current in the coil 90 degrees back after voltage. Both are reactive, only the current across resistance is active.

Parallel resonance is characterized by the fact that at the resonance frequency  $\omega_0$  currents across a coil and a capacitor are equal in module but opposite in phase (vector sum is zero).

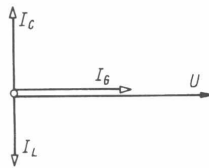


**Figure 3.8 Parallel circuit at resonance, reactive current component equal zero**

Current resonance (Figure 3.8) is expressed by

$$I_C + I_L = 0 \quad (3.21)$$

also

$$\left( \omega_0 C - \frac{1}{\omega_0 L} \right) U = 0 \quad (3.22)$$

Resonant frequency

$$\omega_0 = \frac{1}{\sqrt{LC}} \quad (3.23)$$

The susceptance of a parallel branch at resonance is zero

$$B = B_C - B_L = \omega_0 C - \frac{1}{\omega_0 L} = 0 \quad (3.24)$$

The voltage across the parallel branch reaches its maximal value in comparison to values reached not at resonance

$$U = \frac{I}{G + j\left(\omega_0 C - \frac{1}{\omega_0 L}\right)} = \frac{1}{G} \quad (3.25)$$

At resonance, the branch is strictly resistive and current is in phase with the voltage.

The characteristic impedance (wave impedance) for a parallel branch is given by

$$\rho = \omega_0 L = \frac{1}{\omega_0 C} = \sqrt{\frac{L}{C}} \quad (3.26)$$

The Q-factor for a parallel branch is defined similarly as for a series circuit and given by

$$Q = \omega_0 \frac{\frac{1}{2} C |U_m|^2}{G U^2} = R \omega_0 C = \frac{R}{\rho} \quad (3.27)$$

but the expression is different from (3.6). Both equation ((3.6) and (3.27)) are given for a particular circuit and can not be generalized.

Deviation from resonant frequency in a parallel circuit is given by

$$\xi = -\frac{B}{G} \quad (3.28)$$

Admittance as a function of deviation from resonant frequency

$$Y = |Y| e^{-j\varphi} = G \sqrt{1 + \xi^2} e^{-j\varphi} \quad (3.29)$$

At resonance we have  $\varphi_0 = 0$ ,  $Y_0 = |Y_0| = G$ , therefore the relative admittance and impedance have the form

$$\left. \begin{aligned} \frac{|Y|}{|Y_0|} &= \sqrt{1 + \xi^2} \\ \frac{|Z|}{|Z_0|} &= \frac{1}{\sqrt{1 + \xi^2}} \end{aligned} \right\} \quad (3.30)$$

Assuming changing frequency  $\omega$  and constant absolute value of current  $|I|$  the Ohm's law for absolute values

$$|U| = |Z| |I| \quad (3.31)$$

Therefore, the characteristic in Figure 3.9 shows the changes of  $|Z|/|Z_0|$  as a function of the deviation from resonant frequency which is equal to the curve showing  $|U|/|U_0|$ .

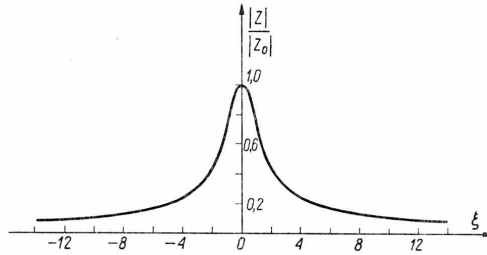


**Figure 3.9 Absolute value of relative impedance as a function of deviation from resonant frequency**

Accompanying the characteristic of absolute value of relative impedance the characteristic of an admittance phase angle is given in Figure 3.10. It has the form of the function  $\text{arctg}$  multiplied by minus one.

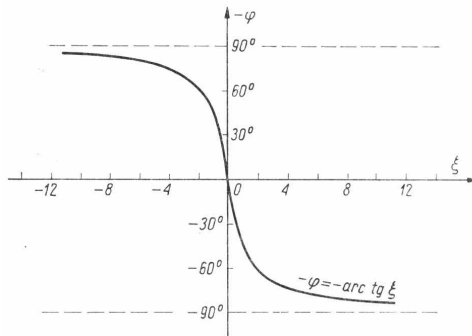


**Figure 3.10 Admittance phase angle in parallel GLC branch**

According to the definition of characteristic impedance, the values of L and C may be expressed as

$$L = \frac{\rho}{\omega_0}, \quad C = \frac{1}{\omega_0 \rho} \quad (3.32)$$

and the susceptance may be expressed as a function of characteristic impedance

$$B = \omega C - \frac{1}{\omega L} = \left( \frac{\omega}{\omega_0} - \frac{\omega_0}{\omega} \right) \frac{1}{\rho} \quad (3.33)$$

Similarly as for parallel branch the relative deviation from resonant frequency

$$\delta = \frac{\omega}{\omega_0} - \frac{\omega_0}{\omega} = \frac{f}{f_0} - \frac{f_0}{f} \quad (3.34)$$

and

$$\xi = Q\delta \quad (3.35)$$

A quite interesting and unusual situation may be present in a parallel circuit with two branches RL and RC (Figure 3.11). Currents at resonant frequency are shown in Figure 3.12 where the compensation of reactive currents takes place.

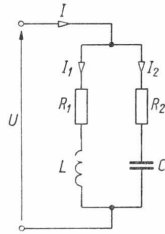


Figure 3.11 Circuit with parallel braches RL and RC

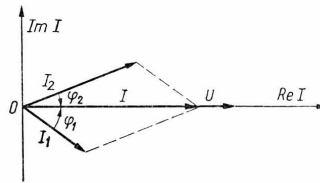


Figure 3.12 Currents in a parallel RL and RC circuit at resonance

The compensation condition is given by

$$|I_1| \sin \varphi_1 + |I_2| \sin \varphi_2 = 0 \quad (3.36)$$

also

$$B_1 + B_2 = 0 = -\frac{X_1}{|Z_1|^2} - \frac{X_2}{|Z_2|^2} \quad (3.37)$$

Applying (3.37) to the circuit in Figure 3.11 we obtain

$$-\frac{\omega L}{R_1^2 + \omega^2 L^2} + \frac{\frac{1}{\omega C}}{R_2^2 + \frac{1}{\omega^2 C^2}} = 0 \quad (3.38)$$

rewriting this we get

$$\omega^2 L \left( R_2^2 - \frac{L}{C} \right) = \frac{1}{C} \left( R_1^2 - \frac{L}{C} \right) \quad (3.39)$$

where  $L/C$  is equal to the squared value of characteristic impedance.

If the resistances of both branches are equal to characteristic impedance

$$R_1 = R_2 = \sqrt{\frac{L}{C}} \quad (3.40)$$

then by every frequency the resonance of currents appears. This is a rare example of a frequency **insensitive** circuit. In this particular case, the circuit impedance is

$$Z = \frac{\left(\sqrt{\frac{L}{C}} + j\omega L\right)\left(\sqrt{\frac{L}{C}} - j\frac{1}{\omega C}\right)}{\sqrt{\frac{L}{C}} + j\omega L + \sqrt{\frac{L}{C}} - j\frac{1}{\omega C}} = \sqrt{\frac{L}{C}} \quad (3.41)$$

also the impedance is purely resistive and equal to the characteristic impedance.

For two different resistances the resonant frequency is given as

$$\omega_0' = \frac{1}{\sqrt{\frac{L}{C}}} \sqrt{\frac{\frac{L}{C} - R_1^2}{\frac{L}{C} - R_2^2}} \quad (3.42)$$

If the student is interested in the analysis of more complicated cases it is strongly advisable to refer to [3].

### 3.4. Literature

- [1] John Bird, "Electrical Circuit Theory and Technology", Elsevier, Linacre House, Jordan Hill, Oxford OX2 8DP, UK, 2007, pp. 349-368
- [2] Tadeusz Łobos, Jacek Rezmer, Przemysław Janik, Zbigniew Wacławek, "Prony and nonlinear regression methods used for determination of transient parameters in wind energy conversion system", IEEE Lausanne PowerTech, Switzerland, 1-5 July 2007, 6 pages
- [3] Tadeusz Cholewicki, "Elektrotechnika Teoretyczna", WNT, Warszawa 1973 pp. 391-422
- [4] Stanisław Bolkowski, „Teoria obwodów elektrycznych”, WNT, Warszawa, 1995 pp. 150-168

## 4. Analog filter design methodology for harmonic cancelation

### 4.1. Problem formulation

One of the various sources of harmonics are widespread lightning systems. Modern lighting systems - street lighting, interior lighting, illumination of buildings must meet multi-criteria

demands imposed by standards and users. One of the demands is reduction of harmonics and interharmonics and guaranteeing good power quality.

Traditional and compact fluorescent lamps, powered via a stabilizing-ignition system, sodium and mercury discharge lamps, light sources powered via power converters contribute significantly to improving the lighting quality and reducing energy costs. Unfortunately, the common feature of all these devices is the non-linearity [1]. The disadvantageous feature is strengthened by other nonlinear devices powered from the same pcc .

Main feature of the nonlinear load is strongly non-sinusoidal current drawn from the grid. This current causes non-sinusoidal voltage drops on transformers' impedances and power lines. It distorts the voltage at pcc, to which other users are connected. Nonlinear loads are the source of power quality deterioration [2], [3].

Non-sinusoidal voltages and currents cause technical problems and obstruct the function of network components (e.g. automation and protection units), additionally negatively influence other loads [4].

Reduction of harmonics in distribution systems is forced as a result of technical reasoning. Also legal regulations imposed on distribution companies and manufacturers of electrical equipment determine acceptable levels of voltage and current distortion [5], [6], [7].

There is a need for a simple and effective way of reducing the content of harmonics and interharmonics. Analog filters [8] are in use, but a detailed and tedious design process for every application side is required. This article presents the theoretical basis for an efficient filter design, together with sample calculations and simulations carried out for selected characteristic harmonics. The aim of the authors was to deliver an accurate and easy tool to design filters distinguishing selected harmonics and interharmonics. Therefore, the implementation of filters may be very precise and effective. Without detailed calculation for each installation side, application of "average" filter is not advisable.

## 4.2.Higher order Harmonics originating in nonlinear loads

Nonlinear lighting circuits draw periodical, non-sinusoidal currents  $i$ . Generally, periodic current can be expressed as the sum of sine waves, forming a Fourier series [8]

$$i_0(t) = I_{m1} \sin(\omega_0 t + \psi_1) + \sum_{k>1}^{\infty} I_{mk} \sin(\omega_k t + \psi_k) \quad (4.1)$$

where  $I_{mk}$  means the amplitude of the  $k$ -th harmonic component,  $\omega_k$  is angular velocity and  $\psi_k$  initial phase shows a signal distorted by 5,7,9 and 11 harmonics.

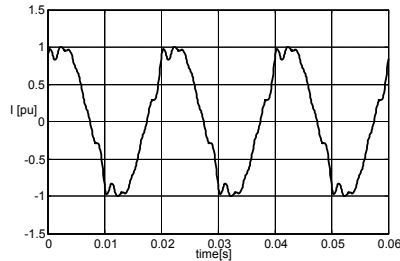


**Figure 4.1 Distorted current signal**

Harmonics have a direct impact on cables, especially neutral, and transformers. Integer multiples of third harmonic add up in the neutral. Current in which may be, in an extreme case, up to three times higher than in the phase wire. The presence of higher harmonics in the current causes additional heating of cables, therefore, it is dangerous for the insulation. The presence of higher harmonics in voltage increases the current drawn by the capacitors, since the capacitor impedance decreases with increasing frequency.

The magnetic flux in the transformer originating from the third current harmonic is closed outside the core, resulting in the formation of eddy currents in other parts of the transformer [9]. Additional energy losses heat up the transformer interior, so accelerate the aging process of isolation [2].

Higher harmonics also have an adverse impact on the protection [4], in particular the operation of differential-current protection. Harmonics cause also false measuring of electricity meters. They are dangerous for the insulation of cables and compensating capacitor banks, causing heating and damage to insulation. Harmonics cause resonances which are difficult to predict and result in damage to measuring transformers [3].

Higher voltage harmonics are especially dangerous for drives [2]. They generate additional heat loss together with fluctuating value of torque on the shaft.

### 4.3. Currents drawn by a non-sinusoidal load, general characteristic

Consider a system consisting of a non-linear receiver, connected to the grid (Figure 4.2, left), which in simple terms can be represented in terms of the actual source of sinusoidal voltage (Figure 4.2, right).

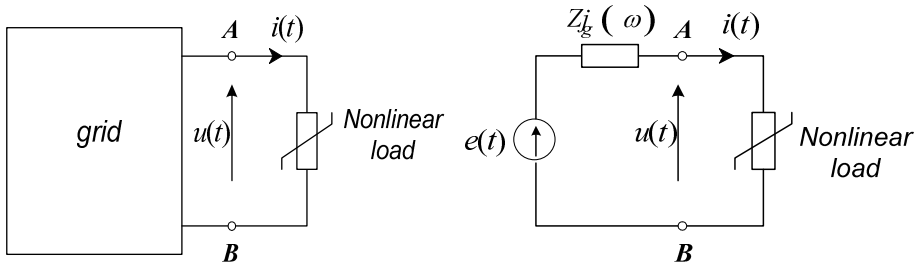


Figure 4.2 non-linear load connected to the grid (l), representation of the network with voltage source (r)

We limit the discussion to steady state. Then, even assuming sinusoidal voltage, the load draws deformed, nonlinear current, containing higher harmonics. Due to the voltage drop across the impedance  $Z_g$  (Fig. 2), the load will be fed by non-sinusoidal voltage anyway.

The complete elimination of higher harmonics from the currents and voltages waveforms is not possible. We can only minimize the distortion, separating the distortion sources from the grid. Distorted waveforms will be “closed” in a certain “loop”, and load is powered by the fundamental harmonic only. Separators are subsystems with appropriately selected frequency characteristics, such as resonant circuits or filters.

Supposing, that a non-linear load drew the current given by (4.1). Actually, other harmonics may be present due to preexisting voltage distortion. An effective way to determine harmonic (interharmonic) content in the current is direct measurement of the spectrum.

Starting from the compensating theorem [8],[10] and (4.1) we can replace the load by a battery of current sources connected in parallel, each corresponding to the specific harmonic current (Figure 4.3).



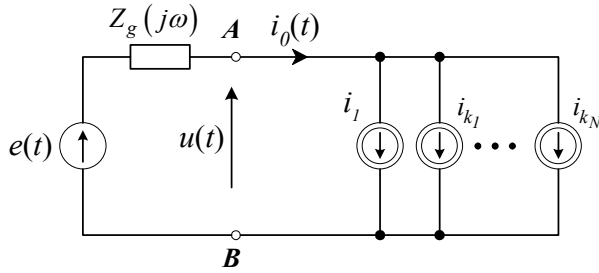


Figure 4.3 Load represented as a battery of current sources

If we place ideal serial resonant branches between the source and the load (Figure 4.4), tuned respectively to each of the higher harmonics, the currents of those frequencies will be completely "separated" from the grid, and the current drawn from the system will contain only the component of fundamental frequency

$$i'(t) = I'_{m1} \sin(\omega_0 t + \psi'_1) \quad (4.2)$$

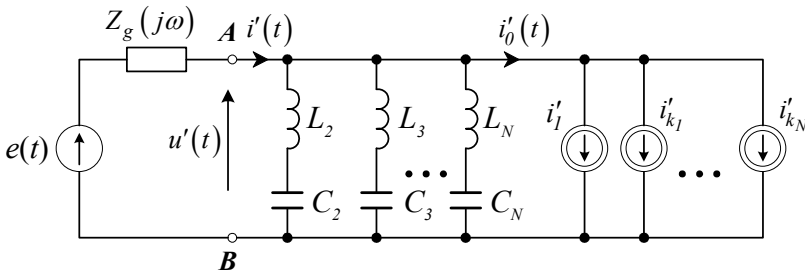
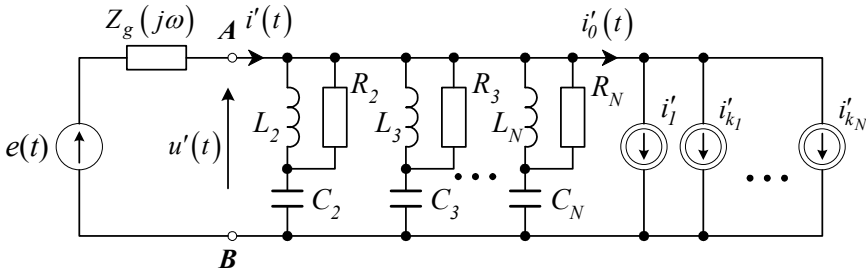


Figure 4.4 Load with ideal resonant branches

However, application of resonant circuits with a very high quality factor is dangerous due to the possibility of significant over-voltages or over-currents. Therefore, instead of ideal branches, circuits in which there is a possibility of regulating the quality factor, are in use. We can modify the circuit in Figure 4.4 by adding a resistor in parallel to the inductance (Figure 4.5). The quality factor can be changed varying the resistance.



**Figure 4.5 Load with resonant branches including resistor**

To make a bit more in-depth analysis of the system in Figure 4.5, suppose that this circuit, except the load is a linear circuit, for which the principle of superposition applies. On this basis, the circuit can be studied individually for each harmonic. An example of such a system for the k-th harmonic is shown in Figure 4.6.

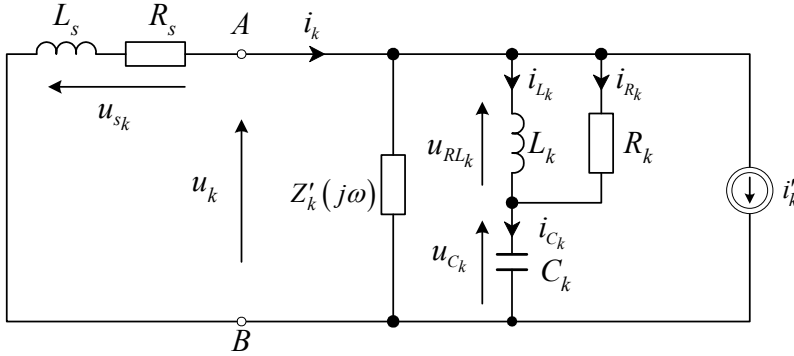


**Figure 4.6 Circuit for the k-th harmonic reduction**

Assigning the impedance of the k-th resonance circuit by  $Z_k(j\omega_k)$  and a summary of all other impedances for the rest of harmonics by  $Z'_k(j\omega_k)$  we can define the current of the k-th harmonic as

$$\underline{I}_k = \frac{Z_k(j\omega_k) // Z'_k(j\omega_k)}{Z_k(j\omega_k) // Z'_k(j\omega_k) + Z_s(j\omega_k)} \underline{I}'_k \quad (4.3)$$

where

$$Z_k(j\omega_k) // Z'_k(j\omega_k) = \frac{Z_k(j\omega_k) Z'_k(j\omega_k)}{Z_k(j\omega_k) + Z'_k(j\omega_k)} \quad (4.4)$$

If we select the impedances of resonance circuit in such a way that

$$|Z_k(j\omega_k)| \ll |Z'_k(j\omega_k)| \quad (4.5)$$

then, the complex value of the k-th current harmonic is given by

$$\underline{I}_k \approx \frac{Z_k(j\omega_k)}{Z_k(j\omega_k) + Z_s(j\omega_k)} \underline{I}'_k \quad (4.6)$$

We can therefore conclude that for absolute values of impedances  $Z_k(j\omega_k)$  small enough at resonance frequencies, then the harmonic content in current and supply voltage  $u(t)$ , will be significantly reduced, in comparison to the circuit in Fig. 3. A brief description of the basic

concepts necessary to analyze resonant circuits is given the special respect to the design method presented here.

#### 4.4. Basic dependencies in the resonant circuit selected for the filter

The basic feature describing a resonant circuits is its impedance, defined as a complex function of a real input variable, mostly frequency. Using the impedance function we can compute important parameters - resonance frequency, impedance at resonance, bandwidth. Let us consider a circuit shown in Figure 4.7.

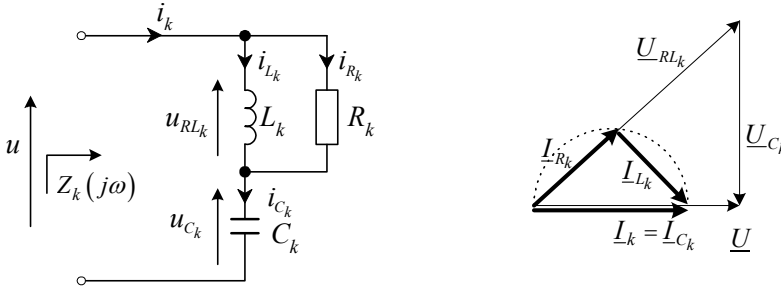


Figure 4.7 Resonance branch and corresponding vector diagram at phase resonance

Assuming that the vectors in Figure 4.7 represent sinusoidal functions with the pulse  $\omega$ , the complex impedance is defined as the ratio of complex voltage to the complex current value

$$Z_k(j\omega) = \frac{U}{I_k} = \frac{R_k j\omega L_k}{R_k + j\omega L_k} + \frac{1}{j\omega C_k} = \frac{R_k \omega^2 L_k^2}{R_k^2 + \omega^2 L_k^2} + j \left[ \frac{R_k^2 \omega L_k}{R_k^2 + \omega^2 L_k^2} - \frac{1}{\omega C_k} \right] \quad (4.7)$$

Hence, considering the phase resonance condition

$$\text{Im } Z_k(j\omega) = \frac{R_k^2 \omega L_k}{R_k^2 + \omega^2 L_k^2} - \frac{1}{\omega C_k} = 0 \quad (4.8)$$

We compute the frequency  $f$  (angular frequency  $\omega$ ) at resonance

$$\omega_k = \frac{1}{\sqrt{L_k C_k - \left(\frac{L_k}{R_k}\right)^2}}, \quad f_k = \frac{1}{2\pi \sqrt{L_k C_k - \left(\frac{L_k}{R_k}\right)^2}} \quad (4.9)$$

using the computed value of  $\omega_k$  we can compute the impedance at resonance

$$\omega = \omega_k \Rightarrow Z_k(j\omega_k) = Z_{k0} = \frac{R_k \omega_k^2 L_k^2}{R_k^2 + \omega_k^2 L_k^2} = \frac{R_k \frac{1}{L_k C_k - \left(\frac{L_k}{R_k}\right)^2} L_k^2}{R_k^2 + \frac{1}{L_k C_k - \left(\frac{L_k}{R_k}\right)^2} L_k^2} = \frac{L_k}{R_k C_k} \quad (4.10)$$

Quality factor Q is an important feature characterizing a resonant circuit. It is defined as a ratio of the maximal energy of the electromagnetic field and energy radiated as heat at resonance during one period [8].

$$Q = 2\pi \frac{W_{\max}}{T_0 P_0} \quad (4.11)$$

Where  $W_{\max}$  - maximal energy of the electromagnetic field,  $P_0$  – average power radiated during one period,  $T_0$  – period of the waveform under consideration. For the circuit in Figure 4.7 the expression for the quality factor is given by

$$Q_k = \frac{\frac{1}{\omega_k C_k}}{Z_{k0}} = \frac{R_k}{\omega_k L_k} = R_k \sqrt{\frac{C_k}{L_k}} \quad (4.12)$$

The quality factor is followed by another useful parameter – transmission bandwidth. Transforming ((4.7)) into ((4.13)) we obtain corresponding plot of the impedance absolute value near the resonant frequency (Figure 4.8)

$$|Z_k(j\omega)| = \sqrt{\frac{R_k^2 (1 - L_k C_k \omega^2)^2 + (\omega L_k)^2}{(\omega C_k)^2 [R_k^2 + (\omega L_k)^2]}} \quad (4.13)$$

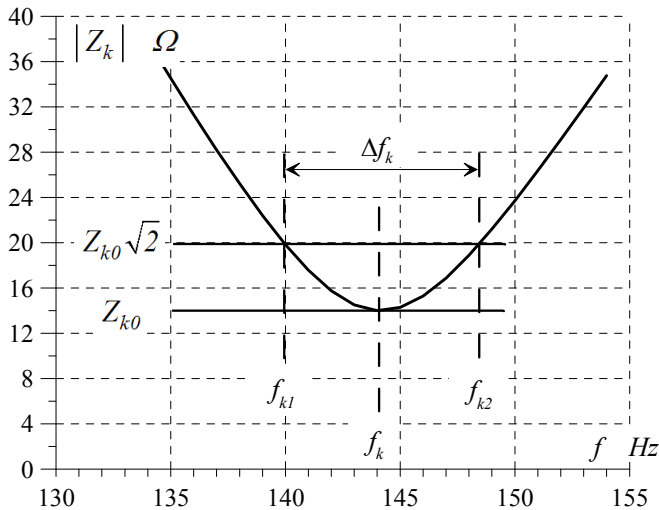


**Figure 4.8 Computation of the transmission bandwidth**

We observe (Figure 4.8) that the transmission bandwidth is given as the difference of frequencies  $f_{k1}$  and  $f_{k2}$  for which the impedance absolute value is  $\sqrt{2}$  higher than at resonance (power reduced by half).

Exact expression for transmission bandwidth can be given only for relatively simple circuits. In the presented case we apply approximated approach describing the impedance as a function of fractional deviation from the resonant frequency

$$x = \frac{\omega}{\omega_k} = \frac{f}{f_k} \quad (4.14)$$

Putting (4.14) into (4.7) and using (4.9), (4.10) and (4.12) we get a new expression for the impedance

$$Z_k(x) = \frac{Q_k^2 Z_{k0}}{Q_k^2 + x^2 - 1} \left[ x^2 + j \frac{(Q_k^2 - 1)^{\frac{3}{2}}}{Q_k^2 x} (x^2 - 1) \right] \quad (4.15)$$

Usually, Q factor is significantly higher than 1. Assuming analysis around resonance frequency, we can say that

$$\left. \begin{array}{l} Q_k \gg 1 \\ x \approx 1 \end{array} \right\} \quad (4.16)$$

then

$$Z_k(x) \cong Z_{k0} [1 + j2Q_k(x-1)] \quad (4.17)$$

and

$$|Z_k(x)|^2 \cong Z_{k0}^2 [1 + 4Q_k^2(x-1)^2] \quad (4.18)$$

defining

$$x_1 = \frac{f_{k1}}{f_k}, \quad x_2 = \frac{f_{k2}}{f_k} \quad (4.19)$$

we obtain

$$1 + 4Q_k^2(x_{1,2} - 1)^2 = 2 \quad (4.20)$$

therefore

$$x_{1,2} = 1 \mp \frac{1}{2Q_k} \quad (4.21)$$

Finally, the bandwidth is

$$\Delta f_k = f_{k2} - f_{k1} = (x_2 - x_1) f_k = \frac{1}{Q_k} f_k \quad (4.22)$$

In (4.23) we recognize a plain relationship between Q factor and bandwidth. Quality factor Q may be determined using the resonance characteristic

$$Q_k = \frac{f_k}{\Delta f_k} \quad (4.23)$$

The influence of various Q factor values obtained by (4.24) on the shape of the resonance curve is shown in Figure 4.9, where  $Z_{k0} = 10 \Omega$ ,  $Q_k = 5, 10, 20, 50$ .

$$|Z_k(x)| = \frac{Q_k^2 Z_{k0}}{Q_k^2 + x^2 - 1} \sqrt{x^4 + \frac{(Q_k^2 - 1)^3}{Q_k^4 x^2} (x^2 - 1)^2} \quad (4.24)$$

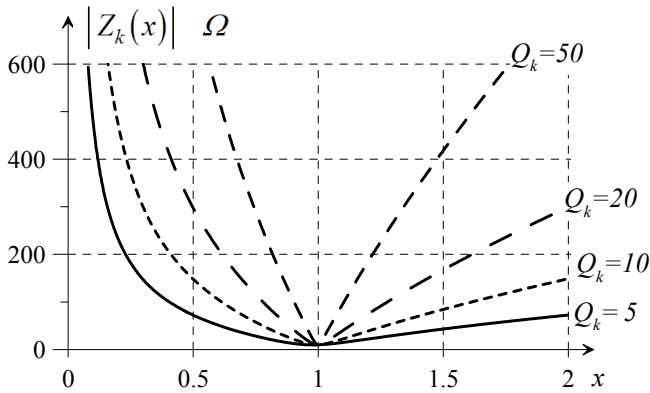


Figure 4.9 Impedance vs. Q factor

Unfortunately, there is a discrepancy between the minimum of impedance and resonance frequency. In practice, it may have a negative impact on filtering accuracy. Therefore, it is advisable to apply a corrective value given by (4.25). It was derived using the small parameter method.

$$f_{k0} \cong f_k \sqrt{1 - \frac{1}{Q_k^2} + \frac{1}{2Q_k^4}} \quad (4.25)$$

#### 4.5. Proposed design for efficient harmonic filtration

Figure 4.10 shows a simplified model of a filter for arbitrary selected harmonics or interharmonics. The idea may be expanded on every frequency, not only an integer multiply of fundamental

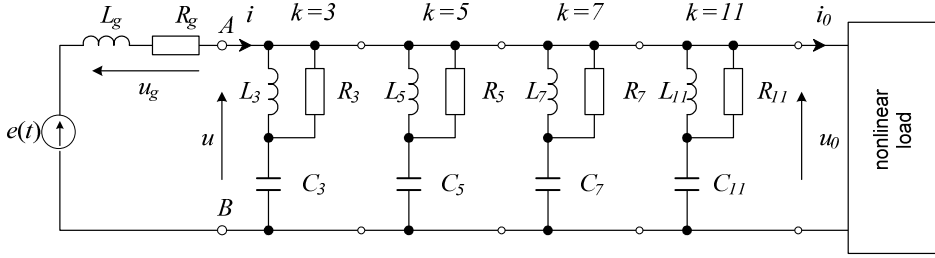


**Figure 4.10 Filter for selected harmonics**

Using the method given above, the set of expression enabling fast and accurate determination of RLC parameters will be presented.

Usually, there are required values for resonance frequency  $f_k$ , impedance at resonance  $Z_{k0}$ , and Q factor (or bandwidth  $\Delta f_k$ ). For Q factor smaller than 10, it is recommended to apply the correction given by (4.25). Then,  $f_k$  is given by

$$f_k \cong \frac{f_{k0}}{\sqrt{1 - \frac{1}{Q_k^2} + \frac{1}{2Q_k^4}}} \quad (4.26)$$

From (4.10) and (4.12) we get

$$R_k = Q_k^2 Z_{k0} \quad (4.27)$$

Then we compute the wave impedance  $\rho$

$$\rho^2 = \frac{L_k}{C_k} = \frac{R_k^2}{Q_k^2} = Q_k^2 Z_{k0}^2 \quad (4.28)$$

From(4.28) and (4.9) we obtain

$$L_k = \frac{1}{2\pi f_k} \frac{Q_k^2}{\sqrt{Q_k^2 - 1}} Z_{k0} \quad (4.29)$$

and

$$C_k = \frac{L_k}{\rho_k^2} = \frac{L_k}{Q_k^2 Z_{k0}^2} = \frac{1}{2\pi f_k} \frac{1}{\sqrt{Q_k^2 - 1}} \frac{1}{Z_{k0}} \quad (4.30)$$

#### 4.6.Computation of filtration parameters

Mathematical expressions from previous chapters were used in realization of a four section filter for a priori chosen harmonics

$$\begin{aligned} f_{03} &= 150 \text{ Hz}, & f_{05} &= 250 \text{ Hz}, \\ f_{07} &= 350 \text{ Hz}, & f_{11} &= 550 \text{ Hz} \end{aligned} \quad (4.31)$$

The absolute value of impedance for each resonance frequency can be chosen independently. Equal value was assumed for every harmonics in order to simplify the presentation

$$Z_{03} = Z_{05} = Z_{07} = Z_{011} = 14 \Omega \quad (4.32)$$

Similarly, the Q factor for every component filter was equalized. Four different cases are summarized in Table 4-1.

**Table 4-1 Various values of the Q factor**

Case No.	1	2	3	4
$Q_3 = Q_5 = Q_7 = Q_{11}$	5	10	20	50

Tables show the RLC and f values for Q factors from Table 4-1.

**Table 4-2 RLC values for the case 1, Q=5**

	$k = 3$	$k = 5$	$k = 7$	$k = 11$
$R$	350Ω	350Ω	350Ω	350Ω
$L$	0.074H	0.044H	0.032H	0.020H
$C$	15.16μF	9.10μF	6.65μF	4.135μF
$f$	153.03Hz	255.05Hz	357.07Hz	561.11Hz

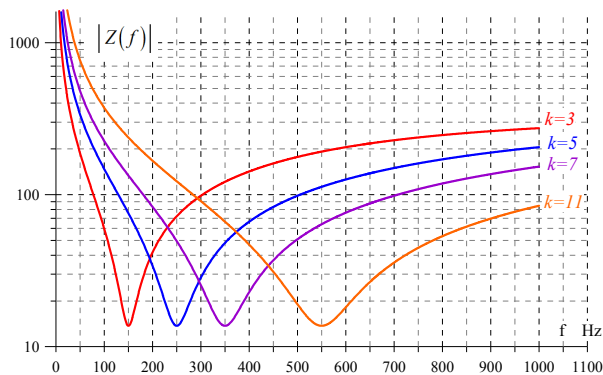


**Figure 4.11 Absolute value of impedance for Q=5**



Table 4-3 RLC values for the case 1, Q=10

	$k = 3$	$k = 5$	$k = 7$	$k = 11$
$R$	1400Ω	1400Ω	1400Ω	1400Ω
$L$	0.148H	0.89H	0.637H	0.040H
$C$	7.579μF	4.547μF	3.248μF	2.067μF
$f$	150.75Hz	251.25Hz	351.75Hz	552.76Hz

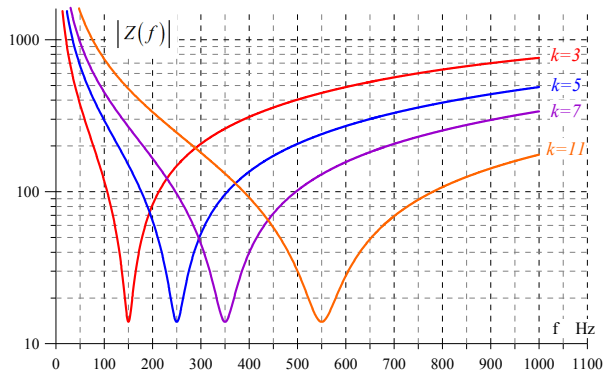


Figure 4.12 Absolute value of impedance for Q=10

Table 4-4 RLC values for the case 1, Q=20

	$k = 3$	$k = 5$	$k = 7$	$k = 11$
$R$	1400Ω	1400Ω	1400Ω	1400Ω
$L$	0.148H	0.89H	0.637H	0.040H
$C$	7.579μF	4.547μF	3.248μF	2.067μF
$f$	150.75Hz	251.25Hz	351.75Hz	552.76Hz

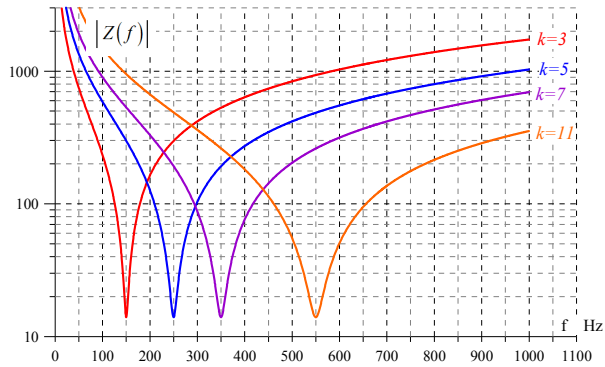


Figure 4.13 Absolute value of impedance for Q=20

Table 4-5 RLC values for the case 1, Q=50

	$k = 3$	$k = 5$	$k = 7$	$k = 11$
$R$	35k $\Omega$	35k $\Omega$	35k $\Omega$	35k $\Omega$
$L$	0.743H	0.446H	0.318H	0.203H
$C$	1.516 $\mu$ F	0.909 $\mu$ F	0.650 $\mu$ F	0.413 $\mu$ F
$f$	150.03Hz	250.05Hz	350.07Hz	550.11Hz

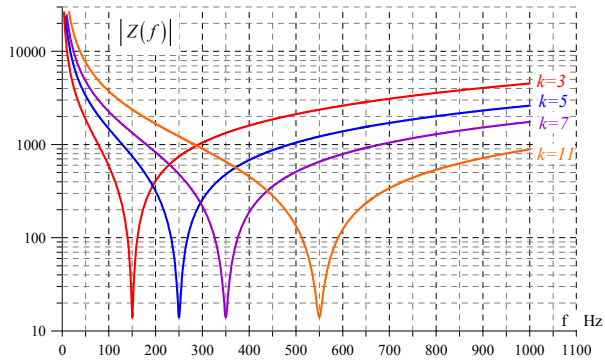
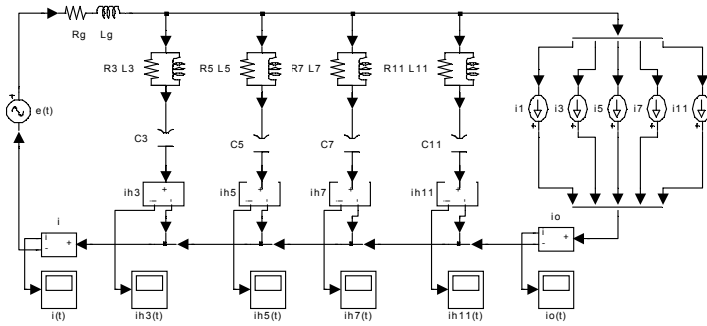


Figure 4.14 Absolute value of impedance for Q=50

#### 4.7. Simulation of nonlinear load working with a filter

Simulation is an effective way to test the presented approach to filter design. The filter was implemented in Power System Blockset [11], a part of Matlab [12] and shown in Figure 4.15.



**Figure 4.15 Simulated one phase system**

To show clearly the filtration effect, the presence of 3, 5, 7, 9, 11 current harmonic was assumed. Every harmonic with an amplitude of 20% of the fundamental. Due to a significant difference between the impedance of the network  $Z_g$  and the impedance  $Z_f$  of the filter (50 to 14) the effect of filtering is very clear (Fig. 15). The module of impedance  $Z_f$  should be selected depending on the impedance of the network, the expected effect of filtration and maximum overcurrent and overvoltage in the filter.

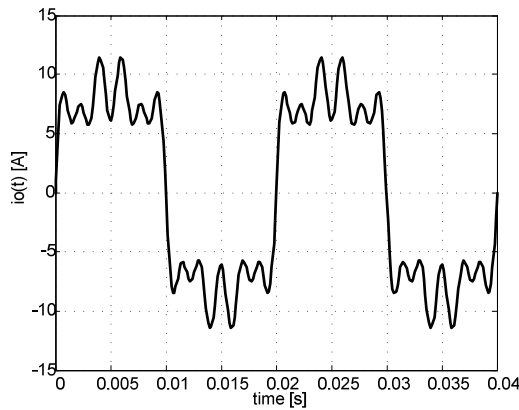


**Figure 4.16 Current drawn by nonlinear load**

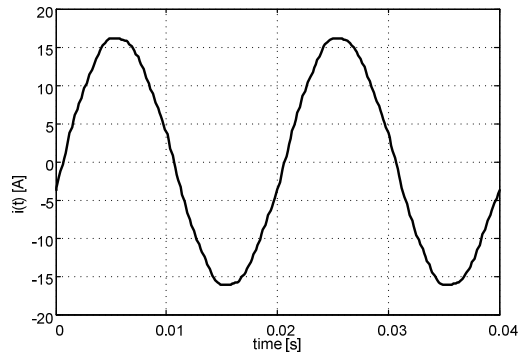


Figure 4.17 Current drawn from the pcc

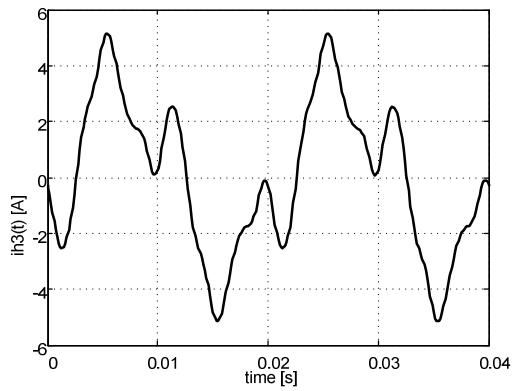


Figure 4.18 Current in the filter branch for 3-th harmonic

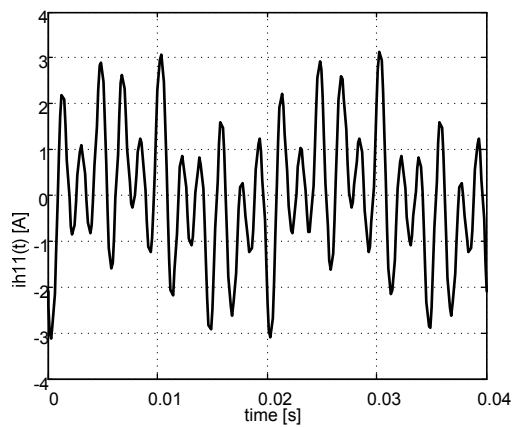


Figure 4.19 Current in the filter branch for 11-th harmonic

Figure 4.18 and Figure 4.19 shows currents flowing in the branches of the filter, designed for 3 and 11 harmonics. These graphs show the effectiveness of filtration.

An effective way to eliminate harmonics is an appropriate use of analog filters. Selecting an adequate filter is primarily reduced to the analysis of the load structure and harmonics levels in the current. The next step is to find a filter structure with appropriate parameters.

#### **4.8.Literature**

- [1] F. C. de la Rosa, Harmonics and power systems (Boca Raton FL:, CRC Press 2006)
- [2] R. Dugan, Electrical Power Systems Quality, (McGraw-Hill, New York 1996)
- [3] J. Arrilaga, N. R. Watson, Power System Quality Assessment (Chichester England, John Wiley & Sons, 2000)
- [4] F. Wang, M. H. J. Bollen, Quantifying the potential impacts of disturbances on power system protection, Proceedings of 'Developments in Power System Protection Conference', Amsterdam 9-12 April, 2002, 262-266
- [5] EN 50160, Standard, Voltage Characteristics In Public Distribution Systems
- [6] PN-EN 61000-3-2, Standard, Limits for harmonic current emissions (equipment input current up to and including 16A per phase).
- [7] IEC 662, Standard, Sodium Vapor Lamps
- [8] J.Bird, Electric circuit theory and technology (London, Elsevier, 2007)
- [9] MGM Transformer online: [www.mgm-transformer.com](http://www.mgm-transformer.com)
- [10] U. A. Bakshi, A. V. Bakshi, Circuit Theory (Shanivar Pet, Pune, 2009)
- [11] The Matworks: Power System Blockset. User's Guide, (The Math Works Inc. 2000)
- [12] The Matwroks: Matlab. The Language of Technical Computing. Using Matlab, (The Math Works Inc. 2001)

### **5. Fourier Techniques for Spectral Analysis**

Harmonics have always been present in power systems. Recently, due to the widespread use of a power electronics system resulting in an increase in their magnitude, they have become a key issue in installations [1]. A harmonic distortion can be considered as a sort of pollution of the electric system which can cause problems if the sum of harmonics currents exceeds certain limits [1].

Fourier transform is one of the most powerful tools in a spectral analysis. The assessment of harmonics content in currents and voltages is usually done with Fourier Transform. In this chapter, the outline of the discrete Fourier Transform will be given, and is based mainly on [2].

### 5.1. Discrete Time Fourier Transform Definition

Let us firstly formulate and explain the definition.

The Fourier Transform of a discrete series DTFT  $X(e^{j\omega})$  of the signal  $x[n]$  is defined as

$$X(e^{j\omega}) = \sum_{n=-\infty}^{\infty} x[n] e^{-j\omega n} \quad (5.1)$$

Generally,  $X(e^{j\omega})$  is a complex function of a real variable  $\omega$  and may be written as a sum of real and imaginary part

$$X(e^{j\omega}) = X_{re}(e^{j\omega}) + jX_{im}(e^{j\omega}) \quad (5.2)$$

$X_{re}(e^{j\omega})$  and  $X_{im}(e^{j\omega})$  are the real and imaginary parts of  $X(e^{j\omega})$

and consequently real functions of the independent variable  $\omega$ .

Sometimes, the exponential form of DTFT is more suitable and readable

$$X(e^{j\omega}) = |X(e^{j\omega})| e^{j\theta(\omega)} \quad (5.3)$$

where  $\theta(\omega)$

$$\theta(\omega) = \arg\{X(e^{j\omega})\} \quad (5.4)$$

and returns directly the amplitude spectrum and phase spectrum. Therefore,

$|X(e^{j\omega})|$  is the absolute value of the function or **amplitude spectrum** and

$\theta(\omega)$  is the phase as a function of frequency or briefly **phase spectrum**. Both quantities are functions of real variable  $\omega$ .

Assuming that  $x[n]$  is a real function (almost all signals in the power quality area), characteristic features can be noticed

- $|X(e^{j\omega})|$  and  $X_{re}(e^{j\omega})$  are even functions of  $\omega$
- $\theta(\omega)$  and  $X_{im}(e^{j\omega})$  are odd functions of  $\omega$ .

Both are a consequence of complex exponential function properties, compactly written as

$$X(e^{j\omega}) = |X(e^{j\omega})| e^{j\theta(\omega+2\pi k)} = |X(e^{j\omega})| e^{j\theta(\omega)} \quad (5.5)$$

for any integer  $k$ .

Computation of Fourier Transform of a power sequence describing a causal system has been chosen to illustrate practical use of the definition of DTFT.

The signal, e.g. impulse response of the mentioned system

$$x[n] = a^n \cdot 1[n] \quad (5.6)$$

where  $|a| < 1$  to guarantee convergence.

DTFT is given as

$$X(e^{j\omega}) = \sum_{n=-\infty}^{\infty} a^n \cdot 1[n] e^{-j\omega n} = \sum_{n=0}^{\infty} a^n e^{-j\omega n} = \sum_{n=0}^{\infty} (ae^{-j\omega})^n = \frac{1}{1-ae^{-j\omega}} \quad (5.7)$$

and again  $|ae^{-j\omega}| = |a| < 1$  for convergence.

Amplitude and phase spectrum of DTFT (5.8) for  $a = 0.5$  may be presented graphically.

$$X(e^{j\omega}) = \frac{1}{1-0.5e^{-j\omega}} \quad (5.8)$$

Figure 5.1 shows the amplitude spectrum of (5.8) and Figure 5.2 shows the corresponding phase spectrum.

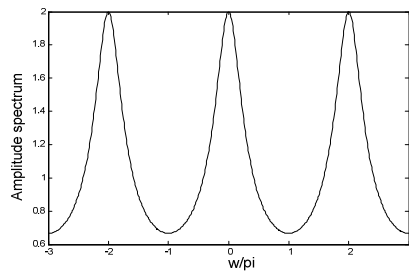


**Figure 5.1** Amplitude spectrum

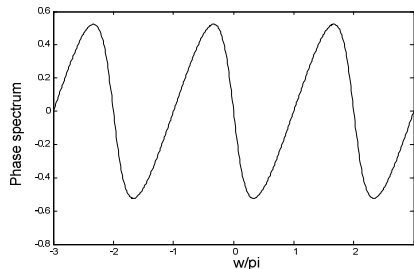


**Figure 5.2** Phase spectrum

The two pictures above indicate two important general features of the transform:

- DTFT of the sequence  $x[n]$  is a continuous function of frequency  $\omega$ .
- DTFT of the sequence  $x[n]$  is a periodic function of  $\omega$  with the period  $2\pi$ .

## 5.2. Discrete Fourier Transform Definition

In practice the Discrete Fourier Transform DFT, an alternation of DTFT is in use. The definition and examples will be given below.

The relationship between the finite sequence  $x[n]$  (bounded in its length)  $0 \leq n \leq N-1$  and its DTFT  $X(e^{j\omega})$  may be obtained through equidistant sampling of the function  $X(e^{j\omega})$  on the  $\omega$  axes in the interval  $0 \leq \omega \leq 2\pi$  at points  $\omega_k = 2\pi k / N$ ,  $0 \leq k \leq N-1$ .

So, the defining equation may be written

$$X[k] = X(e^{j\omega}) \Big|_{\omega = 2\pi k / N} = \sum_{n=0}^{N-1} x[n] e^{-j2\pi kn / N} \quad (5.9)$$

where  $0 \leq k \leq N-1$ .

is a complex series of the length  $N$  in frequency domain.

Discrete series  $X[k]$  is called a **Discrete Fourier Transform (DFT)** of the sequence  $x[n]$ .

Introducing the supposition  $W_N = e^{-j2\pi / N}$  the DFT may be given in frequently used form

$$X[k] = \sum_{n=0}^{N-1} x[n] W_N^{kn} \quad (5.10)$$

where  $0 \leq k \leq N-1$ .

There is a way to invert the transformation and return to the finite time series. The procedure, called **Inverse Discrete Fourier Transform IDFT**, is given by

$$x[k] = \frac{1}{N} \sum_{k=0}^{N-1} X[k] W_N^{-kn} \quad (5.11)$$

where  $0 \leq n \leq N-1$ .

An example illustrates the practical use of the DFT definition.

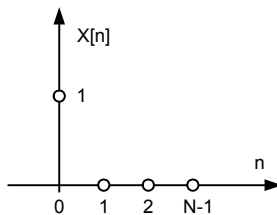




**Figure 5.3** Discrete signal of the length N.

The DFT of the signal in Figure 5.3 contains also N points in the frequency domain

$$X[k] = \sum_{n=0}^{N-1} x[n] W_N^{kn} = x[0] W_N^0 = 1 \quad (5.12)$$

where  $0 \leq k \leq N-1$ . All points have the same value, one.

Another example considers a signal given by

$$x[n] = \begin{cases} 1, & n = m \\ 0, & 0 \leq n \leq m-1, m+1 \leq n \leq N-1 \end{cases} \quad (5.13)$$

the corresponding DFT

$$X[k] = \sum_{n=0}^{N-1} x[n] W_N^{kn} = x[m] W_N^{km} = W_N^{km}, \quad 0 \leq k \leq N-1 \quad (5.14)$$

where  $0 \leq k \leq N-1$ .

It is very convenient for the practical numerical computation to present the DFT equation in

a matrix form. DFT given as  $X[k] = \sum_{n=0}^{N-1} x[n] W_N^{kn}$  may be compactly written in the matrix

form

$$\mathbf{X} = \mathbf{D}_N \mathbf{x} \quad (5.15)$$

where

$$\mathbf{X} = [X[0] \quad X[1] \quad \dots \quad X[N-1]]^T \quad (5.16)$$

represents the signal in frequency domain,

$$\mathbf{x} = [x[0] \quad x[1] \quad \dots \quad x[N-1]]^T \quad (5.17)$$

is the signal in time domain to be transformed and

$$\mathbf{D}_N = \begin{bmatrix} 1 & 1 & 1 & \dots & 1 \\ 1 & W_N^1 & W_N^2 & \dots & W_N^{(N-1)} \\ 1 & W_N^2 & W_N^4 & \dots & W_N^{2(N-1)} \\ \vdots & \vdots & \vdots & \ddots & \vdots \\ 1 & W_N^{(N-1)} & W_N^{2(N-1)} & \dots & W_N^{(N-1)^2} \end{bmatrix} \quad (5.18)$$

is the transformation matrix.

Also the Inverse Discrete Fourier Transform defined by  $x[n] = \frac{1}{N} \sum_{k=0}^{N-1} X[k] W_N^{-kn}$  may be

written in a matrix form

$$\mathbf{x} = \frac{1}{N} \mathbf{D}_N^{-1} \mathbf{X} \quad (5.19)$$

where

$$\mathbf{D}_N^{-1} = \begin{bmatrix} 1 & 1 & 1 & \dots & 1 \\ 1 & W_N^{-1} & W_N^{-2} & \dots & W_N^{-(N-1)} \\ 1 & W_N^{-2} & W_N^{-4} & \dots & W_N^{-2(N-1)} \\ \vdots & \vdots & \vdots & \ddots & \vdots \\ 1 & W_N^{-(N-1)} & W_N^{-2(N-1)} & \dots & W_N^{-(N-1)^2} \end{bmatrix} \quad (5.20)$$

is the inverse transformation matrix.

The transformation matrix and inverse transformation matrix are joined by the expression

$$\mathbf{D}_N^{-1} = \frac{1}{N} \mathbf{D}_N^* \quad (5.21)$$

### 5.3. Discrete Fourier Transform expressed using trigonometric functions

The well known Euler's formula (5.22) allows us to rewrite the equations for DFT

$$e^{-j\phi} = \cos(\phi) - j \sin(\phi) \quad (5.22)$$

into the trigonometric form

$$X[k] = \sum_{n=0}^{N-1} x[n] [\cos(2\pi nk / N) - j \sin(2\pi nk / N)] \quad (5.23)$$

where

$X[k]$  is the  $k$ -th component of DFT, meaning  $X[0], X[1], \dots, X[N-1]$ ,

$k$  is the index of samples of DFT in frequency domain, meaning  $k = 0, 1, 2, 3, \dots, N-1$ ,

$x[n]$  is the sequence of input samples, meaning  $x[0], x[1], \dots, x[N-1]$ ,

$n$  is the index of input samples in time domain, meaning  $n = 0, 1, 2, 3, \dots, N-1$ ,

$N$  is the number of samples of the input sequence and the number of frequency points in the DFT sequence.

Indices  $n$  for the input samples and  $k$  for the samples of DFT always increase from 0 to  $N-1$  in the standard notation of DFT. That means, for  $N$  input samples in time domain, DFT computes the spectrum content of the input signal at  $N$  equidistant points of the frequency axes.

That means, for  $N$  input samples in time domain, DFT computes the spectrum content of the input signal at  $N$  equidistant points of the frequency axes.

The value of  $N$  is therefore an important parameter of DFT, with a direct impact on:

- the number of required input samples
- the spectral resolution in frequency domain
- the time needed for processing a signal of length  $N$  to the DFT representation

To illustrate the practical application of DFT some examples are shown.

**Example I.**

The detailed computation of four values in frequency domain will be shown.

If  $N = 4$ , then both  $n$ , and  $k$  increase from 0 to 3. The particular expression for DFT has the form:

$$X[k] = \sum_0^3 x[n] [\cos(2\pi nk/4) - j \sin(2\pi nk/4)] \tag{5.24}$$

Writing all spectral terms of DFT for the first sample,  $k = 0$ , we obtain

$$\begin{aligned} X[0] = & \\ & x(0) \cos(2\pi \cdot 0 \cdot 0/4) - jx(0) \sin(2\pi \cdot 0 \cdot 0/4) + \\ & x(1) \cos(2\pi \cdot 1 \cdot 0/4) - jx(1) \sin(2\pi \cdot 1 \cdot 0/4) + \\ & x(2) \cos(2\pi \cdot 2 \cdot 0/4) - jx(2) \sin(2\pi \cdot 2 \cdot 0/4) + \\ & x(3) \cos(2\pi \cdot 3 \cdot 0/4) - jx(3) \sin(2\pi \cdot 3 \cdot 0/4) \end{aligned} \tag{5.25}$$

For second sample of DFT,  $k = 1$  the equation is

$$\begin{aligned} X[1] = & \\ & x(0) \cos(2\pi \cdot 0 \cdot 1/4) - jx(0) \sin(2\pi \cdot 0 \cdot 1/4) + \\ & x(1) \cos(2\pi \cdot 1 \cdot 1/4) - jx(1) \sin(2\pi \cdot 1 \cdot 1/4) + \\ & x(2) \cos(2\pi \cdot 2 \cdot 1/4) - jx(2) \sin(2\pi \cdot 2 \cdot 1/4) + \\ & x(3) \cos(2\pi \cdot 3 \cdot 1/4) - jx(3) \sin(2\pi \cdot 3 \cdot 1/4) \end{aligned} \tag{5.26}$$

The third sample is obtained in the same way,  $k = 2$

$$\begin{aligned} X[2] = & \\ & x(0) \cos(2\pi \cdot 0 \cdot 2/4) - jx(0) \sin(2\pi \cdot 0 \cdot 2/4) + \\ & x(1) \cos(2\pi \cdot 1 \cdot 2/4) - jx(1) \sin(2\pi \cdot 1 \cdot 2/4) + \\ & x(2) \cos(2\pi \cdot 2 \cdot 2/4) - jx(2) \sin(2\pi \cdot 2 \cdot 2/4) + \\ & x(3) \cos(2\pi \cdot 3 \cdot 2/4) - jx(3) \sin(2\pi \cdot 3 \cdot 2/4) \end{aligned} \tag{5.27}$$

The final one in this example,  $k = 3$

$$\begin{aligned}
X[3] = & \\
& x(0)\cos(2\pi \cdot 0 \cdot 3/4) - jx(0)\sin(2\pi \cdot 0 \cdot 3/4) + \\
& x(1)\cos(2\pi \cdot 1 \cdot 3/4) - jx(1)\sin(2\pi \cdot 1 \cdot 3/4) + \\
& x(2)\cos(2\pi \cdot 2 \cdot 3/4) - jx(2)\sin(2\pi \cdot 2 \cdot 3/4) + \\
& x(3)\cos(2\pi \cdot 3 \cdot 3/4) - jx(3)\sin(2\pi \cdot 3 \cdot 3/4)
\end{aligned} \tag{5.28}$$

Looking at the results above we can formulate an important remark:

Every sample of  $X[k]$  DFT is a “point after point” summation of a product term consisting of subsequent values of the input series and a complex term  $\cos(\phi) - j \sin(\phi)$ .

We see in that example that the frequencies of sinusoidal components depend on the sampling frequency  $f_p$ , and the number of samples  $N$ .

**Example II.**

If we sample an analog signal with the ratio of 500 samples per second and compute afterward a 16-point DFT from these samples, then the fundamental frequency of the sinus waves to which we correlate the signal to be transformed is

$$f_p / N = 500 / 16 = 31,25\text{Hz} \tag{5.29}$$

Computed values of  $X(k)$  DFT called “stripes”, are determined at points being exact multiplies of the fundamental frequency. In presented case, the specific values are

$X[0]$  - 1. strip with analysis frequency =  $0 \times 31,25 = 0$  Hz.

$X[1]$  - 2. strip with analysis frequency =  $1 \times 31,25 = 31,25$  Hz,

$X[2]$  - 3. strip with analysis frequency =  $2 \times 31,25 = 62,5$  Hz,

$X[3]$  - 4. strip with analysis frequency =  $3 \times 31,25 = 93,75$  Hz.

.....

$X[15]$  - 16. strip with analysis frequency  $15 \times 31,25 = 468.75$  Hz.

The values of  $N$  subsequent points on the frequency axes are given by

$$f_a = \frac{mf_p}{N} \tag{5.30}$$

The resolution of DFT is given as ratio of the sampling frequency to the number of samples

$$\Delta f = \frac{f_p}{N} \tag{5.31}$$

Instantaneous power of the signal  $X_p[k]$  is expressed as a square of the absolute value of the spectrum.

$$X_p(k) = |X(k)|^2 = X_{re}^2(k) + X_{im}^2(k) \quad (5.32)$$

**Example III.**

An input signal  $x(t)$  should be sampled. The signal contains two spectral components with the frequencies 1 kHz and 2 kHz, and is given as

$$x(t) = \sin(2\pi \cdot 1000 \cdot t) + \frac{1}{2} \sin(2\pi \cdot 2000 \cdot t + \frac{3\pi}{4}) \quad (5.33)$$

Afterwards, 8-point DFT of the sampled signal should be computed.

The approach to the problem may be the following:

Choosing a sampling frequency  $f_p$ , we get equidistant samples every  $T_p = 1/f_p$ . We need exactly 8 input samples, allowing the computation of 8 - points DFT. Eight elements of the series  $x[n]$  are equal to  $x(t)$  sampled at the time instants  $nT_p$

$$x[n] = x(nT_p) = \sin(2\pi \cdot 1000 \cdot nT_p) + \frac{1}{2} \sin(2\pi \cdot 2000 \cdot nT_p + \frac{3\pi}{4}) \quad (5.34)$$

If we choose the sampling frequency  $f_p = 8000$  samples/second, then DFT determines spectral components of the signal  $x[n]$  at certain points of the frequency axes  $k \cdot \frac{f_p}{N}$ , which is at 0 kHz, 1 kHz, 2 kHz ... 7 kHz.

Numerical values  $x[n]$  of the sampled signal given by (5.34) are:  $x[0]= 0,3535$ ,  $x[1]= 0,3535$ ,  $x[2]= 0,6464$ ,  $x[3]= 1,0607$ ,  $x[4]= 0,3535$ ,  $x[5]=-1,0607$ ,  $x[6]= -1,3535$ ,  $x[7]= -0,3535$ .

These values of samples  $x[n]$  are shown as dots on the continuous line  $x(t)$  on figures below illustrating the DFT.

Let us now compute the DFT values.

For  $k = 1$ , or the DFT component with the frequency 1 kHz,  $\frac{kf_p}{N} = \frac{8000}{8}$ , the equation in this case has the form:

$$X(1) = \sum_{n=0}^7 x[n] \cos\left(\frac{2\pi n}{8}\right) - jx[n] \sin\left(\frac{2\pi n}{8}\right) \quad (5.35)$$

Substituting the values of samples  $x[n]$  into the equation and putting the cos terms into the left column and the sin terms into the right column we obtain

$X[1]=$	$0,3535 \cdot 1,0$	$-j(0,3535 \cdot 0,0)+$	for n=0
	$+ 0,3535 \cdot 0,707$	$-j(0,3535 \cdot 0,707)+$	for n=1
	$+ 0,6464 \cdot 0,0$	$-j(0,6464 \cdot 1,0)+$	for n=2
	$+ 1,0607 \cdot -0,707$	$-j(1,0607 \cdot 0,707)+$	for n=3
	$+0,3535 \cdot -1,0$	$-j(0,3535 \cdot 0,0)+$	for n=4
	$-1,0607 \cdot -0,707$	$-j(-1,0607 \cdot -0,707)+$	for n=5
	$-1,3535 \cdot -0,0$	$-j(-1,3535 \cdot -1,0)+$	for n=6
	$-0,3535 \cdot 0,707$	$-j(0,3535 \cdot -0,707)=$	for n=7
=	$0,3535 +$	$0$	
	$+ 0,250$	$-j0,250 +$	
	$0$	$-j0,6464 +$	
	$- 0,750$	$-j0,750+$	
	$-0,3535+$	$0$	
	$+0,750$	$-j0,750+$	
	$0$	$-j1,3535$	
	$-0,250=$	$+j0,250=$	
$X[1]=$	$0-j4,0$	$= 4e^{-j90^\circ}$	

It should be noticed, that the sin and cos lines used in the analysis have the frequency of 1kHz (Figure 5.4), which is one period in the sampling interval.

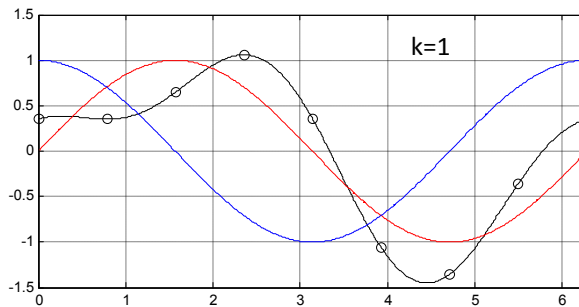


**Figure 5.4** Signal  $x(t)$  and sin, cos curves with 1 kHz used for sampling

The computational results shows that the input signal  $x[n]$  contains a component with the frequency 1kHz. Detailed information of the component for  $k = 1$  :

Absolute value of the first component  $X(1)$

$$|X(1)| = 4 \quad (5.36)$$

Phase

$$X_{\phi}(1) = \arctg\left(\frac{X_{imag}(1)}{X_{real}(1)}\right) = -90^{\circ} \quad (5.37)$$

Instantaneous power

$$X_p(1) = |X(1)|^2 = 16 \quad (5.38)$$

Let us now compute the second component for  $k = 2$ .

We correlate  $x[n]$  with the sin and cos curves of the frequency 2 kHz. These sin and cos curves in Figure 5.5 have  $k = 2$  whole periods in the sampling interval (in previous case only one).

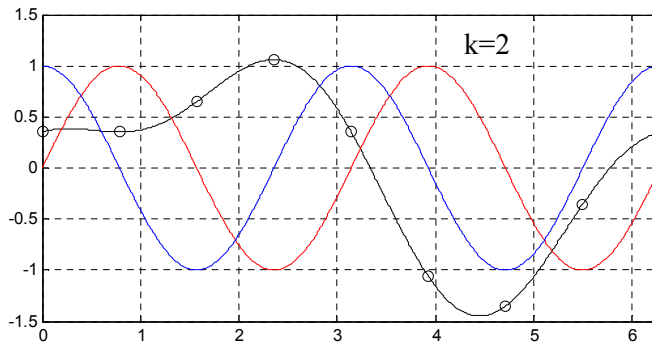


**Figure 5.5** Signal  $x(t)$  and sin, cos curves with 2 kHz used for sampling

Substituting the values of samples  $x[n]$  into the equation (5.35) for  $k = 2$  gives the result:

$$X(2) = 1,414 + j1,414 = 2e^{j45^{\circ}} \quad (5.39)$$

The input signal  $x[n]$  contains a term of frequency 2 kHz, its relative amplitude is 2 and its phase angle to the cos curve of frequency 2 kHz is  $45^{\circ}$ .

In a similar manner, we compute the third component for  $k = 3$ .

For  $k = 3$ , we correlate  $x[n]$  with sin and cos line of the frequency 3 kHz (Figure 5.6).

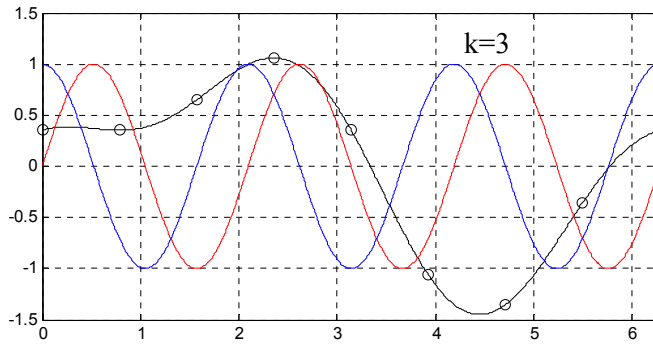


**Figure 5.6** Signal  $x(t)$  and sin, cos curves with 3 kHz used for sampling

We should notice again, that they have  $k=3$  full periods in the sampling window. Substituting the values of the samples  $x(n)$  to the equation (5.35) and for  $k=3$  returns

$$X(3) = 0 - j0 = 0 \quad (5.40)$$

DFT yields that  $x[n]$  do not contain a term with the frequency 3 kHz.

We continue in a similar manner the computation of DFT for the subsequent values of the parameter  $k$ .

For  $k=4$  the result of computation according to (5.35) is

$$X(4) = 0, 0 - j0, 0 = 0 \quad (5.41)$$

For  $k=5$  the result of computation according to (5.35) is also zero

$$X(5) = 0, 0 - j0, 0 = 0 \quad (5.42)$$

and curves used for  $k=5$  are shown in Figure 5.7

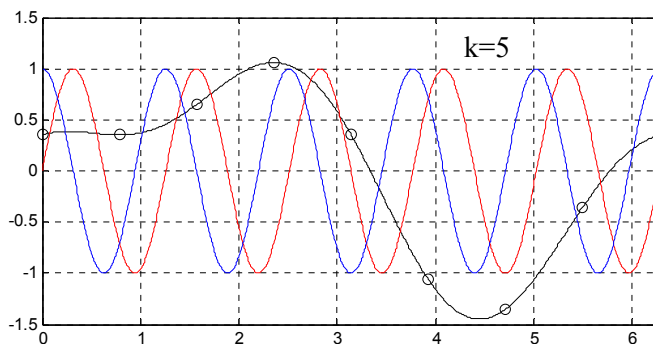


**Figure 5.7** Signal  $x(t)$  and sin, cos curves with 5 kHz used for sampling



For  $k = 6$  the result of computation according to (5.35) is non zero

$$X(2) = 1,414 + j1,414 = 2e^{j45^\circ} \quad (5.43)$$

and curves used for  $k = 6$  are shown in Figure 5.8.

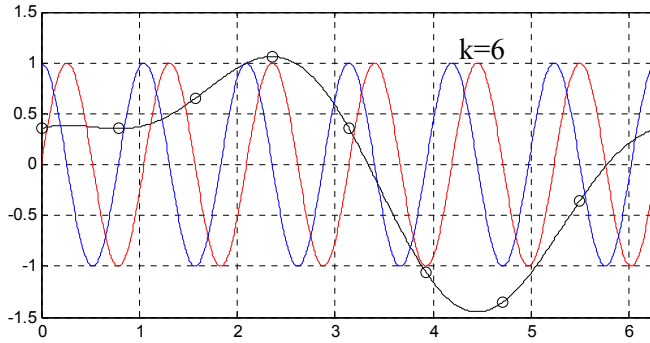


**Figure 5.8** Signal  $x(t)$  and sin, cos curves with 6 kHz used for sampling

Also for  $k = 7$  the result of computation according to (5.35) is non zero

$$X(7) = 0 + j4 = 4e^{j90^\circ} \quad (5.44)$$

and curves used for  $k = 7$  are shown in Figure 5.9.

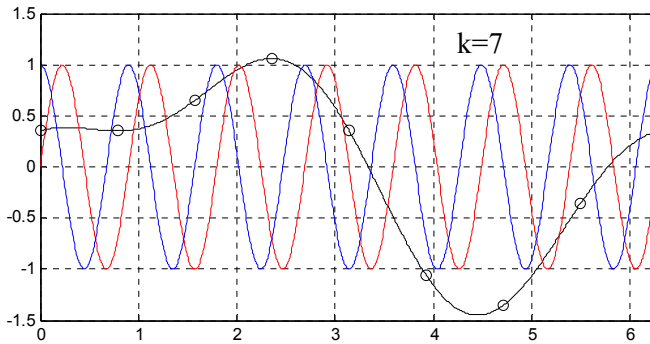


**Figure 5.9** Signal  $x(t)$  and sin, cos curves with 7 kHz used for sampling

Finally, for  $k = 0$  we use for computation  $\cos(0) - j \sin(0)$  and obtain

$$X(0) = \sum_{n=0}^{N-1} x(n) [\cos(0) - j \sin(0)] = \sum_{n=0}^{N-1} X(n) \quad (5.45)$$

substituting sampled data

$$X(0) = 0,3535 + 0,3535 + 0,6464 + 1,0607 + 0,3535 - 1,0607 - 1,3535 - 0,3535 = 0 \quad (5.46)$$

The value  $X(0)$  in the frequency domain determines the constant term in the spectrum of the signal  $x[n]$ .

Plotting the output values  $|X(k)|$  as a function of frequency, we obtain an **amplitude spectrum** of the input sequence  $x[n]$  (Figure 5.10).

We should notice, that the picture shows for the sequence  $x[n]$ , two spectral components 1 kHz ( $k = 1$ ) and 2 kHz ( $k = 2$ ). Additionally, the first component of the frequency 1 kHz has twice as high amplitude as the second component with the frequency 2 kHz.

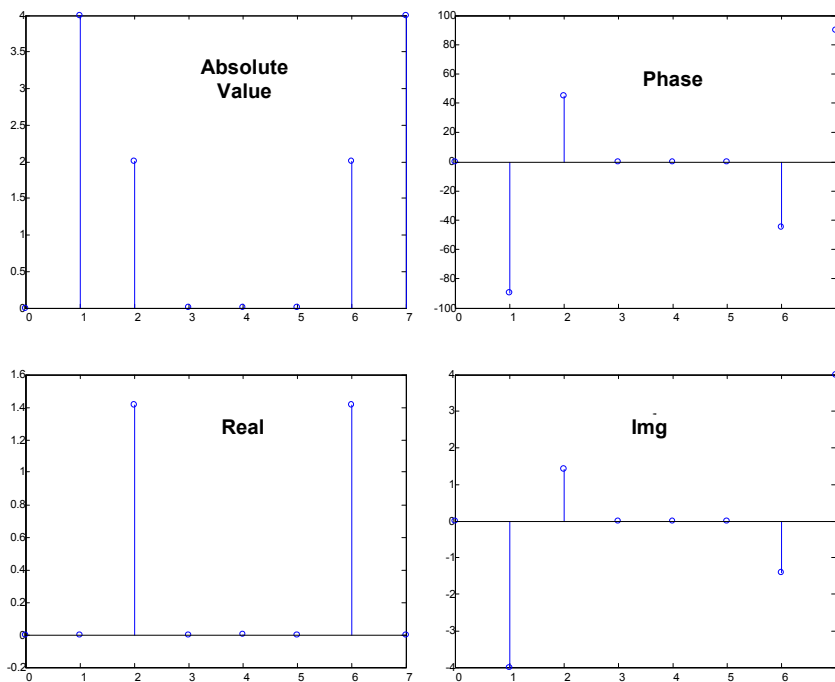


**Figure 5.10** DFT Results: abs value, phase, real and imaginary part of all eight components

Looking at Figure 5.10 two natural question may be asked.

Firstly, what is the meaning of amplitudes for  $k = 6$  and  $k = 7$ ? Secondly, why do the amplitudes seem to be four times as high as we would expect them to be?

The answer to the two questions reveals two important features of the DFT. Every single output value  $X(k)$  is a sum of subsequent products of input sequence samples and the sin and cos components, whose frequencies are so chosen, that they have  $k$  full periods in the whole range of  $N$  samples. Additionally, the output terms of DFT are symmetrical.

#### 5.4. Properties of DFT

We firstly take a closer look at the **symmetry** property. If the input sequence  $x[n]$  is real then, the complex output values of DFT for arguments  $k \geq \frac{N}{2}$  are superfluous in regard to output values for the arguments ranging from  $k = 0$  to  $k = \frac{N}{2} - 1$ .  $k$ -th Output value of DFT has the same amplitude as the  $(N-k)$ -th output value. The phase angle of the  $m$ -th output value of DFT is equal to the phase angle of  $(N-m)$ -th output value of DFT with the minus sign.

We may compactly write the properties using complex conjugate numbers denoted with (\*).

$$X(k) = X^*(N - k) \quad (5.47)$$

Let us once again take a look at the signal analysis presented above.

In the example under consideration, we see in **Figure 5.10** that  $X(5)$ ,  $X(6)$  and  $X(7)$  are complex conjugated values with  $X(3)$ ,  $X(2)$  and  $X(1)$ , respectively. The real part of  $X(k)$  has the property of **even symmetry** (see **Figure 5.10**) and imaginary part of DFT has the property of odd symmetry (see **Figure 5.10**).

Therefore, to obtain the DFT of the signal  $x[n]$ , it is enough to compute the first  $\frac{N}{2}$  values of  $X(k)$ , where  $0 \leq k \leq \frac{N}{2} - 1$ . • If the real input function is even  $x(n) = x(-n)$ , then  $X(k)$  is always real and even. On the other hand, if the real input function is odd,  $-x(n) = x(-n)$ , then  $X_{Re}(k)$  is always equal to zero, and  $X_{Im}(k)$  is non zero.

Let us now take a closer look at the **linearity** property of DFT. It is a very important property, because It says that the DFT of a sum of two components is equal to the sum of transforms of each term independently. Substituting

$$x_{sum}(n) = x_1(n) + x_2(n) \quad (5.48)$$

into the equation (5.1) in order to obtain  $X_{sum}(k)$  we get

$$\begin{aligned}
X_{sum}(k) &= \sum_{n=0}^{N-1} (x_1[n] + x_2[n]) e^{-j2\pi kn/N} = \\
&= \sum_{n=0}^{N-1} x_1[n] e^{-j2\pi kn/N} + \sum_{n=0}^{N-1} x_2[n] e^{-j2\pi kn/N} = \\
&= X_1(k) + X_2(k)
\end{aligned} \tag{5.49}$$

The proper interpretation of the **amplitudes of DFT** requires more explanations. Once again, we will consider the computational example presented in **Figure 5.10**.

The results  $|X(1)|=4$ ,  $|X(2)|=2$  are ambiguous, because the components of the input signal  $x[n]$  had the amplitudes 1 and 0,5 respectively.

If the real input signal contains a sin component with the amplitude  $A_0$  and an integer number of periods in the interval of  $N$  input samples then the amplitude of DFT for this particular sin signal is  $M_r$ , where

$$M_r = A_0 \frac{N}{2} \tag{5.50}$$

If the input signal for DFT contains a constant term  $D_0$ , then the amplitude of the constant output component  $X(0)$  DFT is equal to

$$X(0) = \frac{D_0}{N} \tag{5.51}$$

Considering the previous case of the real input signal for the component with frequency 1000 Hz  $A_0=1$  and  $N=8$ , we obtain

$$M_r = 1 \cdot \frac{8}{2} = 4 \tag{5.52}$$

as shown in our example.

In the literature on DFT, the transformation is sometimes defined with an included scaling term

$$X(k) = \frac{2}{N} \sum_{n=0}^{N-1} x[n] e^{-j2\pi nk/N} \tag{5.53}$$

The scaling term  $2/N$  guaranties, that the amplitudes of  $X(k)$  are equal to the amplitudes of the sin components in the input signal in time domain. Unfortunately, there is additional computational “cost” included in the operation – division by  $N$ .

Commercial software packages include often the following relationships:

$$X(k) = \frac{1}{\sqrt{N}} \sum_{n=0}^{N-1} x[n] e^{-j2\pi nk/N} \tag{5.54}$$

and

$$x_2[n] = \frac{1}{\sqrt{N}} \sum_{k=0}^{N-1} X_2(k) e^{j2\pi nk/N} \quad (5.55)$$

for direct and inverse DFT.

The scaling terms  $\frac{1}{\sqrt{N}}$  seem a little bit ambiguous, but they are in use, to avoid the change of scaling coefficients by transforming in both directions.

### 5.5. Shifting theorem in DFT

There is another property of the DFT, known as shifting theorem. As it has tremendous impact on practical computations a whole chapter has been dedicated to it. The shifting theorem states that:

**The shift in time of a periodic input sequence  $x(n)$**

**manifests itself as a constant phase shift in the angles associated with DFT results.**

If we decide to sample  $x[n]$  beginning with  $n$  equal to a particular constant  $n = k$ , as a opposition to  $n = 0$ , then DFT of the time shifted samples is given by

$$X_k(m) = e^{j2\pi km/N} X(m) \quad (5.56)$$

From (5.56) we see that if the point at which we start sampling  $x[n]$  is shifted to the right by  $k$  samples, then the output spectrum  $X_k(m)$  of DFT is expressed  $X(m)$ , with every complex term  $X(m)$  multiplied by a linear phase shift  $e^{j2\pi km/N}$ , actually shifting the phase by  $2\pi km/N$ .

On the other hand, if the point at which we start to sample  $x(n)$  is shifted to the left side by  $k$  samples, then the spectrum  $X_k(m)$  is expressed as  $X(m)$  multiplied by  $e^{-j2\pi km/N}$ .

In order to illustrate the shifting phenomenon, the same discrete signal from the previous example has been sampled with a delay (or more precisely a shift) of  $k = 3$  samples.

$$x(t) = \sin(2\pi \cdot 1000 \cdot t) + \frac{1}{2} \sin(2\pi \cdot 2000 \cdot t + \frac{3\pi}{4}) \quad (5.57)$$

Figure 5.11 shows the original signal defined through (5.57) in the time domain.

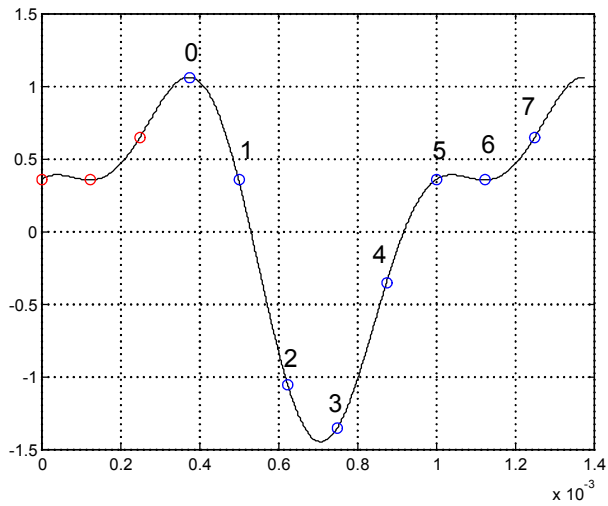


Figure 5.11 Sampling of  $x(t)$  in both examples

The new, shifted series  $x(n)$  contains points labeled with numbers (see picture) with the values:

$$\begin{aligned}
 x(0) &= 1,0607, & x(1) &= 0,3535, \\
 x(2) &= -1,0607, & x(3) &= -1,3535, \\
 x(4) &= -0,3535, & x(5) &= 0,3535, \\
 x(6) &= 0,3535, & x(7) &= 0,6464
 \end{aligned}$$

Computing DFT of the above series,  $X_k(m)$  we obtain results given in Table 5-1 and presented graphically in

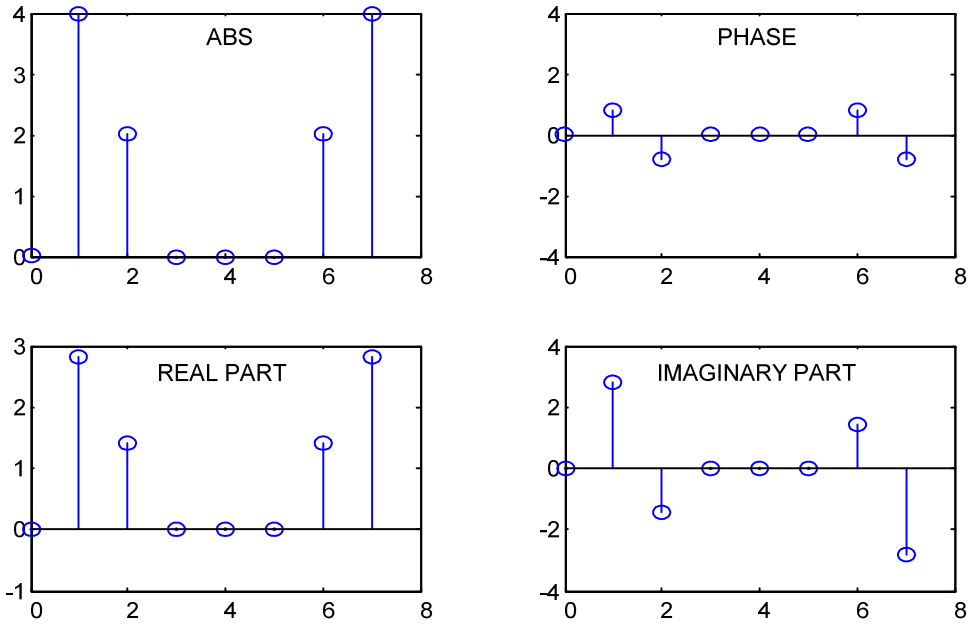
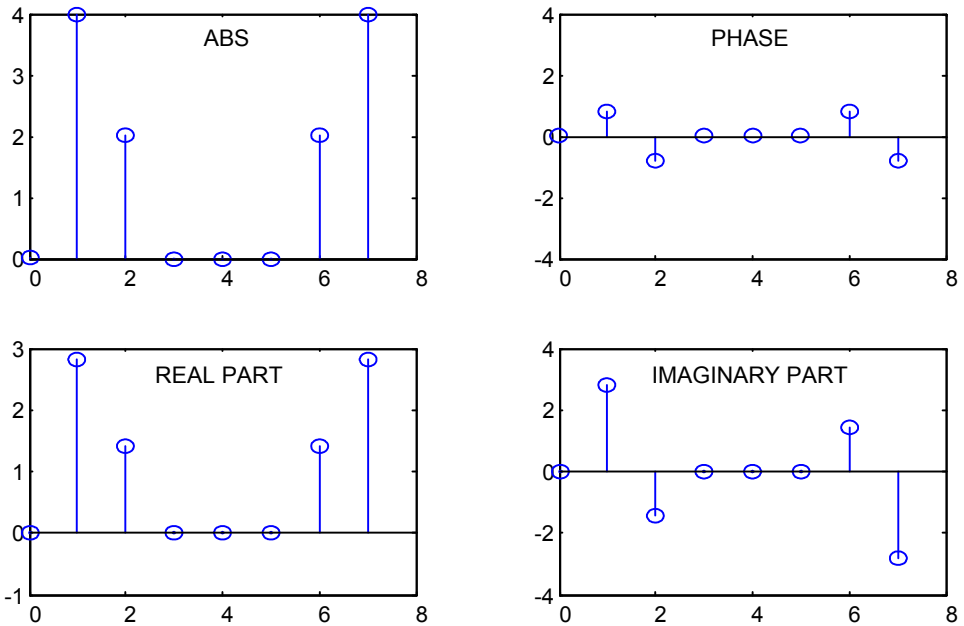


Figure 5.12.

Table 5-1 Shifted DFT values

m	amplitude	phase	real part	imaginary part
0	0	0	0	0
1	4	+45	2,8284	2,8284
2	2	-45	1,4141	-1,4141
3	0	0	0	0
4	0	0	0	0
5	0	0	0	0
6	2	+45	1,4141	-1,4141
7	4	-45	2,8284	-2,8284



**Figure 5.12** DFT Results for the 2 example: absolute value of  $X_k(m)$ , phase  $X_k(m)$ , real part  $X_k(m)$ , imaginary part  $X_k(m)$ .

From the computation results we see, that the amplitude of  $X_k(m)$  is unchanged in relation to the amplitude of  $X(m)$  of the non-shifted signal. The observations may be presented briefly:

The amplitude of DFT related to the original signal did not change despite sampling in shifted interval.

The phase of DFT, however, changes with relation to the moment when we start sampling of the signal  $x(n)$ .

Now, considering the component of DFT  $X_k(m)$ , for  $m = 1$  we check the phase of the shifted signal.

Recalling that  $X(1)$  from the 1 example DFT had an amplitude 4 and the phase -90 we have for  $k = 3$  and  $N = 8$ :

$$X_3(1) = e^{j2\pi k \frac{m}{N}} \cdot X(1) = e^{j2\pi \frac{3}{8}} \cdot 4e^{-j\frac{\pi}{2}} = 4e^{j\frac{\pi}{4}} \quad (5.58)$$

Therefore,  $X_3(m)$  has an amplitude 4 and phase +45 degree.



## 5.6. Inverse Discrete Fourier Transform

There is a simple way to come back from the spectral components to the original signal in time domain. The standard expression for inverse discrete Fourier Transform IDFT is given shortly in the exponential notation

$$x(n) = \frac{1}{N} \sum_{m=0}^{N-1} X(m) e^{j2\pi mn/N} \quad (5.59)$$

or applying the sin and cos terms

$$x(n) = \frac{1}{N} \sum_{m=0}^{N-1} X(m) \left[ \cos\left(2\pi m \frac{n}{N}\right) + j \sin\left(2\pi m \frac{n}{N}\right) \right] \quad (5.60)$$

**Discrete time signals may be regarded as a sum of sinusoidal terms with various values of frequencies. The values  $X(m)$  of DFT are  $N$  complex values, determining the amplitude and phase of every term of the sum.**

The inverse transform will be explained further on an example.

If we compute IDFT substituting the results from the 1 example into the equation (3), then we will go back from the frequency domain to the time domain and we will obtain the values of the original signal  $x(n)$ .

$$\begin{aligned} x[2] &= \frac{1}{8} \sum_{m=0}^{N-1} X(m) e^{j2\pi m 2/8} \\ x[2] &= \frac{1}{8} \left( X(0) e^{j\pi 0/8} + X(1) e^{j\pi 4/8} + X(2) e^{j\pi 6/8} + X(3) e^{j\pi 8/8} + \dots + X(7) e^{j\pi 14/8} \right) \quad (5.61) \\ x[2] &= 0,6464 \end{aligned}$$

and

$$\begin{aligned} x[0] &= 0,3535, \quad x[1] = 0,3535, \quad x[2] = 0,6464, \quad x[3] = 1,0607, \\ x[4] &= 0,3535, \quad x[5] = -1,0607, \quad x[6] = -1,3535, \quad x[7] = -0,3535. \end{aligned}$$

We should notice that the expression for IDFT, given by the equation (3), differs from the equation for DFT only with the scaling term  $1/N$  and the change of the sign of the exponent. Apart from the difference in scaling of values, all properties of DFT, may also be related to the IDFT.

## 5.7. DFT Leakage (Ambiguity) and its minimization

The previous examples of DFT have shown accurate results, because input sequences  $x(n)$  had been chosen carefully from a set of sinusoidal signals.

In a general case, DFT of sampled signals may lead to **ambiguous** results in the frequency domain.

**The DFT property, known as spectrum leakage, results in the fact that DFT values are only an approximation of the spectrum for signals after the sampling (discretization).**

There are methods minimizing that effect, but it is not possible to eliminate it completely.

DFT is bounded to operate on a finite number  $N$  of input samples, which are sampled with the frequency  $f_p$ . As a result we get  $N$ - point transform for discrete values of frequency:

$$f_m = \frac{mf_p}{N}; \quad m = 0, 1, 2, \dots, N-1 \quad (5.62)$$

for which the values of DFT are computed.

**DFT gives accurate results, only if the input sequence energy is located exactly at frequencies given in equation (5), for which we do the analysis. That are integer multiplies of the fundamental frequency  $f_p/N$ .**

Presented theoretical dependencies will be illustrated with a practical computational example.

If the input signal contains a term with an intermediate frequency e.g.  $1,5 f_p / N$  between the values  $mf_p/N$  for which we compute DFT, then the input component will be visible by all  $N$  output values of DFT.

Let's compute a 64-points DFT for a series obtained after sampling three periods of a sinusoid (Figure 5.13). Computed DFT shows that the signal do not contain a component with a frequency other then  $m=3$ . The correlation of an input sequence and sinusoids for  $m$  different from 3 is equal to zero.

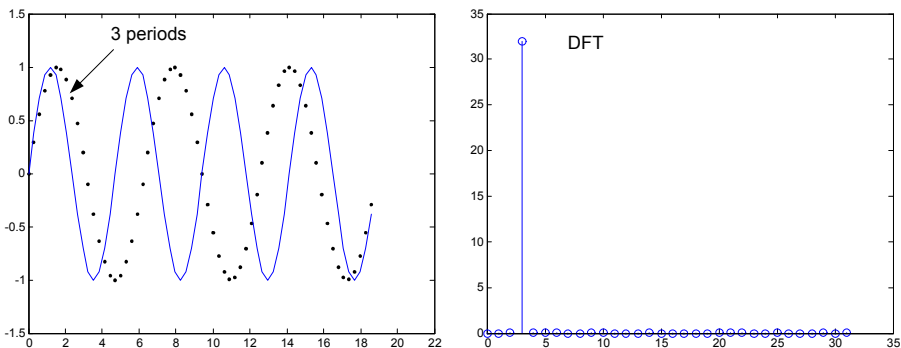


**Figure 5.13** 64-points DFT (left) input sequence, (right) absolute value of DFT, the first part of the result

We have now an input series containing 3,4 periods for 64 samples. Because this input sequence does not have an integer number of periods represented by the 64 samples, the energy “leaks” to all commuted samples of DFT, as shown in Figure 5.14 (right).

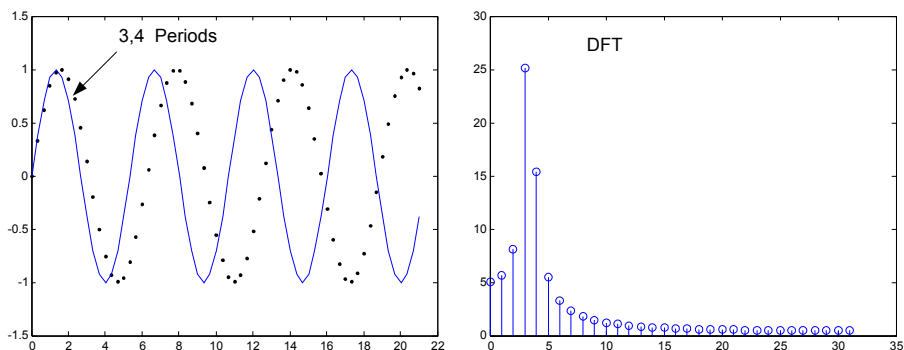


**Figure 5.14** 64-points DFT (left) input sequence, (right) absolute value of DFT the first part of the result

DFT sample e.g. for  $m = 4$  is not equal to zero, because, the sum of products of the input series and the term for frequency analysis at  $m = 4$  is not equal to zero.

That is a leakage, which means every input signal with a frequency not equal to the particular frequency for which the DFT has been computed at the moment, leaks to all other DFT samples.

The leakage effect is inevitable when we compute DFT of a real time series with a finite length.

Knowing the reason and importance of leakage we should consider the minimization possibilities. Try to answer the question how to predict and minimize the leakage effect.

For a real sinusoidal signal with  $k$  periods in  $N$ -points input time sequence, the values of frequency stripes of  $N$ -points DFT as a function of index  $m$  are approximated with the function sinc (sinus cardinalis)

$$X(m) = \frac{N}{2} \cdot \frac{\sin[\pi(k-m)]}{\pi(k-m)} \quad (5.63)$$

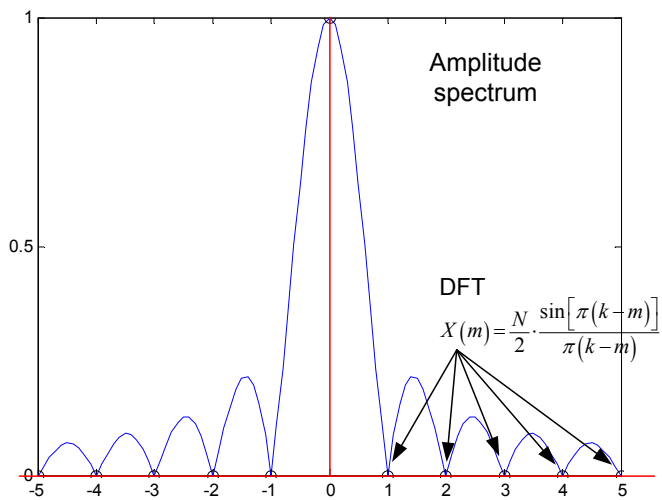
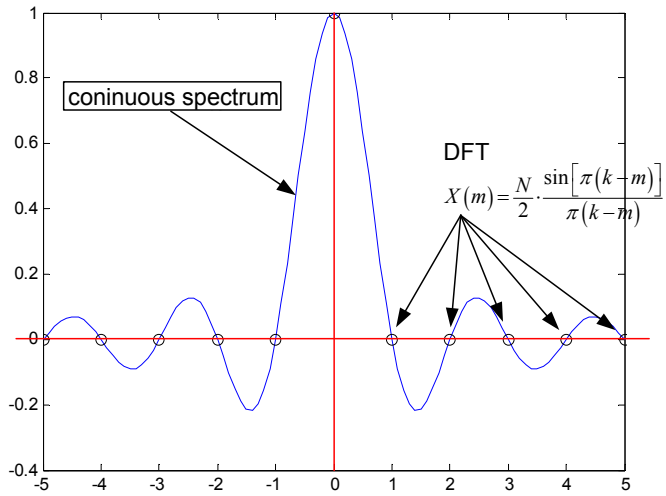


Figure 5.15 DFT for N-point input sequence, containing k periods of real sinusoid: (above) spectrum as a function of m-th sample DFT, (below) amplitude spectrum.

The curve in the picture 5 (above), containing the **main lobe** and periodic picks and valleys known as **side lobes**, may be regarded as N point spectrum of real sinusoidal time series with k full periods in N-points input time interval.

The DFT values are discrete samples, which are on the curves in Figure 5.15, which means DFT will be the sampled version of the continuous spectrum.

If the input signal has exactly an integer number of periods k, the leakage will not appear. The reason for that: the angle in the numerator of equation (5.63) is an integer multiply of  $\pi$ , then the sinus of it is equal to zero.

If the input sinusoid has an integer number of periods in the interval of the length N, then the output values of DFT are located on the continuous spectrum curve exactly on the **zero crossing points** of that curve.

As usual, an example will explain in detail the presented theory.

A real sinusoid with the frequencies 8 kHz, 8,5 kHz, 8,75 kHz, and amplitude 1, has been sampled with the frequency 32kHz. For 32-points DFT the distance between samples is  $f_p/N=1\text{kHz}$ . DFT results are shown in Figure 5.16 and Figure 5.17.

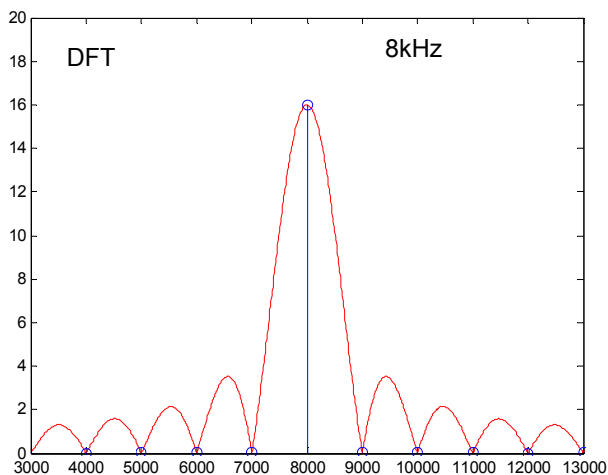


**Figure 5.16** DFT for 32-points sinusoidal input sequence , signal frequency  $f=8\text{kHz}$ ,

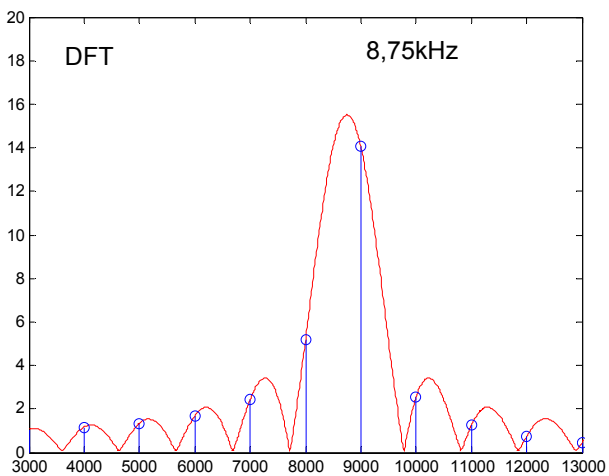
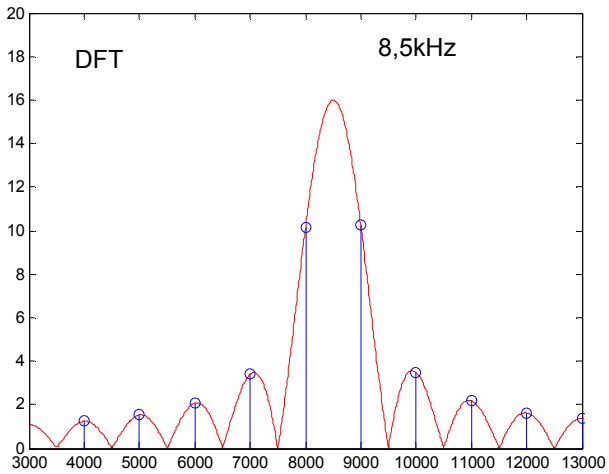


**Figure 5.17** DFT for 32-points sinusoidal input sequence (above) signal frequency  $f=8,5\text{kHz}$ , (below)  $f=8,75\text{kHz}$

The results of DFT leakage are troublesome, because the values of stripes correlated with low amplitude components will be distorted by side lobes of nearby stripes for signals with high amplitude.

An important technique, known as windowing, is the most common way of reducing the leakage. Windowing is reducing the leakage by minimizing the amplitude of side lobes of the function sinc (equation (5.63)).

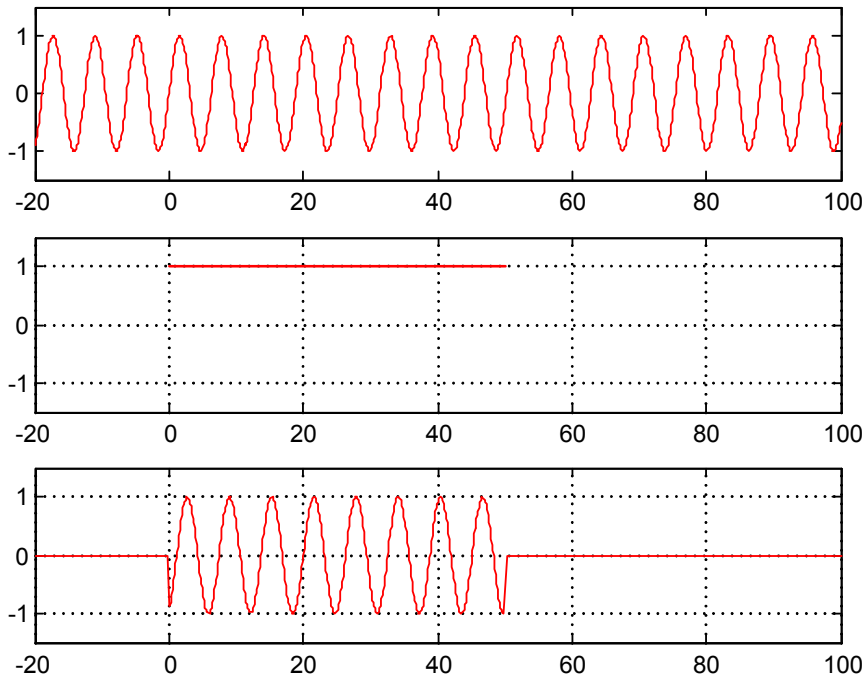


**Figure 5.18** Minimizing discontinuity at the ends of sampling interval: (above) input infinite sinusoid; (middle) a square window adequate to the sampling interval, (bottom) the product of the square window and input sinusoid.

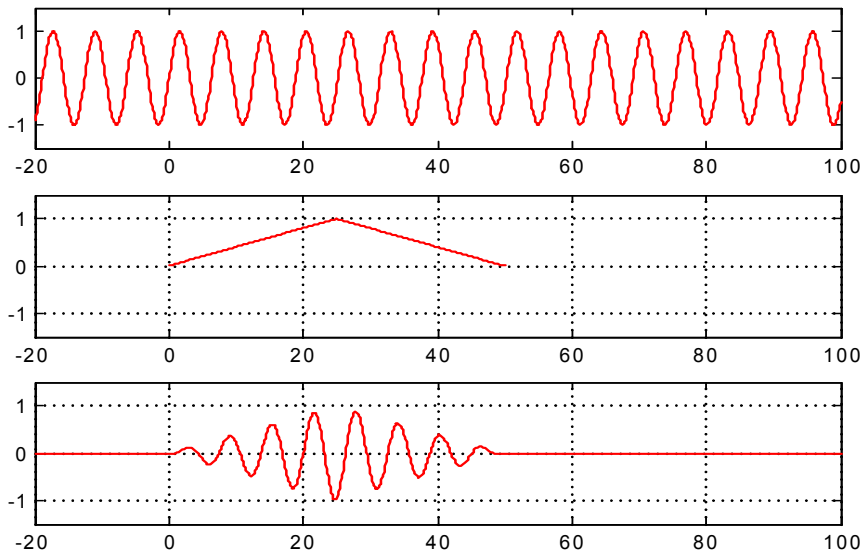


**Figure 5.19** (above) input sinusoid of infinite duration; (middle) triangular window function, (bottom) multiplication of the signal and window

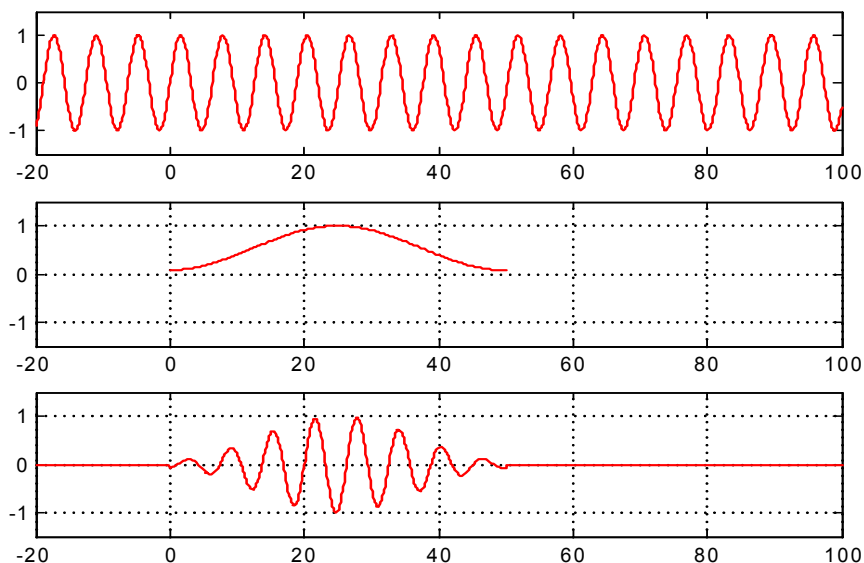


Figure 5.20 (above) input sinusoid of infinite duration (middle) Hanning window, (bottom) multiplication of Hanning window and input sinusoid

Let's consider a signal of infinite duration in time domain shown in Figure 5.18 (above). DFT may be done only on a finite time sequence, as shown in Figure 5.18 (bottom). We may regard DFT of the input signal in Figure 5.18 (bottom) as DFT of the product of infinite input signal from Figure 5.18 (above) and a square window with the amplitude 1 on Figure 5.18 (middle).

Every time, when computing DFT of a finite time series (bottom in Figure), by default we multiply the sequence in sampling interval by a window of ones and other values by zeros. As it turns out, the shape of the function  $\text{sinc} = \sin(x)/x$  is caused by the square window, because the DFT of a square window is a sinc function.

**To minimize the leakage effect caused by the side lobes we must minimize their amplitudes by applying other windows than a square one.**

Imagine that we have multiplied the input signal from Figure 5.19 (above) by a triangular window from Figure 5.19 (middle), in order to obtain a windowed signal shown in picture Figure 5.19 (bottom).

When you look at the Figure 5.19, you notice that the values of the final input signal are equal on both sides of the sampling interval. Reduced discontinuity decreases the level of



relatively high frequency components in the whole DFT values set. That means, the values of side lobes have reduced amplitude due to the application of a triangle window.

There are other window types, which reduce the leakage even better, than the triangle window such as Hanning window form Figure 5.20 (middle). Multiplication of the window in Figure 5.20 (middle) by the input sequence gives us the signal shown in Figure 5.20 (bottom), being the final input for DFT.

### 5.8.Windows types and their properties

To minimize the leakage effect different types of windows are in use.

Assuming, that N original samples of the input signal are indexed by n, where  $0 \leq n \leq N-1$ , we assign N coefficients of the window as w(n), which means, the input sequence x(n) is multiplied by the window w(n), before we start DFT. Therefore DFT  $X_w(m)$  of the windowed input signal x(n) has the form:

$$X_w(m) = \sum_{n=0}^{N-1} w(n) \cdot x(n) e^{j2\pi m \frac{n}{N}} \quad (5.64)$$

- square window also called **boxcar**

$$w(n) = 1, \text{ for } n = 0, 1, 2, \dots, N-1 \quad (5.65)$$

- triangle window (similar to Barletta and Parzen windows)

$$w(n) = \begin{cases} \frac{n}{N/2}; n = 0, 1, 2, \dots, N/2 \\ 2 - \frac{n}{N/2}; n = N/2 + 1, N/2 + 2, \dots, N-1 \end{cases} \quad (5.66)$$

- Hanning window (called also lifted cosinus, Hanna or von Hanna)

$$w(n) = \frac{1}{2} - \frac{1}{2} \cos\left(2\pi \frac{n}{N}\right), \quad n = 0, 1, 2, \dots, N-1 \quad (5.67)$$

- Hamming window

$$w(n) = 0,54 - 0,46 \cos\left(2\pi \frac{n}{N}\right); n = 0, 1, 2, \dots, N-1 \quad (5.68)$$

The spectrum of a square window is a measure to evaluate and compare different types of windows.

There is a definition for a logarithmic amplitude response which helps to normalize and compare spectra of various windows.

The width of main lobes of various windows degrades the spectral resolution of windowed DFT almost twice. However, the advantages of suppressing leakage overweight the worsening of spectral resolution

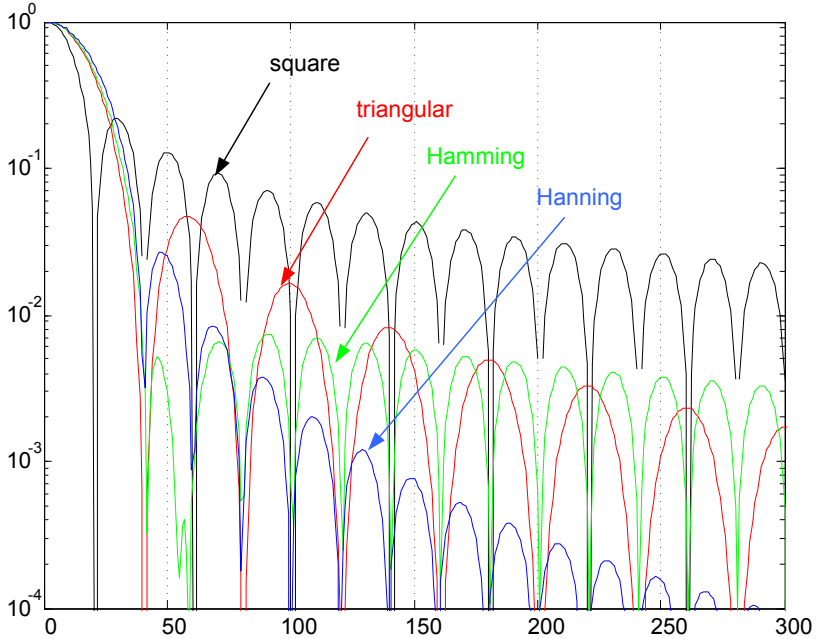


**Figure 5.21** Absolute values of window responses in normalized logarithmic scale

We notice a reduction of first side lobe and drastic reduction of further lobes in Hanning window. Hamming window has even a smaller value of the first side lobe, but the further lobes do not increase as efficiently as Hanning.

That means, the leakage three or four stripes away from main stripe is smaller for Hamming window than for Hanning. But the leakage further away shows an opposite dependence.

If we apply the Hanning window to the example of 3.4 periods in sampling interval, we obtain DFT output values for this windowed signal along with the results for square window. See

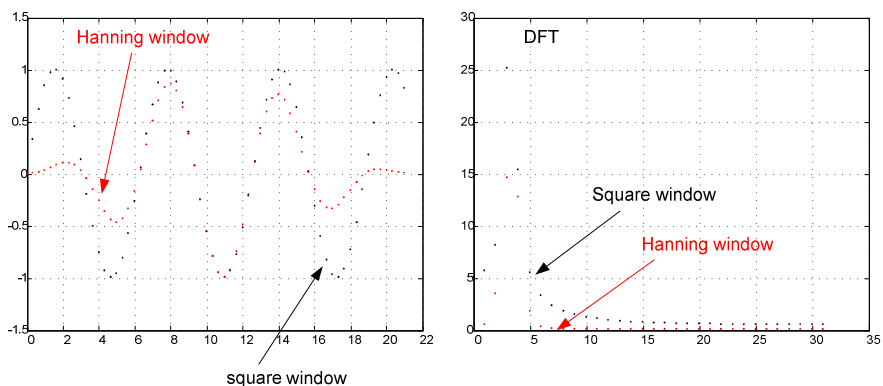


Figure 5.22.

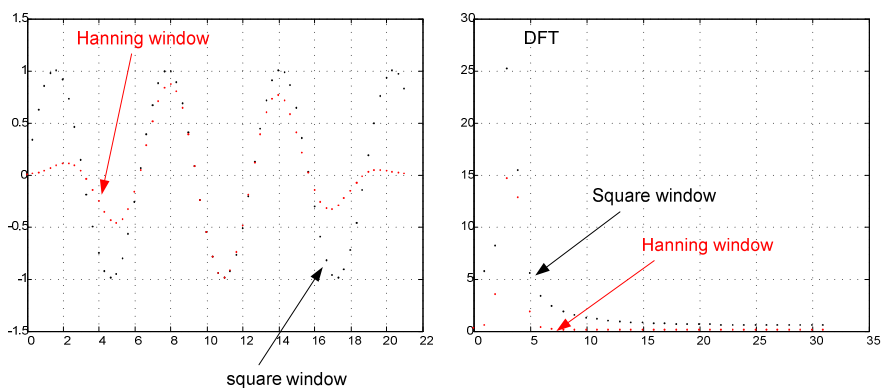


Figure 5.22 Comparison of DFT results for square and Hanning windows

As awaited, the amplitude spectrum for Hanning window is brighter and has a lower maximal value, but the leakage of side lobes is significantly smaller in comparison to the leakage of square window.

Therefore, we may say that the choice of a window is a compromise between the brightening of the main lobe, value of the first lobe and the decrease rate of side lobes with increasing frequency. The application of a certain window depends on a particular situation.

### 5.9. Resolution of the DFT, filling with zeros, sampling in the frequency domain

One of the popular methods of improving frequency resolution of DFT is a method called **zero filling**.

This process requires an addition of zero samples to the original input sequence in order to increase the number of input samples.

Sampling a function continuous in time domain, having a continuous Fourier transform, and afterwards computing DFT from these samples, we see that this DFT gives us sampled approximation of the continuous Fourier transform in frequency domain.

**We may assume that the more samples in the DFT, the better the approximation of the continuous transform is.**

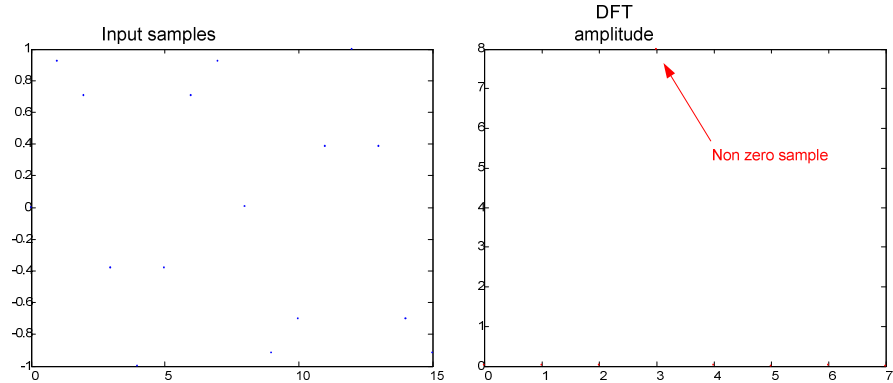


Figure 5.23 Sampling of DFT in frequency domain: 16 samples of input data and  $N = 16$ ;

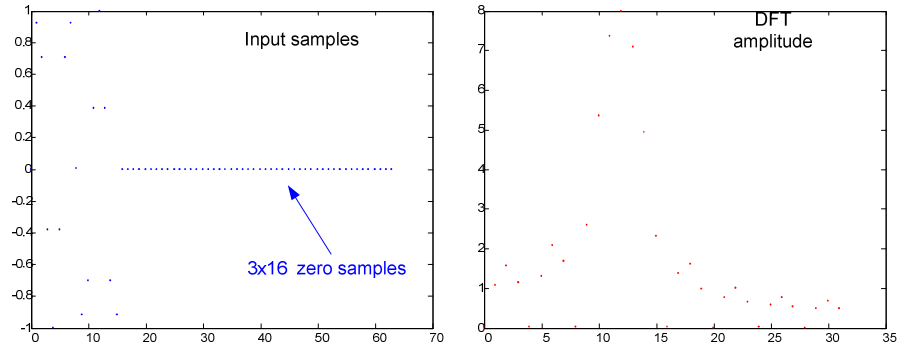
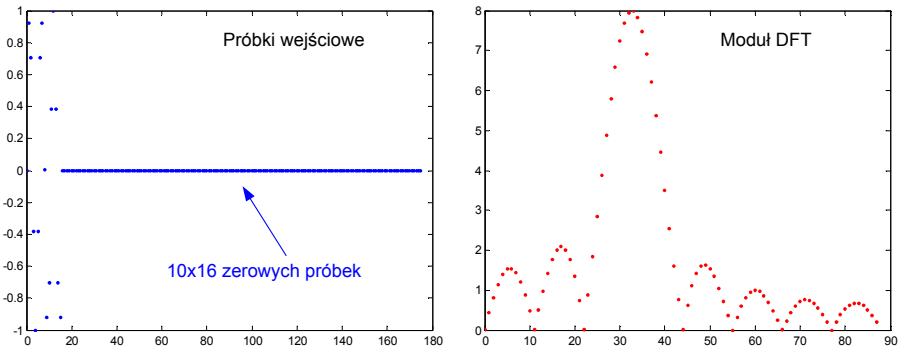


Figure 5.24 Sampling of DFT in frequency domain: 16 samples of input data, 3x16 added zeros



**Figure 5.25 Sampling of DFT in frequency domain: 16 samples of input data, 10x16 added zeros**

Adding zeros to the input sequence improves the spectral resolution of DFT, but there is a practical border determining how much we can gain through adding zero samples.

In practice, if we want to introduce both zero filling and windowing, we should be careful **not to apply a window to the whole signal after addition of zeros.**

## 5.10. Literature

- [1] Angelo Baghini, Handbook of power quality, Wiley, Chichester, 2008, pp. 187-259
- [2] R. G. Lyons Understanding digital signal processing Addison Wesley Longman, 1997
- [3] S.J. Orfandis, Introduction to Signal Processing, Prentce Hall, 1996
- [4] A. V. Oppenheim, R. W. Schaffer, Discrete-Time Signal Processing, Prentce Hall, 1999

## **6. Symmetrical components for current and voltage unbalance assessment**

Three phase voltages and currents should be symmetrical during the operation of a power system. Therefore, the voltages at generators taps are of the same magnitude and displaced equally to each other at an angle of 120 degrees. Components of the power system (lines, transformers, switch gears, etc. ) are designed and build in order to guarantee linearity and symmetry. The greatest difficulty brings the appropriate connection of single phase loads differing significantly in operational characteristics. Attention must be paid to equal distribution of them.

In everyday practice it is hardly possible to obtain an ideal voltage symmetry at all nodes of the electrical sources. Similarly, currents are very often unsymmetrical.

The main sources of unbalance in voltage and current are low-voltage and medium voltage one phase appliances. The operation of single-phase loads results in various currents in all feeding lines. As a consequence, unequal voltage drops appear on system nodes. An arc furnace is an example of a three-phase load introducing unbalance conditions. The characteristic of a melting process evolves different impedances of high current paths.

System components, especially overhead lines contribute to the unbalance phenomenon. The geometry of most popular electrical masts forces an unequal position of the conductors in relation to each other and to the earth.

Faults, excluding three phase balanced faults, and other abnormal operation condition contribute additionally to the levels of unbalance.

In this chapter the mathematical description of the unbalance phenomena will be presented. Unbalance factors and border values given in standards will be presented.

The theoretical ideas of the chapter are from [7].

## 6.1. Mathematical Background

The concluding idea derived from a three phase system analysis suggests that it is much easier to deal with a symmetrical system than with a nonsymmetrical one. Computation of currents, voltages and powers is conceptually less demanding and more stride forward.

### 6.1.1. Complex transformation parameter $a$

Generally, the analysis of an unsymmetrical electrical system may be transformed into an analytical problem of a special set of symmetrical systems. The superposition of results gives the original currents and voltages.

In other words, the symmetrical component method is basically a modelling technique that permits a systematic analysis and design of three phase systems. Decoupling a detailed three phase network into three simpler sequence networks reveals complicated phenomena in more simplistic terms. Sequence network results can then be superimposed to obtain three phase results. See Figure 6.1.

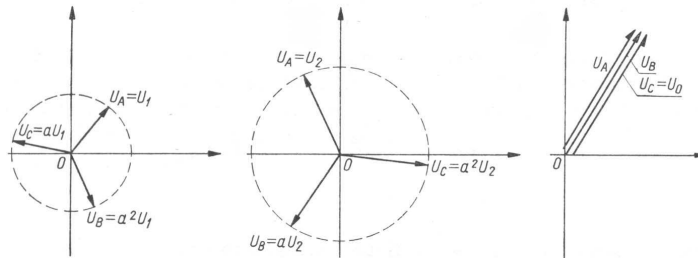


Figure 6.1 Positive sequence, negative sequence and zero sequence voltage systems

To express quantities algebraically, the complex operator  $a$  is used. This denotes a phase shift by  $+120^\circ$  and multiplication by unit magnitude.

$$a = e^{j120^\circ} = \cos 120^\circ + j \sin 120^\circ = -0.5 + j \frac{\sqrt{3}}{2} \quad (6.1)$$

therefore

$$\begin{cases} a^2 = -0.5 - j \frac{\sqrt{3}}{2} \\ a^3 = 1 \end{cases} \quad (6.2)$$

Geometric addition of three vectors  $a$   $a^2$   $a^3$  gives us an equilateral triangle

$$1 + a + a^2 = 0 \quad (6.3)$$

Basic algebraic dependences for the  $a$  operator are given in expressions

$$a - a^2 = \left(-0,5 + j\frac{\sqrt{3}}{2}\right) - \left(-0,5 - j\frac{\sqrt{3}}{2}\right) = j\sqrt{3} \quad (6.4)$$

and

$$1 - a = ja^2\sqrt{3} \quad (6.5)$$

$$1 - a^2 = -ja\sqrt{3} \quad (6.6)$$

Equations (6.4) to (6.6) have an geometrical representation on the complex numbers plane.

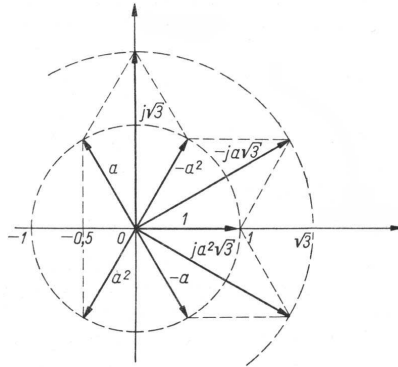


Figure 6.2 geometrical representation of algebraic operations on vectors  $a$   $a^2$

### 6.1.2. Symmetrical components definition

Applying the  $a$  operator of the three voltages may be resolved into three sets of sequence components; according to

$$shift = -k \frac{2\pi}{n} \quad (6.7)$$

where  $n$  is the number of phases and  $k=0,1,2$ . (Figure 6.1)

- Positive Sequence

The voltage in the subsequent phase has a negative displacement of 120 degree

$$(shift = -1 \frac{2\pi}{3})$$

$$\begin{cases} u_{L1} = U_1 \sin(\omega t) \\ u_{L2} = U_1 \sin(\omega t - 120^\circ) \\ u_{L3} = U_1 \sin(\omega t - 240^\circ) \end{cases} \quad (6.8)$$



$$\begin{cases} \underline{U}_{L1} = \underline{U}_1 \\ \underline{U}_{L2} = a^2 \underline{U}_1 \\ \underline{U}_{L3} = a \underline{U}_1 \end{cases} \quad (6.9)$$

- Negative Sequence

The voltage in the subsequent phase has a negative displacement of 240 degree

$$(shift = -2\frac{2\pi}{3})$$

$$\begin{cases} u_{L1} = U_2 \sin(\omega t) \\ u_{L2} = U_2 \sin(\omega t - 240^\circ) \\ u_{L3} = U_2 \sin(\omega t - 120^\circ) \end{cases} \quad (6.10)$$

$$\begin{cases} \underline{U}_{L1} = \underline{U}_2 \\ \underline{U}_{L2} = a \underline{U}_2 \\ \underline{U}_{L3} = a^2 \underline{U}_2 \end{cases} \quad (6.11)$$

- Zero Sequence

The voltage consists of three phasors with equal magnitudes and with zero phase

displacement between them ( $shift = -3\frac{2\pi}{3}$ ).

$$\begin{cases} u_{L1} = U_0 \sin(\omega t) \\ u_{L2} = U_0 \sin(\omega t) \\ u_{L3} = U_0 \sin(\omega t) \end{cases} \quad (6.12)$$

$$\begin{cases} \underline{U}_{L1} = \underline{U}_0 \\ \underline{U}_{L2} = \underline{U}_0 \\ \underline{U}_{L3} = \underline{U}_0 \end{cases} \quad (6.13)$$

The load (Figure 6.3) is powered in the same manner, regardless of the switch position. A cascade connection of three symmetrical generators (zero, positive and negative sequence) constitutes an intuitive equivalent of an unsymmetrical generator G.

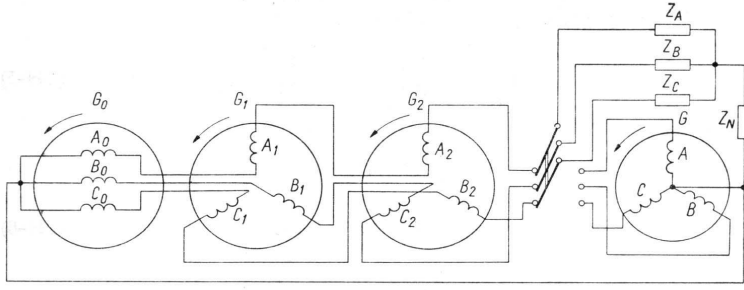


**Figure 6.3 Representation of an unsymmetrical generator G with a cascade connection of zero sequence generator  $G_0$ , positive sequence generator  $G_1$  and negative sequence generator  $G_2$**

### 6.1.3. Symmetrical components of voltage, current, impedance and admittance

Mathematically, the idea presented in Figure 6.3 is expressed by a set of equations

$$\begin{cases} U_{L1} = U_0 + U_1 + U_2 \\ U_{L2} = U_0 + a^2 U_1 + a U_2 \\ U_{L3} = U_0 + a U_1 + a^2 U_2 \end{cases} \quad (6.14)$$

or in matrix notation

$$\begin{bmatrix} U_{L1} \\ U_{L2} \\ U_{L3} \end{bmatrix} = \begin{bmatrix} 1 & 1 & 1 \\ 1 & a^2 & a \\ 1 & a & a^2 \end{bmatrix} \begin{bmatrix} U_0 \\ U_1 \\ U_2 \end{bmatrix} \quad (6.15)$$

S - matrix is called a symmetrical components transformation matrix

$$\mathbf{S} = \begin{bmatrix} 1 & 1 & 1 \\ 1 & a^2 & a \\ 1 & a & a^2 \end{bmatrix} \quad (6.16)$$

The determinant of the S matrix

$$\det \mathbf{S} = 3(a - a^2) = 3j\sqrt{3} \quad (6.17)$$

is non zero, thus S is a nonsingular matrix (it is invertible).

Computing the reverse transformation we obtain

$$\begin{bmatrix} U_0 \\ U_1 \\ U_2 \end{bmatrix} = \frac{1}{3} \begin{bmatrix} 1 & 1 & 1 \\ 1 & a & a^2 \\ 1 & a^2 & a \end{bmatrix} \begin{bmatrix} U_{L1} \\ U_{L2} \\ U_{L3} \end{bmatrix} \quad (6.18)$$

writing down (6.18) similarly as (6.14) we get

$$\begin{cases} U_0 = \frac{1}{3}(U_{L1} + U_{L2} + U_{L3}) \\ U_1 = \frac{1}{3}(U_{L1} + a^2U_{L2} + aU_{L3}) \\ U_2 = \frac{1}{3}(U_{L1} + aU_{L2} + a^2U_{L3}) \end{cases} \quad (6.19)$$

The zero sequence, positive sequence and negative sequence components are obtained directly from phase voltages and contain exactly the same information.

Transformation procedure may be also applied for three phase currents

$$\begin{bmatrix} I_{L1} \\ I_{L2} \\ I_{L3} \end{bmatrix} = \begin{bmatrix} 1 & 1 & 1 \\ 1 & a^2 & a \\ 1 & a & a^2 \end{bmatrix} \begin{bmatrix} I_0 \\ I_1 \\ I_2 \end{bmatrix} \quad (6.20)$$

and reverse transformation

$$\begin{bmatrix} I_0 \\ I_1 \\ I_2 \end{bmatrix} = \frac{1}{3} \begin{bmatrix} 1 & 1 & 1 \\ 1 & a & a^2 \\ 1 & a^2 & a \end{bmatrix} \begin{bmatrix} I_{L1} \\ I_{L2} \\ I_{L3} \end{bmatrix} \quad (6.21)$$

Transformation of currents and voltages are compactly given in matrix notation

$$\mathbf{U} = \mathbf{S}\mathbf{U}_s \quad \mathbf{U}_s = \frac{1}{3}\mathbf{S}_1\mathbf{U} \quad \mathbf{I} = \mathbf{S}\mathbf{I}_s \quad \mathbf{I}_s = \frac{1}{3}\mathbf{S}_1\mathbf{I} \quad (6.22)$$

where

$$\mathbf{S}\mathbf{S}_1 = 3 \cdot \mathbf{I} \quad (6.23)$$

for impedances and admittances we have similar matrix notation

$$\mathbf{Z} = \mathbf{S}\mathbf{z}_s \quad \mathbf{z}_s = \frac{1}{3}\mathbf{S}_1\mathbf{Z} \quad \mathbf{Y} = \mathbf{S}\mathbf{y}_s \quad \mathbf{y}_s = \frac{1}{3}\mathbf{S}_1\mathbf{Y} \quad (6.24)$$

#### 6.1.4. Basic properties of symmetrical components

- Three phase source or load connected in wye and without a fourth zero line indicates no zero sequence current component  $I_0 = 0$ . It is a consequence of Kirchoff law for the node of wye connection  $I_0 = \frac{1}{3}(I_{L1} + I_{L2} + I_{L3})$ .
- In a three phase system of voltages and currents where only one voltage or current is different from zero the three symmetrical components are equal and amount exactly

to  $\frac{1}{3}$  of the line voltage or current. For  $I_{L1} \neq 0$  and  $I_{L2} = 0, I_{L3} = 0$  we get

$$I_0 = I_1 = I_2 = \frac{1}{3} I_{L1}.$$

- In a three phase system of voltages and currents where only one voltage or current is exactly zero the geometrical sum of three symmetrical components is zero  $I_0 + I_1 + I_2 = 0$ .
- In a three phase system of voltages with or without neutral the zero sequence component of L-L voltage is zero  $U_0 = 0$ . It is a consequence of a fact that the geometrical sum of three L-L voltages is zero.
- In the three phase delta connected source or load windings can circulate the zero sequence current component. It is not present in the line currents.

## 6.2. Ohm's law for symmetrical components

A three phase unsymmetrical load is given in Figure 6.4. Starting from the three equations defining the relation between voltage and current (6.25) we formulate the Ohm's law in a matrix form

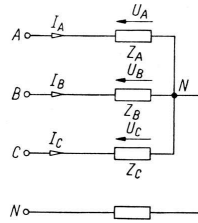


Figure 6.4 Three phase unsymmetrical load

$$\begin{cases} U_A = Z_A I_A \\ U_B = Z_B I_B \\ U_C = Z_C I_C \end{cases} \quad (6.25)$$

$$\begin{bmatrix} U_A \\ U_B \\ U_C \end{bmatrix} = \begin{bmatrix} Z_A & 0 & 0 \\ 0 & Z_B & 0 \\ 0 & 0 & Z_C \end{bmatrix} = \begin{bmatrix} I_A \\ I_B \\ I_C \end{bmatrix} \quad (6.26)$$

where  $\mathbf{Z}'$  is the diagonal impedance matrix

$$\mathbf{Z}' = \begin{bmatrix} Z_A & 0 & 0 \\ 0 & Z_B & 0 \\ 0 & 0 & Z_C \end{bmatrix} \quad (6.27)$$

using the matrix notation

$$\mathbf{U} = \mathbf{Z}'\mathbf{I} \quad (6.28)$$

Substituting  $\mathbf{U} = \mathbf{S}\mathbf{U}_s$   $\mathbf{I} = \mathbf{S}\mathbf{I}_s$  and multiplying both sides of (6.28) by  $\mathbf{S}^{-1}$  we obtain

$$\mathbf{U}_s = \mathbf{S}^{-1}\mathbf{Z}'\mathbf{S}\mathbf{I}_s \quad (6.29)$$

The Ohm's law for symmetrical components

$$\mathbf{U}_s = \mathbf{z}'\mathbf{I}_s \quad (6.30)$$

where

$$\mathbf{z}'_s = \mathbf{S}^{-1}\mathbf{Z}'\mathbf{S} \quad (6.31)$$

after evaluation of (6.31) we get

$$\mathbf{z}' = \begin{bmatrix} z_0 & z_2 & z_1 \\ z_1 & z_0 & z_2 \\ z_2 & z_1 & z_0 \end{bmatrix} \quad (6.32)$$

Finally, a formula (6.25) corresponds with a set of scalar equations for symmetrical components

$$\begin{cases} U_0 = z_0 I_0 + z_2 I_1 + z_1 I_2 \\ U_1 = z_1 I_0 + z_0 I_1 + z_2 I_2 \\ U_2 = z_2 I_0 + z_1 I_1 + z_0 I_2 \end{cases} \quad (6.33)$$

Computation of every symmetrical component of voltage requires all symmetrical components of the current.

Similar concepts may be developed for admittances, therefore we rewrite (6.25) introducing admittances

$$\begin{cases} I_A = Y_A U_A \\ I_B = Y_B U_B \\ I_C = Y_C U_C \end{cases} \quad (6.34)$$

and apply the same procedure described above, finally obtaining

$$\begin{cases} I_0 = y_0 U_0 + y_2 U_1 + y_1 U_2 \\ I_1 = y_1 U_0 + y_0 U_1 + y_2 U_2 \\ I_2 = y_2 U_0 + y_1 U_1 + y_0 U_2 \end{cases} \quad (6.35)$$

Computation of every symmetrical component of current requires all symmetrical components of the voltage.

Generally, the symmetrical component admittance is not an inverse of impedance and is given by

$$\begin{cases} y_0 = \frac{z_0^2 - z_1 z_2}{z_0^3 + z_1^3 + z_2^3 - 3z_0 z_1 z_2} \\ y_1 = \frac{z_2^2 - z_0 z_1}{z_0^3 + z_1^3 + z_2^3 - 3z_0 z_1 z_2} \\ y_2 = \frac{z_1^2 - z_2 z_0}{z_0^3 + z_1^3 + z_2^3 - 3z_0 z_1 z_2} \end{cases} \quad (6.36)$$

### 6.3. Kirchhoff's current law and voltage law for symmetrical components

A three phase wye – wye connected system is shown in Figure 6.5. Kirchhoff's current law is a linear relationship between currents. The sum of currents flowing into  $N_1$  node is equal to the sum of currents flowing out of that node. The transformation of current into symmetrical components (6.21) is also a linear operation. Therefore, the same relationship is valid for currents transformed (or not) into symmetrical components. No further considerations are needed.

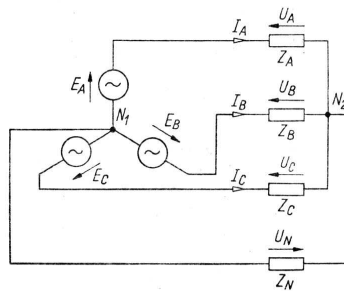


Figure 6.5 A three phase wye - wye connected system.

Kirchhoff's voltage law requires more attention. We start with a selection of three meshes, each consisting from the phase line and neutral. The voltage in every closed loop must be equal to zero, therefore

$$E_A = U_A + U_N \quad E_B = U_B + U_N \quad E_C = U_C + U_N \quad (6.37)$$

The value of source voltage is equal to a voltage drop on phase impedance and the neutral. The first term will be rewritten with accordance to (6.25), corresponding symmetrical components are given by (6.33). The voltage drop on the neutral can be rewritten into

$$U_N = Z_N(I_A + I_B + I_C) = 3Z_N I_0 \quad (6.38)$$

Equation (6.38) includes only one symmetrical component.

Finally, the Kirchhoff's voltage low for symmetrical components is given by

$$\begin{bmatrix} E_0 \\ E_1 \\ E_2 \end{bmatrix} = \begin{bmatrix} z_0 + 3Z_N & z_2 & z_1 \\ z_1 & z_0 & z_2 \\ z_2 & z_1 & z_0 \end{bmatrix} \begin{bmatrix} I_0 \\ I_1 \\ I_2 \end{bmatrix} \quad (6.39)$$

in compact form

$$\mathbf{E}_s = \mathbf{z}_s' \mathbf{I}_s \quad (6.40)$$

where

$$\mathbf{z}_s' = \begin{bmatrix} z_0 + 3Z_N & z_2 & z_1 \\ z_1 & z_0 & z_2 \\ z_2 & z_1 & z_0 \end{bmatrix} \quad (6.41)$$

Comparing the square matrices  $\mathbf{z}_s$  and  $\mathbf{z}_s'$  in the notations of Ohm's law and Kirchhoff's law we see that there is only one different entry at (1,1). Therefore, there is apparent equality between the positive and negative symmetrical components of the source and load voltages  $E_1 = U_1$   $E_2 = U_2$ .

Especially for a symmetrical load ( $Z_A = Z_B = Z_C$ ) we observe a significant simplification. The positive and negative symmetrical component of impedances is zero and we have only  $z_0 = Z_A$ . The matrix equation (6.39) can be rewritten to

$$\begin{cases} E_0 = (z_0 + 3Z_N)I_0 \\ E_1 = z_0 I_1 \\ E_2 = z_0 I_2 \end{cases} \quad (6.42)$$

#### 6.4. Filtering of symmetrical components

Filters of symmetrical components are used in order to deliver adequate values for further processing. Basic ideas and concepts of filtering are presented below.

### 6.4.1. Zero sequence filtering

In a three phase system the neutral wire is conducting a current three times higher than the zero component. Therefore, an ammeter indicates  $3I_0$  (Figure 6.6). There is no need for further filtering. However, in a network without neutral wire three current transformers are needed (Figure 6.6). The ammeter shows  $3kI_0$ .

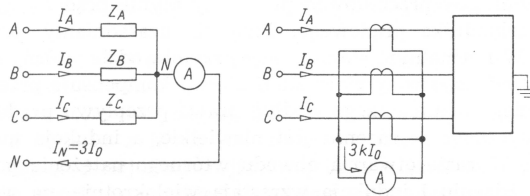


Figure 6.6 Zero sequence component filters in networks with neutral (left) and without neutral (right)

Examples of a voltage symmetrical component filter are shown in Figure 6.7.

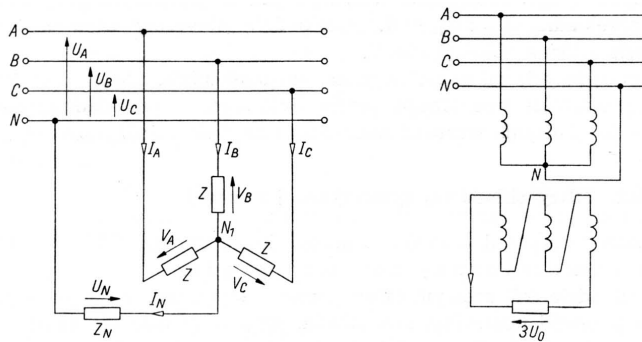


Figure 6.7 voltage symmetrical components filters

In order to filter zero sequence component a wye – connected identical impedances  $Z$  are needed (Figure 6.7 left). The artificial neutral point  $N_1$  is connected with neutral wire via  $Z_N$  impedance. According to the symbols in Figure 6.7 we get

$$I_A + I_B + I_C = I_N \quad (6.43)$$

the sum of voltages may be therefore expressed as

$$V_A + V_B + V_C = Z(I_A + I_B + I_C) = ZI_N \quad (6.44)$$

rewriting formula (6.44) we obtain an expression for the voltage across neutral wire

$$U_N = Z_N I_N = \frac{Z_N}{Z} (V_A + V_B + V_C) \quad (6.45)$$

The line voltages



$$\begin{aligned}
U_A &= V_A + U_N \\
U_B &= V_B + U_N \\
U_C &= V_C + U_N
\end{aligned} \tag{6.46}$$

after summation yield

$$U_A + U_B + U_C = V_A + V_B + V_C + 3U_N \tag{6.47}$$

so, the zero component is given by

$$U_0 = \frac{1}{3}(U_A + U_B + U_C) = \frac{1}{3}(V_A + V_B + V_C) + U_N \tag{6.48}$$

Comparing (6.44) and (6.48) we can express  $U_N$  voltage as a function of the zero sequence component

$$U_N = \frac{3Z_N}{Z + 3Z_N} U_0 \tag{6.49}$$

and the current in the neutral wire

$$I_N = \frac{U_N}{Z_N} = \frac{3}{Z + 3Z_N} U_0 \tag{6.50}$$

is proportional to the zero sequence component in the voltage.

Figure 6.7 (right) shows an example of a zero sequence filter where the voltage is measured on the secondary side of a wye–delta measuring transformer. The voltages on the secondary side are  $U_{AB}, U_{BC}, U_{CA}$  therefore the zero sequence component is given by

$$U_0 = \frac{1}{3}(U_{AB} + U_{BC} + U_{CA}) \tag{6.51}$$

#### 6.4.2. Positive and negative sequence components filtering

There are many approaches to the filtering of positive and negative sequence components. In order to illustrate the question, two filters are presented as examples.

**Figure 6.8** shows a three phase line without neutral wire feeding a wye connected load. Two equal measuring transformers are installed in phase A and C. Transformed currents are denoted as  $I_A, I_C$ . Parallel to the current transformers two impedances are connected  $Z_1, Z_2$ , whose values will be determined further on. The secondary circuit is closed via  $Z_f$  impedance representing an ammeter or a transducer leading  $I_f$  current. A brief analysis of the circuit will be presented.

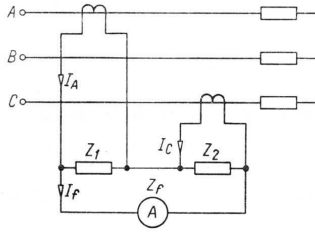


**Figure 6.8 positive and negative sequence component filter for voltage and current**

The sum of voltages in a mesh is given by

$$Z_1(I_A - I_f) + Z_2(I_C - I_f) - Z_f I_f = 0 \quad (6.52)$$

the current  $I_f$  as a function of  $I_A, I_C$  is given by

$$I_f = \frac{Z_1 I_A + Z_2 I_C}{Z_1 + Z_2 + Z_f} \quad (6.53)$$

In a three phase system without neutral the zero sequence is not present, therefore

$$\begin{aligned} I_A &= I_1 + I_2 \\ I_C &= aI_1 + a^2 I_2 \end{aligned} \quad (6.54)$$

Then, we apply (6.54) to (6.53) and obtain an expression for filter current  $I_f$  as a function of the positive  $I_1$  and negative  $I_2$  sequence component

$$I_f = \frac{(Z_1 + aZ_2)I_1 + (Z_1 + a^2 Z_2)I_2}{Z_1 + Z_2 + Z_f} \quad (6.55)$$

And now there are two approaches.

- Measuring positive sequence component in the current:

where the condition for correct measurement is

$$Z_1 + a^2 Z_2 = 0 \quad (6.56)$$

and also

$$Z_1 = -a^2 Z_2 \quad (6.57)$$

One of the solutions is  $Z_2 = R$  than  $Z_1 = e^{j60} R = \frac{R}{2}(1 + j\sqrt{3})$ . The resistance of the coil is

$R_1 = \frac{R}{2}$  and the reactance  $X_1 = \frac{R}{2}\sqrt{3}$ .

- Measuring negative sequence component in the current:

where the condition for correct measurement is

$$Z_1 + aZ_2 = 0 \quad (6.58)$$

and also

$$Z_1 = -aZ_2 \quad (6.59)$$

One of the solutions is  $Z_1 = R$  than  $Z_2 = e^{j60}R = \frac{R}{2}(1 + j\sqrt{3})$ . The resistance of the coil is  $R_2 = \frac{R}{2}$  and reactance  $X_2 = \frac{R}{2}\sqrt{3}$ .

Figure 6.9 shows a circuit for the measurement of positive and negative sequence components in the voltage. The three phase system may be with or without the neutral wire. Two identical measurement voltage transformers give voltages between phase A and B and phase B and C, denoted with  $U_{AB}, U_{BC}$ . Two impedances  $Z_1, Z_2$ , whose values will be determined further on, are connected in series with the measurement transformers. The two secondary meshes have a common branch denoted as  $Z_f$  impedance representing an ammeter or transducer leading  $I_f$  current.

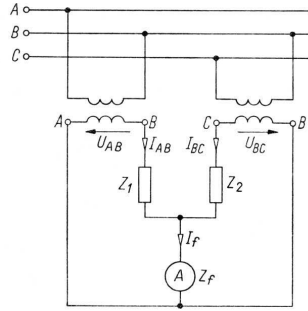


**Figure 6.9 positive and negative sequence component filter of the voltage**

The voltages in the two meshes in Figure 6.9 are given by

$$\left. \begin{aligned} Z_1 I_{AB} + Z_f I_f &= U_{AB} \\ Z_2 I_{BC} + Z_f I_f &= U_{BC} \end{aligned} \right\} \quad (6.60)$$

The current  $I_f$  is also a function of the line to line voltages

$$I_f = \frac{Z_2 U_{AB} + Z_1 U_{BC}}{Z_1 Z_2 + Z_2 Z_f + Z_f Z_1} \quad (6.61)$$

A symmetrical component of line to line voltages is equal to zero. Therefore

$$\left. \begin{aligned} U_{AB} &= U_1 + U_2 \\ U_{BC} &= a^2 U_1 + a U_2 \end{aligned} \right\} \quad (6.62)$$

substituting (6.62) to (6.51) we obtain an expression of the filter current  $I_f$  as a function of symmetrical components  $U_1, U_2$  of the line to line voltages.

$$I_f = \frac{Z_2 + a^2 Z_1}{Z_1 Z_2 + Z_2 Z_f + Z_f Z_1} U_1 + \frac{Z_2 + a Z_1}{Z_1 Z_2 + Z_2 Z_f + Z_f Z_1} U_2 \quad (6.63)$$

And now there are two approaches.

- Measuring of a positive sequence component in the line to line voltage:

The condition for correct measurement is

$$Z_2 + a Z_1 = 0 \quad (6.64)$$

also

$$Z_2 = -a^2 Z_1 \quad (6.65)$$

One of the solutions is  $Z_2 = R$  than  $Z_1 = e^{j60} R = \frac{R}{2}(1 + j\sqrt{3})$ . The resistance of the coil is

$$R_1 = \frac{R}{2} \text{ and the reactance } X_1 = \frac{R}{2}\sqrt{3}.$$

- Measuring of a negative sequence component in the line to line voltage:

The condition for correct measurement is

$$Z_2 + a^2 Z_1 = 0 \quad (6.66)$$

and also

$$Z_2 = -a Z_1 \quad (6.67)$$

One of the solutions is  $Z_1 = R$  than  $Z_2 = e^{j60} R = \frac{R}{2}(1 + j\sqrt{3})$ . The resistance of the coil is

$$R_2 = \frac{R}{2} \text{ and reactance } X_2 = \frac{R}{2}\sqrt{3}.$$

Substituting the values proposed above into (6.63) we obtain simplified expressions for  $I_f$ .

A positive sequence component

$$I_f = \frac{ja^2\sqrt{3}}{Z_1 - ja\sqrt{3}Z_f} U_1 \quad (6.68)$$

A negative sequence component

$$I_f = \frac{ja\sqrt{3}}{Z_1 + ja^2\sqrt{3}Z_f}U_2 \quad (6.69)$$

## 6.5. Determination of unbalance with accordance to international standards

Symmetrical components are primarily used for the analysis of different types of faults. Line to line faults with and without earth connection, line to earth faults, symmetrical faults, etc. Power quality assessment requires the implementation of symmetrical components for the computation of asymmetry factor, mainly based on [3].

### 6.5.1. Unbalance factor

An unbalance factor “K” stands for the measure of unbalance. It is a ratio of negative and (or) zero sequence component to the positive sequence component. The former is, the negative sequence

$$K_{2U} = \frac{U_2}{U_1} \cdot 100\% \quad (6.70)$$

$$K_{2I} = \frac{I_2}{I_1} \cdot 100\% \quad (6.71)$$

and the latter is the expression for a factor related to zero sequence

$$K_{0U} = \frac{U_0}{U_1} \cdot 100\% \quad (6.72)$$

$$K_{0I} = \frac{I_0}{I_1} \cdot 100\% \quad (6.73)$$

Equations from (6.70) to (6.73) refer only to the main component of the voltage or current. For isolated neutral power networks, the term “asymmetry” is more frequently used, it is defined by the ratio of negative to positive sequence only.

The negative sequence component is transformed by a transformer irrespective of the windings connection, therefore quite important. The zero sequence component is present in low voltage networks, and a delta connected transformer prevents it from transferring into higher voltage network. In this case, the unbalance factor is expressed by phase voltages

$$K_{2U} = \left| \frac{U_A + a^2U_B + aU_C}{U_A + aU_B + a^2U_C} \right| \cdot 100\% \quad (6.74)$$

where applying

$$a + a^2 + 1 = 0 \quad (6.75)$$

we obtain

$$K_{2U} = \left| \frac{U_{AB} - aU_{BC}}{U_{AB} - a^2U_{BC}} \right| \cdot 100\% \quad (6.76)$$

and a similar expression for currents

$$K_{2I} = \left| \frac{I_{AB} - aI_{BC}}{I_{AB} - a^2I_{BC}} \right| \cdot 100\% \quad (6.77)$$

### 6.5.2. Evaluation according to standards

Practically, for the computation of unbalance factor we need three phase voltages or two phase to phase voltages, as in (6.70) to (6.77).

Another approach assumes, that the voltage vector of phase A is located on the real axis. The phase voltages are given then as

$$\begin{aligned} U_A &= U_A \\ U_B &= U_B e^{-j\alpha} \\ U_C &= U_C e^{-j(\alpha+\beta)} \end{aligned} \quad (6.78)$$

where  $\alpha$  is an angle between  $U_A$  and  $U_B$ , and  $\beta$  is an angle between  $U_B$  and  $U_C$ . Both angles can be computed by

$$\alpha = \arccos \left( \frac{U_A^2 + U_B^2 - U_{AB}^2}{2U_A U_B} \right) \quad (6.79)$$

$$\alpha = \arccos \left( \frac{U_A^2 + U_B^2 - U_{AB}^2}{2U_A U_B} \right) \quad (6.80)$$

Standards propose different formulas and levels of acceptance. In IEC 61000-2-12 [5] the formula is given by

$$K_{U2} = \sqrt{\frac{6(U_{AB}^2 + U_{BC}^2 + U_{CA}^2)}{U_{AB} + U_{BC} + U_{CA}}} - 2 \cdot 100\% \quad (6.81)$$

allowed levels are 2% and under special conditions 3%.

The commonly referred standard EN 50160 [66] allows the relative negative sequence value as in (6.70) by maximally 2% of 95% of the time.

## 6.6.Literature

- [1] Charles L. Fortescue, "Method of Symmetrical Co-Ordinates Applied to the Solution of Polyphase Networks". Presented at the 34th annual convention of the AIEE (American Institute of Electrical Engineers) in Atlantic City, N.J. on 28 July 1918. Published in: AIEE Transactions, vol. 37, part II, pages 1027-1140 (1918)
- [2] John Horak "A Derivation of Symmetrical Component Theory and Symmetrical Component Networks", Basler Electric Company, Presented before the 59th Annual Georgia Tech Protective Relaying Conference, Atlanta, Georgia, April 27-29, 2005
- [3] Angelo Baggini "Handbook of Power Quality", John Wiley & Sons Ltd, The Atrium, Southern Gate, Chichester, West Sussex PO19 8SQ. England, 2008, pp. 164-185
- [4] J. Lewis Blackburn, "Symmetrical components for power systems engineering", Marcel Dekker Inc., 270 Madison Avenue, New York, 1993, pp. 39-55
- [5] IEC 61000-2-12, Electromagnetic Compatibility – Part 2: Environment – Section 12: Compatibility Levels for low-frequency conducted disturbances and signaling in public medium-voltage power systems
- [6] EN 50160 Voltage Characteristic of Public Distribution Systems
- [7] Tadeusz Cholewicki, "Elektrotechnika Teoretyczna", WNT, Warszawa 1973 pp. 391-422

## 7. Advanced topic. Determination of transient parameters in wind energy conversion system

The aim of the chapter is a presentation of advanced approach to the estimation of disturbances, also assessment of power quality. A wind energy system has been chosen as an interesting and modern network component, unfortunately producing not only green energy but also disturbances. In this particular case, advanced signal processing methods have been successfully applied for signal characterization and will be briefly introduced.

### 7.1.Motivation and problem formulation

The widespread implementation of wind energy conversion systems is a reality. Wind is seen as a clean and renewable energy source, so the development of wind generation

technologies is welcomed and supported by ecologists and governments. In the next years we will have even more generator units connected to the grid [1].

Besides distinctive merits, the connection of wind generators leads to many disturbances, such as: voltage fluctuation, flickers, harmonics, instability, blind power regulation problems, and transients [2]. That disturbance affects power quality. Power quality issues connected with wind generation are not only important because of technical aspects, they are also crucial on the free energy market.

Many of the wind energy converters installed today have a squirrel-cage induction machine connected directly to the grid [4]. This type of the generator cannot perform voltage control and it absorbs reactive power from the grid. Compensating capacitors are often directly connected. That type of installation is cost-saving, and therefore still in use, but from the system analysis point of view it can be considered as the worst case [3].

When capacitors are switched switching transients occur, whose are devastating for sensitive equipment, protection relays and insulation. The impact of transients on power quality indices cannot be neglected [2]. Transient overvoltages can theoretically reach peak values up to 2.0 pu. High current transients can reach values up to ten times of the nominal capacitor current with duration of several milliseconds [6].

The aim is the assessment of transients in an electrical system with an asynchronous generator. The analysis is carried out for real measured signals and for different operation conditions of the wind converter simulated in Matlab in SimPowerSystem Toolbox [5].

The Prony method was considered as an appropriate tool for parameters estimation of transients. It shows some merits in comparison to widely applied FFT. A nonlinear regression method was also applied and compared with Prony method. Precise computation of the starting point of a disturbance was done using wavelets.

## **7.2.Prony metod**

The Prony method is a technique for modelling sampled data as a linear combination of exponential functions [6]. Although it is not a spectral estimation technique, the Prony method has a close relationship to the least squares linear prediction algorithms used for AR and ARMA parameter estimation. Prony method seeks to fit a deterministic exponential model to the data in contrast to AR and ARMA methods that seek to fit a random model to the second-order data statistics.



Assuming N complex data samples, the investigated function can be approximated by p exponential functions:

$$y[n] = \sum_{k=1}^p A_k e^{(\alpha_k + j\omega_k)(n-1)T_p + j\psi_k} \quad (7.1)$$

where

$n = 1, 2, \dots, N$ ,  $T_p$  - sampling period,  $A_k$  - amplitude,  $\alpha_k$  - damping factor,  $\omega_k$  - angular velocity,  $\psi_k$  - initial phase.

The discrete-time function may be concisely expressed in the form

$$y[n] = \sum_{k=1}^p h_k z_k^{n-1} \quad (7.2)$$

where

$$h_k = A_k e^{j\psi_k}, \quad z_k = e^{(\alpha_k + j\omega_k)T_p}$$

The estimation problem is based on the minimization of the squared error over the N data values

$$\delta = \sum_{n=1}^N |\varepsilon[n]|^2 \quad (7.3)$$

where

$$\varepsilon[n] = x[n] - y[n] = x[n] - \sum_{k=1}^p h_k z_k^{n-1} \quad (7.4)$$

This turns out to be a difficult nonlinear problem. It can be solved using the Prony method that utilizes linear equation solutions.

If as many data samples are used as there are exponential parameters, then an exact exponential fit on to the data can be made.

Consider the p-exponent discrete-time function:

$$x[n] = \sum_{k=1}^p h_k z_k^{n-1} \quad (7.5)$$

The p equations of (5) may be expressed in matrix form as:

$$\begin{bmatrix} z_1^0 & z_2^0 & \dots & z_p^0 \\ z_1^1 & z_2^1 & \dots & z_p^1 \\ \vdots & \vdots & \dots & \vdots \\ z_1^{p-1} & z_2^{p-1} & \dots & z_p^{p-1} \end{bmatrix} \begin{bmatrix} h_1 \\ h_2 \\ \vdots \\ h_p \end{bmatrix} = \begin{bmatrix} x[1] \\ x[2] \\ \vdots \\ x[p] \end{bmatrix} \quad (7.6)$$

The matrix equation represents a set of linear equations that can be solved for the unknown vector of amplitudes.

Prony proposed to define the polynomial that has the exponents as its roots:

$$F(z) = \prod_{k=1}^p (z - z_k) = (z - z_1)(z - z_2) \dots (z - z_p) \quad (7.7)$$

The polynomial may be represented as the sum:

$$\begin{aligned} F(z) &= \sum_{m=0}^p a[m]z^{p-m} = \\ &= a[0]z^p + a[1]z^{p-1} + \dots + a[p-1]z + a[p] \end{aligned} \quad (7.8)$$

Shifting the index on (5) from  $n$  to  $n-m$  and multiplying by the parameter  $a[m]$  yield:

$$a[m]x[n-m] = a[m] \sum_{k=1}^p h_k z_k^{n-m-1} \quad (7.9)$$

Equation (9) can be modified into:

$$\sum_{m=0}^p a[m]x[n-m] = 0 \quad (7.10)$$

The right-hand summation in (10) may be recognized as a polynomial defined by (8), evaluated at each of its roots yielding the zero result:

$$\begin{aligned} \sum_{m=0}^p a[m]x[n-m] &= \\ &= \sum_{k=1}^p h_k z_k^{n-p} \left\{ \sum_{m=0}^p a[m]z_k^{p-m-1} \right\} \end{aligned} \quad (7.11)$$

The equation can be solved for the polynomial coefficients. In the second step the roots of the polynomial defined by (8) can be calculated. The damping factors and sinusoidal frequencies may be determined from the roots  $z_k$ .

For practical situations, the number of data points  $N$  usually exceeds the minimum number needed to fit a model of exponentials, i.e.  $N > 2p$ . In the overdetermined data case, the linear equation (11) should be modified to:

$$\sum_{m=0}^p a[m]x[n-m] = e[n] \quad (7.12)$$

The estimation problem is based on the minimization of the total squared error:

$$E = \sum_{n=p+1}^r |e[n]|^2 \quad (7.13)$$

### 7.3. Nonlinear regression method

Nonlinear regression is a general technique to fit a curve through data. It fits data to any equation that defines Y as a function of X and one or more parameters. It finds the values of those parameters that generate the curve that comes closest to the data (minimizes the sum of the squares of the vertical distances between data points and curve). That technique requires a model of the analyzed signal. In the case of capacitor bank switching, the signal model of transient component can be defined as

$$x(t) = A_1 \sin(\omega_1 t + \varphi_1) + A_2 e^{-\alpha t} \sin(\omega_2 t + \varphi_2) \quad (7.14)$$

where  $A$  - amplitudes,  $\alpha$  - damping factor and  $\omega$  - angular velocities are unknown and should be estimated. Practically, the signal is observed (or measured) during a finite duration of time and  $N$  samples of this signal are available. The measured discrete time signal  $y[nT_p]$  can be specified as

$$\begin{aligned} y(nT_p) = & A_1 \sin(\omega_1 nT_p + \varphi_1) + \\ & + A_2 e^{(-\alpha nT_p)} \sin(\omega_2 nT_p + \varphi_2) + e(nT_p) = \\ & x(nT_p) + e(nT_p) \end{aligned} \quad (7.15)$$

for  $n = 1, 2, 3 \dots N$ .

As previously  $T_p$  - is the sampling period,  $N$  - the number of samples and  $e$  the estimation error correlated with each sample, which includes random noise and other distortions.

The problem of nonlinear regression can be formulated as an optimization problem, where the goal is to minimize the difference between the physical observation and the prediction from the mathematical model. More precisely, the goal is to determine the best values of the unknown parameters  $A$ ,  $\alpha$ ,  $\omega$ ,  $\varphi$  in order to minimize the squared errors between the measured values of the signal and the computed ones. Thus, the optimization problem can be formulated as follows:

Find a vector  $\mathbf{w} = [A_1, A_2, \alpha, \omega_1, \omega_2, \varphi_1, \varphi_2]^T$  which minimizes the objective function

$$E(\mathbf{w}) = \sum_{n=1}^N e^2(nT_p) = \sum_{n=1}^N [y(nT_p) - x(nT_p)]^2 \quad (7.16)$$

That is a well known standard of the least squares problem. To solve that problem, the Quasi-Newton method was applied [7]. At each iteration, the problem is to find a new iterate  $w_{k+1}$  of the form:

$$\mathbf{w}_{k+1} = \mathbf{w}_k + \tau \mathbf{d} \quad (7.17)$$

where  $\tau$  is a scalar step length parameter and  $\mathbf{d}$  is the search direction. Using the quasi-Newton method, a line search is performed in the direction

$$\mathbf{d} = -\mathbf{H}_k^{-1} \cdot \nabla E(\mathbf{w}_k) \quad (7.18)$$

where  $\mathbf{H}^{-1}$  is an approximation of the inverse Hessian matrix.

The DFP formula was used for approximation of the inverse of Hessian matrix

$$\mathbf{H}_{k+1}^{-1} = \mathbf{H}_k^{-1} + \frac{\mathbf{s}^k (\mathbf{s}^k)^T}{(\mathbf{q}^k)^T \mathbf{s}^k} - \frac{(\mathbf{H}_k^{-1} \mathbf{q}^k) (\mathbf{H}_k^{-1} \mathbf{q}^k)^T}{(\mathbf{q}^k)^T \mathbf{H}_k^{-1} \mathbf{q}^k} \quad (7.19)$$

where  $\mathbf{q}_k = \nabla E(\mathbf{w}_{k+1}) - \nabla E(\mathbf{w}_k)$  is a gradient increment and  $\mathbf{s}_k = \mathbf{w}_{k+1} - \mathbf{w}_k$  is a variable increment.

#### 7.4. Wavelet Transform

The wavelet transform is a useful tool in signal analysis. Wavelets can be applied for the precise computation of the beginning of a disturbing event, as it is in this paper.

The continuous Wavelet Transform (WT) of a signal  $x(t)$  is defined as

$$X_{a,b} = \frac{1}{\sqrt{|a|}} \int_{-\infty}^{+\infty} x(t) \psi\left(\frac{t-b}{a}\right) dt \quad (7.20)$$

where  $\psi(t)$  is the mother wavelet, and other wavelets

$$\psi_{a,b}(t) = \left(\frac{1}{\sqrt{a}}\right) \psi\left(\frac{t-b}{a}\right) dt \quad (7.21)$$

are its dilated and translated versions, where  $a$  and  $b$  are the dilation parameter and translation parameter respectively,  $a \in R^+ - \{0\}$ ,  $b \in R$  [8].

The discrete WT (DWT), instead of CWT, is used in practice [8]. Calculations are made for a chosen subset of scales and positions. This scheme is conducted by using filters and computing so called approximations and details. The approximations (A) are the high-scale,

low frequency components of the signal. The details (D) are the low-scale, high-frequency components. The DWT coefficients are computed using the equation

$$X_{a,b} = X_{j,k} = \sum_{n \in Z} x[n]g_{j,k}[n] \quad (7.22)$$

where  $a = 2^j$ ,  $b = k2^j$ ,  $j \in N$ ,  $k \in Z$ .

The wavelet filter  $g$  plays the role of  $\psi$  [8].

The decomposition (filtering) process can be iterated, so that one signal is broken down into many lower resolution components. This is called the wavelet decomposition tree [8].

For detection of transients a multi-resolution analysis tree (Figure 7.1) based on wavelets has been applied [9]. Each one of wavelet transform subbands is reconstructed separately from each other, so as to get  $k+1$  separated components of a signal  $x[n]$ . The MATLAB *multires* function [10] calculates the approximation to the  $2k$  scale and the detail signals from the  $2^1$  to the  $2k$  scale for a given input signal. It uses the analysis filters  $H$  (lowpass) and  $G$  (highpass) and the synthesis filters  $RH$  and  $RG$  (lowpass and highpass respectively) (Figure 7.2).

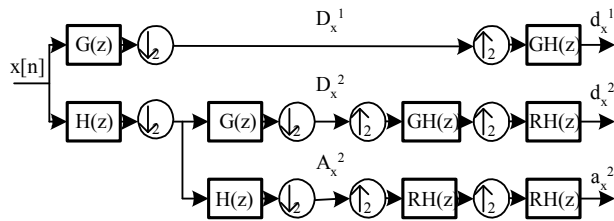


Figure 7.1 . Analysis-Synthesis tree for the MATLAB *multires* function

As a wavelet the symlets function was used. The symlets are nearly symmetrical wavelets proposed by Daubechies as modifications to the “db” family - orthogonal wavelets characterized by a maximal number of vanishing moments for some given support (Figure 7.3).

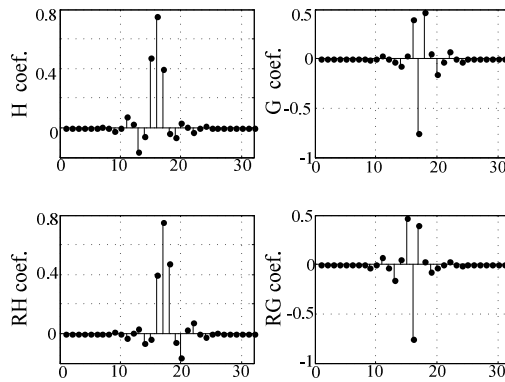


Figure 7.2 Filters coefficients for symlets wavelet

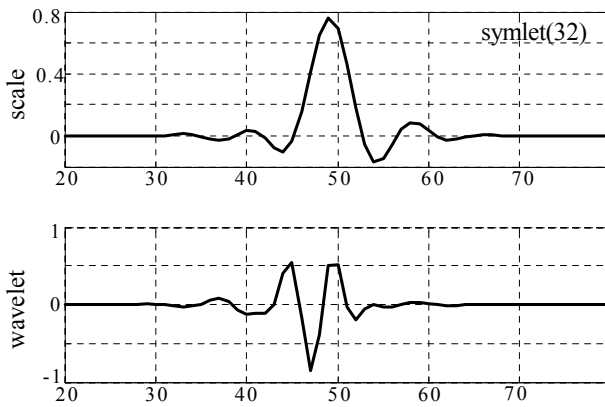


Figure 7.3 Scale and wavelet symlets function for 32 coefficients

### 7.5.Simulation of induction generator with capacitors

The wind generator with compensating capacitors is shown in Figure 7.4. The simulation was done in Matlab using the SimPowerSystem Toolbox [5].

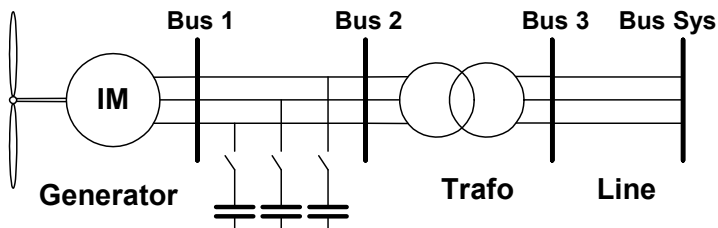


Figure 7.4 Induction generator with compensating capacitors

A wind turbine generates power corresponding to mechanical torque on the rotating shaft of the turbine. Produced power depends on a rotor speed and a pitch angle and is often given in a table form [10]. The turbine characteristic used in this simulation is shown in Figure 7.5.

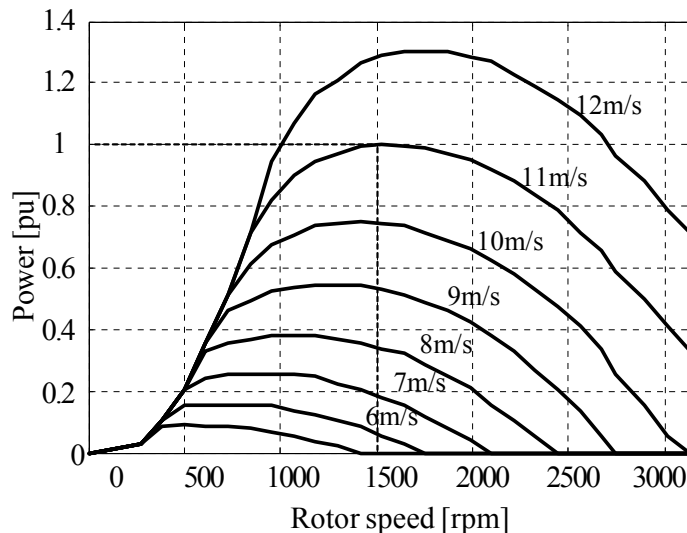


Figure 7.5 Induction generator output power vs. angular velocity

The pitch control dynamic can be neglected in a power system transient analysis [4]. The simulated generator is a 150 kW, 400 V, 1487 rpm, induction machine. It is connected to the grid through a Dyg 25/0.4 kV distribution transformer whose nominal power was varied between 0.5 and 2 MW during the research process and other parameters were set with accordance to [11]. A typical 5 km overhead line [11] connected the generator to a system. The system was represented by an equivalent source with short circuit capacity of 100 MVA and X/R ratio of 7. The induction generator reactive power demand varies with the produced real power [2]. During the research, different compensation levels were simulated. Simulation results correlate with measured values.

### 7.6. Parameters of transients computed using Prony algorithm and Nonlinear Regression

Firstly, to evaluate the performance of the proposed procedure simulated signals has been used.

For variable wind speeds, the exact compensation of reactive power using a capacitor bank is difficult [2]. The reactive power variation should be taken into account even if additional capacitors are switched on and off during the operation.

Assumption of full reactive power compensation at freely chosen wind speed implies capacitance adjustment of the compensating capacitor for every particular case. Table 7-1 contains results of the signal parameters estimation using Prony model (PRO) and nonlinear regression (NLR). The sampling frequency was 5 kHz. Two components in the signal were assumed and estimated: the main 50 Hz frequency [No.2] and the additional capacitor bank switching transient [No.1]. Three wind speeds were chosen – 8 m/s, 10 m/s, 12 m/s. For these wind speeds, the capacitor was adjusted to fully compensate reactive power. The influence of a capacitor change on transient parameters is clearly visible (Table 7-1). For higher wind speeds and therefore greater capacitance value, the amplitudes of the transients were higher and the transients' frequency lower. Time constant did not change significantly.

**Table 7-1 TRANSIENTS PARAMETERS FOR QC=80.4 KVAR AND WIND SPEEDS OF 12 M/S, 10 M/S AND 8 M/S**

SignalCom./ Method [No. –Mth.]	I [A]	$\tau$ [s]	f [Hz]	$\psi$ [rd]
wind speed 8 m/s				
1.-PRO	579.4	0.0095	526.6	-0.15
1.-NLR	579.7	0.0095	526.5	-0.14
2.-PRO	105.7		49.66	-2.37
2.-NLR	107.2		49.64	-2.36
wind speed 10 m/s				
1.-PRO	624.8	0.0095	501.6	-0.15
1.-NLR	625.2	0.0095	501.6	-0.15
2.-PRO	231.1		49.82	-2.47
2.-NLR	233.3		49.81	-2.47
wind speed 12 m/s				
1.-PRO	710.6	0.0095	456.5	-0.16
1.-NLR	711.1	0.0095	456.5	-0.16
2.-PRO	394.4		49.86	-2.49
2.-NLR	396.7		49.86	-2.48

Figure 7.6 shows one phase current after a capacitor switching at wind speed of 8 m/s. The computed signals parameters are included in Table 7-1.



The parameter estimation using the Prony model or a nonlinear regression gave more detailed information than Fourier spectrum estimation. Figure 7.7 depicts the spectrum of the current shown in Figure 7.6. Two components in the signal are visible, but there is no information about an amplitude, time constant or phase. However, Fourier method does not need any assumption about the unknown signal model.

Apart from the capacitor and generator, also transformer, cable, short circuit level of the system and other parameters influence the signal parameters.

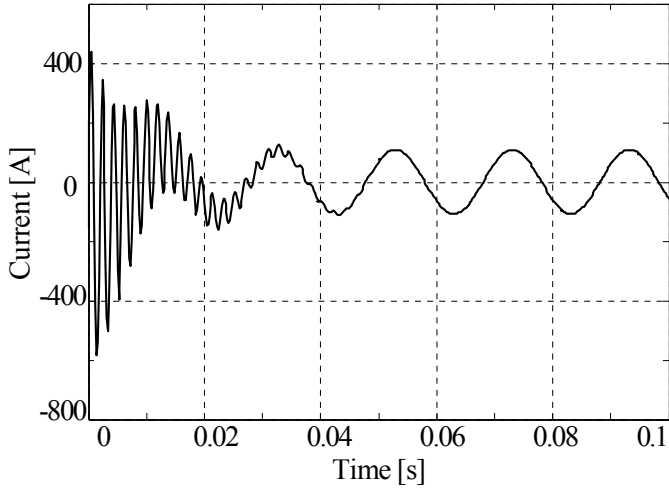


Figure 7.6 Current resulting from capacitor ban switching by wind speed of 08 m/s

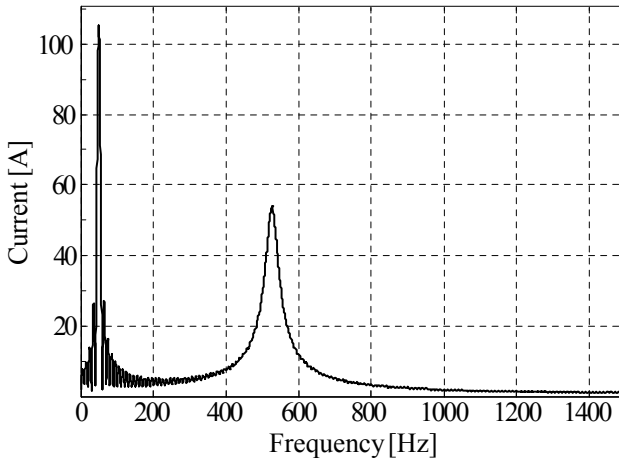


Figure 7.7 Fourier spectrum of the capacitor switching current

After getting encouraging results on simulated signals, real measured values has been chosen for a further research activity.

Nonlinear regression and the Prony model were applied to estimate the parameters of the measured signals.

The measurements were done on a system connected to a 500 kW induction generator with two step compensation capacitors. A measuring recorder was connected to the high voltage side of a 11kV/400V, Dyn11, transformer. The signal was sampled at 6250 Hz.

The most accurate detection of the beginning of transients has been achieved for 32 coefficients of symlets wavelet filters. The 1 scale detail signal enabled detection of transients with accuracy 2-3 sampling intervals. The measured current waveform and the 1st scale details of that signal are shown in Figure 7.8. The transients resulting from the both switching operations were analyzed. The windowed current waveform showing the first switching transient in detail is shown in Figure 7.9. Figure 7.10 depicts the Fourier spectrum of the signal in Figure 7.9.

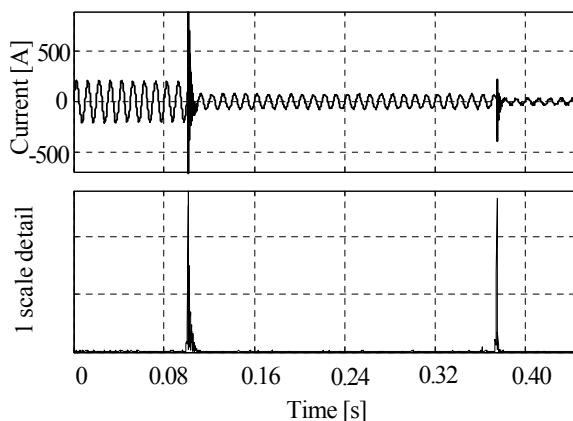


**Figure 7.8 Recorded current waveform and 1 scale detail signal**

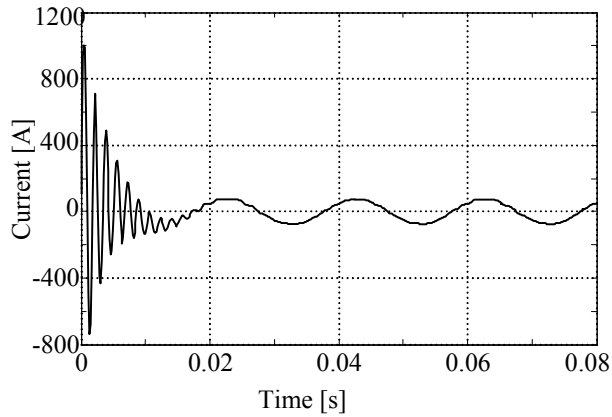


Figure 7.9 . Transient current after switching of the first compensating capacitor

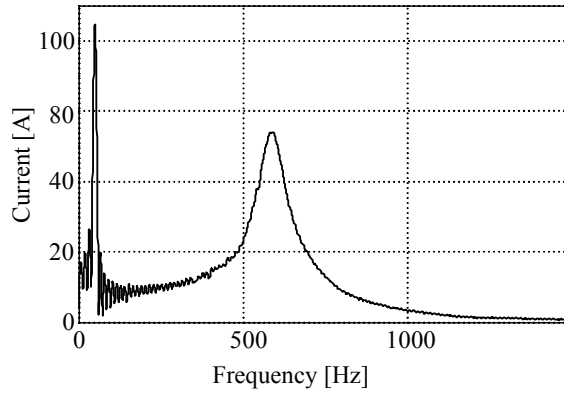


Figure 7.10 Spectrum of current by switching of first capacitor

As previously, computed signal parameters values are presented in a compact form in Table II. The Fourier spectrum in Figure 7.10 indicates additional small components in the signal. The signal model applied for nonlinear regression assumed only two components, so the rest was considered to be noise.

Table 7-2 TRANSIENTS PARAMETERS

SignalCom./ Method [No. -Mth.]	I [A]	$\tau$ [s]	f [Hz]	$\psi$ [rd]
first capacitor switching				
1.-PRO	1127	0.0039	590.5	-1.80

1.-NLR	1123	0.0039	589.1	-1.78
2.-PRO	84.07		49.98	-0.81
2.-NLR	81.20		49.27	-0.69
second capacitor switching				
1.-PRO	406	0.0032	512.2	1.57
1.-NLR	442	0.0027	512.4	1.57
2.-PRO	27.32		51.01	1.39
2.-NLR	27.15		50.83	1.44

### 7.7. Concluding remarks

The research results show that the Prony model and nonlinear regression are useful for transient estimation in systems with wind generators and compensating capacitors. Those methods enabled an accurate estimation of the amplitude, time constant, phase and frequency of transients' components of simulated and measured signals. The current waveform and its parameters depend on system elements and its operating mode. Those dependences could be observed during simulation of various cases.

The application of both Prony Model and nonlinear regression required a signal model. Fourier transform, as a nonparametric method, did not require a signal model or even the number of components, but could not compute signal parameters except for frequency. Using nonlinear regression, the problem of local minima was observed. The unconsidered setting of the initial parameters can lead to a local minimum and inadequate results. Additionally, two signal components were predefined, so the rest was considered noise. Application of the Prony method did not show the problem of local minima. The order of the signal model could be easily extended to detect additional components. Both methods delivered similar results, however, application of the Prony model seems more suitable for an estimation of signal parameters.

### 7.8. Literature

- [1] T. Hammons, "Status of Integrating renewable electricity production in Europe into the grids", Proceedings Universities Power Engineering Conference, Cork, Ireland, ,p.73.
- [2] Z. Lubosny, Wind Turbine Operation in Electric Power Systems, Springer Verlag, Berlin Heidelberg (Germany), 2003, ch. 3 and 4
- [3] Ch. Chompoo-inwai, L. Wei-Jen, P. Fuangfoo, M. Williams, J. R. Liao, "System Impact

- Study for the Interconnection of Wind Generation and Utility System", IEEE Trnas. on Industry Applications, vol. 41, 2005, pp. 163-168
- [4] A. Tabesh, R. Iravani, 2005, "Transient Behavior of Fixed-Speed Grid-Connected Wind Farm", Transactions International Conference on Power Systems Transients, Paper No. IPST05-068
- [5] The Mathworks, SimPowerSystems User's Guide, The Math Works Inc, 2000
- [6] T. Lobos, J. Rezmer, H-J. Koglin, "Analysis of Power System Transients using Wavelets and Prony Method". Proceedings IEEE Power Tech Conference, Porto, Portugal, September 2001, paper ID EMT-103
- [7] A. M. Bhatti, Practical Optimization Methods. Springer Verlag, New York , USA, 2000, pp. 288-302
- [8] M. Misiti, Y. Misity, G. Oppenheim, J-M. Poggi, Wavelet Toolbox User's Guide, MathWorks, 1996
- [9] S. G. Mallat, "A theory of multiresolution signal decomposition: the wavelet representation", IEEE Trans. Pattern Analysis and Machine Intelligence, vol. PAMI 11, July 1998, pp. 647-693
- [10] S.G. Sanchez, N.G. Prelcic, S.J.G. Galan, (1996, Apr.) Uvi Wave-Wavelet Toolbox for Matlab (ver 3.0), University of Vigo, [Online].Available: [http://www.tsc.uvigo.es/~wavelets/uvi\\_wave.html](http://www.tsc.uvigo.es/~wavelets/uvi_wave.html)
- [11] SIEMENS: Electrical Engineering Handbook, 1987

## 8. Computational application of power quality assessment: dips

A power quality issue includes different phenomena usually associated with deviation of the voltage as well as current from its ideal waveform. The main aim of the activities dedicated to power quality assessment is concentrated on a digital signal processing method associated with general classification of power quality phenomena. Proposed in the literature classification [1],[2],[3],[4] divides power quality in two main groups: variations and events. The extended expression of mentioned group depicts Fig. 8.1.

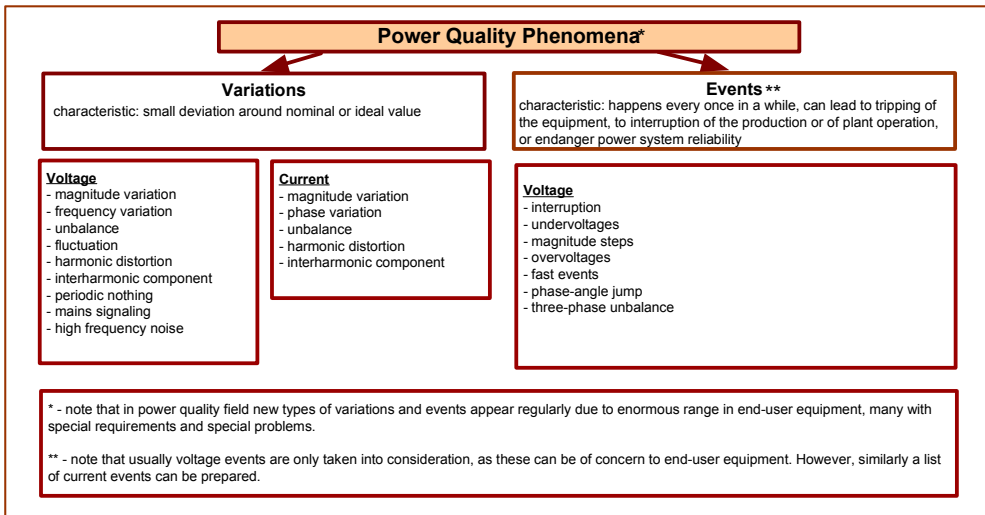


Fig. 8.1 General classification of power quality phenomena

This chapter is dedicated to undervoltage event member, called voltage dips (or sags). In standard nomenclatures dips term is associated with IEC documents and sags can be found in IEEE Standards. Generally, a voltage dip is a reduction in the supply voltage magnitude followed by the voltage recovery after a short period of time. Dips manifests itself in a short duration reduction in rms voltage. The origin of the dips are usually joined with short-circuit faults (transmission system faults, remote distribution systems faults, local distribution system faults), starting of large motors, a short interruption and fuses. In order to localize this event in wider group of undervoltages, some parameters should be specified: level of the rms voltage magnitude reduction and duration time. Referring to IEC Standards, dips are

considered as a reduction in rms voltage to value between 90% and 1% of the declared value, followed by a recovery between 10ms (0.5 cycles of fundamental component 50Hz) and 1 minute later. For the IEEE Standards a voltage drop is only a sags if during a drop the voltage is between 90% and 10%. One word of a comment requires also a phrase “declared value”, considered as reference value for a threshold level. There are arguments in favour of using the pre-fault voltage and there are arguments in favour of using nominal voltage. From practical point of view, usually the base for calculation level of drop the nominal voltage is used i.e. 0.4kV for low voltage, 10kV, 20kV for medium voltage. Classification of all voltage magnitude events including dips definition is expressed in Fig. 8.2.

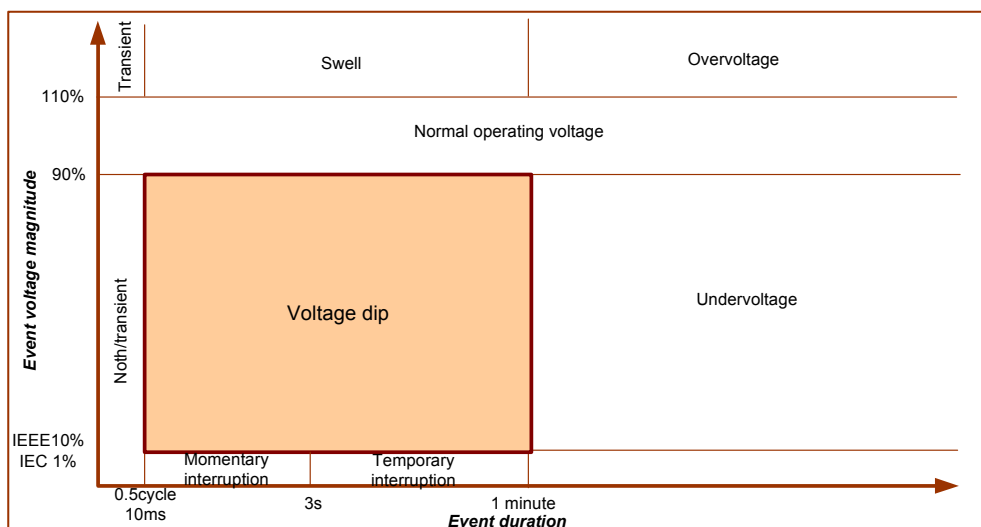


Fig. 8.2. Classification of all voltage magnitude events including dips definition

Taking into a count the quoted definition of voltage dips, proper classification of this event requires an estimation of voltage magnitude as well as time duration during the dip. Thus, it is desirable to know some advantages and disadvantages of the algorithms which allow to detect voltage dips on the basis of recorded voltage waveform. Three approaches can be distinguished: **classical rms voltage method** and **peak voltage method** associated with direct time analysis and **fundamental voltage component method** based on frequency analysis.

This chapter introduces mathematical backgrounds as well as a practical application of mentioned algorithms in Matlab environment with comparison and examples.

### **8.1.Methods of voltage magnitude estimation**

As it was mentioned in the introduction, there is a crucial need for permanent tracking of rms voltage. A detection of its drop below 90% of a reference value can be treated as a threshold for possible dip event. Among the algorithms dedicated to this task we can distinguish methods utilizing direct sampled value (time analysis) and those required spectrum estimation (frequency analysis). A time analysis represent such algorithm as "**rms voltage method**" or "**peak voltage method**". Frequency approach requires "**fundamental voltage component method**".

No matter what kind of method we select to apply tracking of the rms voltage along the signal, the mechanism is the same – shifting executive window which leads to time trend of a magnitude variation. It means that the main algorithm responsible for a magnitude estimation is applied only for a particular portion of samples, designated by the window, many times for its particular location. Finally, we achieve many local values of rms voltage associated with a position of the window along the time axis. The representation of these local rms values along the time axis gives desirable trend of voltage variation during the event. Standard window width is half cycle of fundamental component for EN 50160 and one cycle of fundamental component for IEC 61000. The trend of voltage variation can be achieved in a high-quality mode if window is shifted sample by sample as well as in monitoring mode when window shifts window by window with additional options of averaging time like 200ms or 10 minutes. The described mechanism for high-quality mode is shown in Fig. 8.3.



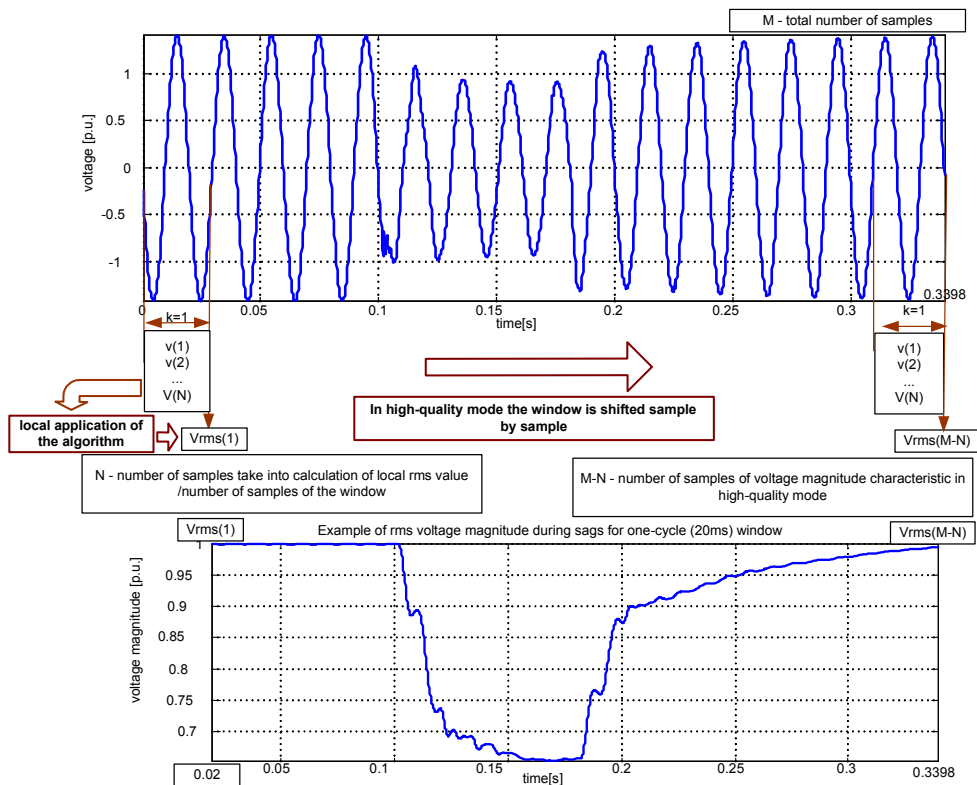


Fig. 8.3. Mechanism of rms voltage trend during the event: high-quality mode, one-cycle algorithm

### “rms voltage” method

This method is based on the classical definition of rms value of periodical signals [1],[3],[4],[5]:

$$V_{rms1}(k) = \sqrt{\frac{1}{N} \sum_{i=k}^{i=k+N-1} v^2(i)} \quad (8.1)$$

where:  $k=(1,2...M-N)$ ,  $M$  – the total length of an investigated voltage signal  $v$  in samples,  $i=(k,k+1...k+N-1)$  – indicates a set of samples  $v(i)$  taken into calculation of local  $V_{rms1}(k)$ , always on the basis of  $N$  samples,  $N$  – a number of samples taken for calculation – usually equals an integer multiplication of a number of samples per one cycle of fundamental component.

Note, we obtain that first value of estimated rms voltage  $V_{rms1}(1)$  on the basis of first  $N$  samples. Thus, following by the time axis the first value of estimated rms voltage is localized in time moment equals  $N*dt$  where  $dt$  is a sampling step. The next points of desirable

$V_{rms1}(k)$  are calculated using shifting window. For a high quality calculation the shift is fine, that means sample by sample. In monitoring quality mode the rms value is calculated once per cycle or half-cycle. Additionally, the averaging time is introduced concerning one value for selected numbers of cycles (half-cycles) i.e. 200ms averaging time means that we achieve one value from 10 one-cycle values or 20 half-cycles values.

“peak voltage” method

Similarly to the previous approach, we expect to achieve a function of time that corresponds to rms voltage changes during the events. Here for each samples over the proceeding window of the voltage, the maximum of absolute value is calculated. Again, the length of executive window should contain integer multiplication of a number of samples per one cycle of fundamental component. Finally, we can estimate rms voltage for particular localisation of the window by [1],[3],[4],[5]:

$$V_{rms2}(k) = \frac{\max\{|v(i)|\}}{\sqrt{2}}, i = (k, k+1, \dots, k+N-1) \quad (8.2)$$

where:  $k = (1, 2, \dots, M-N)$ ,  $M$  – the total length of investigated voltage signal  $v$  in samples,  $i = (k, k+1, \dots, k+N-1)$  – indicates a set of samples  $v(i)$  taken into calculation of local  $V_{rms2}(k)$ , always on the basis of  $N$  samples,  $N$  – a number of samples taken for calculation – usually equals an integer multiplication of a number of samples per one cycle of fundamental component.

Similarly, followed by the time axis first value of estimated rms voltage is localized in time moment equals  $N*dt$  where  $dt$  is the sampling step. The next points of desirable  $V_{rms2}(k)$  are calculated using the shifting window till the end of recorded data. For a high quality calculation the shift is fine, which means sample by sample shift. In a monitoring quality mode the rms value is calculated once per cycle or per half-cycle.

“fundamental voltage component” method

This approach introduces a frequency domain with a classical method for spectrum estimation method that Fourier analysis is. In a continuous-time domain we can calculate Fourier transform and inverse Fourier transform in order to obtain a desirable fundamental component  $f_0$ :

$$v_0(t) = \frac{1}{2\pi} \int_{-\infty}^{+\infty} V(j\omega) \cdot e^{j\omega t} d\omega \Leftarrow V(j\omega) = \int_{-\infty}^{+\infty} v(t) \cdot e^{-j\omega t} dt, \quad (8.3)$$

In a discrete time-domain, we reintroduce this approach applying Fast Fourier Transform (FFT). The idea of tracking rms voltage in time is equally preserved compared to previous method i.e. a local value of rms voltage are associated with a particular position of executive window along time axis. However, the algorithm of local rms voltage utilizes frequency approach this time [1],[3],[4],[5]:

$$V_{rms3}(k) = \left| V(m) \right|_{m=m50} \Leftarrow V(m) = FFT(v(i)), i = k, k+1, \dots, k+N-1 \quad (8.4)$$

$$m50 = 50 / df = 50 / fs / N$$

where:  $k = (1, 2 \dots M-N)$ ,  $M$  – the total length of investigated voltage signal  $v$  in samples,  $i = (k, k+1 \dots k+N-1)$  – indicates a set of samples  $v(i)$  taken into calculation of local  $V_{rms3}(k)$ , always on the basis of  $N$  samples,  $N$  – a number of samples taken for calculation – usually equals an integer multiplication of number of samples per one cycle of fundamental component.

On the basis of local  $N$  samples of a windowed signal  $v(i)$  the FFT is performed. It transfers the set of local  $v(i)$  data into a frequency domain represented now by a local vector  $V(m)$ . Note that  $V(m)$  contains a complex value. The next step is to select from this vector an element associated with fundamental 50Hz component. In order to do it, we have to recalculate the index  $m$  which represents 50Hz on the basis of sampling frequency ( $fs$ ) and a number of frequency bins, here equals  $N$ . Defining frequency resolution as  $df = fs/N$ , we can uncover an index associated with fundamental component  $m50 = 50/df$ . Finally, we identify complex vector describing magnitude as well as phase of fundamental component as  $V(m50)$ .

Even though we use a frequency approach, we still intend to track the rms voltage in time. Thus, followed by the time axis, the first value of estimated rms voltage is localized in time moment equals  $N \cdot dt$  where  $dt$  is the sampling step. The next points of desirable  $V_{rms3}(k)$  are calculated using a shifting window till the end of recorded data. For a high quality calculation the shift is fine, which means sample by sample shift. In a monitoring quality mode the rms value is calculated once per cycle.

**Warning:** Applying FFT algorithm, we have to be conscious of some limitations. This algorithm gives desirable effect if the number of samples taken for FFT calculation equals integer value of samples per one cycle of fundamental component. If not, the leakage effect

must be considered. Thus, application of this approach in case of half-cycle window is more complicated. One of the proposed solution is to take a half-cycle window and build second half-cycle window as:

$$v(i) = \{v(k), v(k+1), \dots, v(k+N-1), -v(k), -v(k+1), \dots, -v(k+N-1)\}, \text{ only for } N = \text{half-cycle window}$$

(8.5)

## 8.2. Application of rms trend calculation in Matlab

Reconnaissance in a signal processing area manifest itself in crucial need for some details about the origin of the phenomena (physical sphere) and parameters of quantisation, especially a sampling rate (digital sphere).

Before we start working with analysis of the phenomena, it is necessary to perform some initial calculations concerning sampling rate, definition of time axis etc.

This section demonstrates investigations of real measured voltage phenomena during decaying fault in low voltage distribution systems under a storm condition Fig. 8.4. File is also available in Matlab format at <http://eportal.eny.pwr.wroc.pl/> as *sag\_dg.mat*. From the digital point of view sampling rate is 10.240kHz. Vectors consist of 4096 samples. In order to demonstrate the phenomena and to associate time axis with recording parameters some initial calculation should be performed.

Initial calculation:

sampling rate (sampling frequency)  $f_s = 10.240kHz$

time step (time resolution)  $dt = \frac{1}{f_s} = \frac{1}{10240} = 9.7656e-005s$

time axis  $t = [0 : 1 : 4096 - 1] * dt = [0 : dt : 0.4 - dt]s$

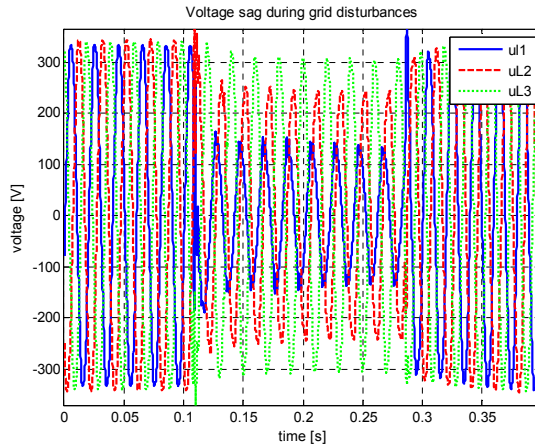


Fig. 8.4. Visualisation of example of investigated dip phenomena

The aim of this chapter is to present some example algorithms in Matlab environment and results concerning discussed methods of rms calculation as well as the influence of the window width.

Table 8-1. Demonstration algorithm of rms trend calculation using classical “rms voltage” method

Fig. 8.5. Investigated one-phase signal and its rms trend characteristic using half-cycle “rms voltage” method

Table 8-2. Demonstration algorithm of rms trend calculation using “peak voltage” method

Fig. 8.6. Investigated one-phase signal and its rms trend characteristic using half-cycle “peak voltage” method.

Table 8-3. Demonstration algorithm of rms trend calculation using “fundamental voltage component” method

Fig. 8.7. Investigated one-phase signal and its rms trend characteristic using half-cycle “fundamental voltage component” method

**Table 8-1. Demonstration algorithm of rms trend calculation using classical “rms voltage” method**

```

-----SIGNAL-----
clear all, close all
load sag_gd;
%sag_gd.mat contain uL1 uL2 uL3 4096 samples
%fs=10240Hz
%It covers 20 cycles (period of fundamental component)
%4096 total number of samples
%2048 samples/ 10cycle
%204.8 samples/ 1cycle, round 204 sample/cycle
x=uL1;
h=plot(t,x)
set(h,'LineWidth',2);
xlabel('time [s]')
ylabel('voltage [V]')
grid on
axis('tight')
-----INITIAL PARAMETERS-----
icycle=1/2; %icycle- executive window width in cycles of fundamental component
fo=50; %fundamental component 50Hz
To=1/fo; %one cycle of the fundamental component in [s]
tN=icycle*To; %executive window width in [s]
N=round(icycle*To/dt) %executive window width in [samples]
%-----
%TIME ANALYSIS - Vrms1- rms voltage: 1-phase, high quality
%-----
%Vrms1 - vector of local rms voltage
%calculated on the basis of N samples of the signal
%High quality mode - every next Vrms1 are obtained
%by shifting the window along signal sample by sample.
%Note - first value of Vrms1 can be obtained after recording of
%assumed N samples of executive window (tN in seconds).
%Thus we should rescale time axis in Figure representing rms voltage
%starting from tN and finish with end of the signal ->t1
%For high quality mode we preserve time step in t1 as dt
for k=1:length(x)-N
    k
    n=[k:k+N-1]; %identification of windowed samples
    xn=[x(n)]; %windowed signal samples taken for calculation of local rms
    Vrms1(k)=sqrt(1/N*sum(xn.^2));
end
t1=t(N+1:length(x));
figure
h=plot(t1,Vrms1)
set(h,'LineWidth',2)
xlabel('time [s]')
ylabel('voltage magnitude [V]')
title(['Vrms1: ',num2str(icycle),'-cycle window'])
grid on
axis('tight')
%-----

```

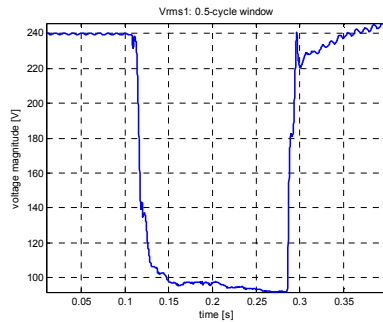
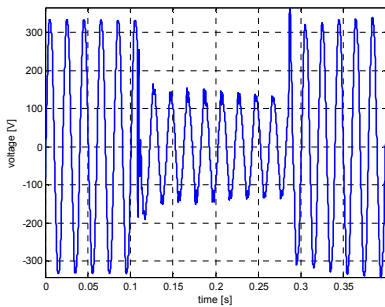


**Fig. 8.5. Investigated one-phase signal and its rms trend characteristic using half-cycle “rms voltage” method**

**Table 8-2. Demonstration algorithm of rms trend calculation using “peak voltage” method**

```

-----SIGNAL-----
clear all, close all
load sag_gd;
%sag_gd.mat contain uL1 uL2 uL3 4096 samples
%fs=10240Hz
%t covers 20 cycles (period of fundamental component)
%4096 total number of samples
%2048 samples/ 10cycle
%204.8 samples/ 1cycle, round 204 sample/cycle
x=uL1;
h=plot(t,x)
set(h,'LineWidth',2);
xlabel('time [s]')
ylabel('voltage [V]')
grid on
axis('tight')
-----INITIAL PARAMETERS-----
icycle=1/2; %icycle- executive window width in cycles of fundamental component
fo=50; %fundamental component 50Hz
To=1/fo; %one cycle of the fundamental component in [s]
tN=icycle*To; %executive window width in [s]
N=round(icycle*To/dt) %executive window width in [samples]
%-----
%TIME ANALYSIS - Vrms2 - peak voltage: 1-phase, high quality
%-----
%Vrms2 - vector of local rms voltage
%calculated on the basis of N samples of the signal
%High quality mode - every next Vrms2 are obtained
%by shifting the window along signal sample by sample.
%Note - first value of Vrms2 can be obtained after recording of
%assumed N samples of executive window (tN in seconds).
%Thus we should rescale time axis in Figure representing rms voltage
%starting from tN and finish with end of the signal ->t1
%For high quality mode we preserve time step in t1 as dt
for k=1:length(x)-N
    k
    n=[k:k+N-1]; %identification of windowed samples
    xn=x(n); %windowed signal samples taken for calculation of local rms
    Vrms2(k)=1/sqrt(2).* (max(abs(x(n))));
end
t2=t(N+1:length(x));
figure
h=plot(t2,Vrms2)
set(h,'LineWidth',2)
xlabel('time [s]')
ylabel('voltage magnitude [V]')
title(['Vrms2: ',num2str(icycle),'-cycle window'])
grid on
axis('tight')

```

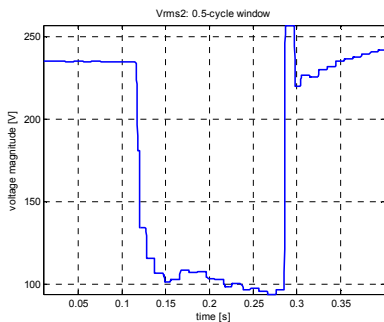
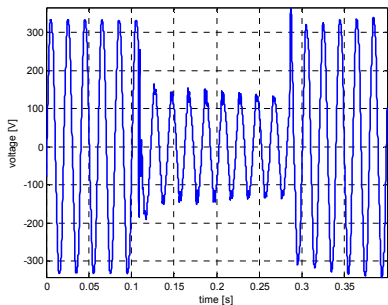


**Fig. 8.6. Investigated one-phase signal and its rms trend characteristic using half-cycle “peak voltage” method.**

**Table 8-3. Demonstration algorithm of rms trend calculation using “fundamental voltage component” method**

```

%-----SIGNAL-----
clear all, close all
load sa9_gd;
%sa9_gd.mat contain uL1 uL2 uL3 4096 samples
%fs=10240Hz
%It covers 20 cycles (period of fundamental component)
%4096 total number of samples
%2048 samples/ 10cycle
%204.8 samples/ 1cycle, round 204 sample/cycle
x=uL1;
h=plot(t,x)
set(h,'LineWidth',2);
xlabel('time [s]')
ylabel('voltage [V]')
grid on
axis('tight')
%-----INITIAL PARAMETERS-----
icycle=1/2; %icycle- executive window width in cycles of fundamental component
fo=50; %fundamental component 50Hz
To=1/fo; %one cycle of the fundamental component in [s]
tN=icycle*To; %executive window width in [s]
N=round(icycle*To/dt) %executive window width in [samples]
%-----
%FREQUENCY ANALYSIS - Vrmsfundamental voltage component
%-----
switch icycle
case 0.5
p=To/dt; %p-delta phase shift
m=[0:N-1]; %frequency axis in [binNnumber]
fanalysis=(fs*m)/(N*2); %frequency axis in [Hz]
m50=round(50*(N*2)/fs+1); %bin of 50Hz
for k=1:(length(x)-N);
k
n=[k:k+N-1]; %identification of windowed samples
xN=[x(n),-x(n)]; %special series windowed signal samples taken for FFT
localspectrumu=fft(xN,N*2);
%local complex rms voltage of fundamental component
fundamental50uc=localspectrumu(m50)*exp(-j*(2*pi/p)*(k-1))./(sqrt(2));
s1=2/(N*2); %scale factor for magnitude
real50u(k)=real(fundamental50uc).*s1; %real part of local rms voltage of fundamental component
img50u(k)=imag(fundamental50uc).*s1; %imaginary part of local rms voltage of fundamental component
s2=180/pi;%scale factor for phase in angle
phase50u(k)=(angle(fundamental50uc)+pi/2)*s2; %local phase of fundamental component as sin
end
Vrms3=sqrt((real50u).^2+(img50u).^2);
t3=t(N+1:length(x));
otherwise
p=To/dt; %p-delta phase shift
m=[0:N-1]; %frequency axis in [bin number]
fanalysis=(fs*m)/(N); %frequency axis in [Hz]
m50=round(50*(N)/fs+1); %bin of 50Hz
for k=1:(length(x)-N);
k
n=[k:k+N-1]; %identification of windowed samples
xN=[x(n)]; %windowed signal samples taken for FFT
localspectrumu=fft(xN,N);
%local complex rms voltage of fundamental component
fundamental50uc=localspectrumu(m50)*exp(-j*(2*pi/p)*(k-1))./(sqrt(2));
s1=2/(N); %scale factor for magnitude
real50u(k)=real(fundamental50uc).*s1; %real part of local rms voltage of fundamental component
img50u(k)=imag(fundamental50uc).*s1; %imaginary part of local rms voltage of fundamental component
s2=180/pi;%scale factor for phase in angle
phase50u(k)=(angle(fundamental50uc)+pi/2)*s2; %local phase of fundamental component as sin
end
Vrms3=sqrt((real50u).^2+(img50u).^2);
t3=t(N+1:length(x));
end
figure
h=plot(t3,Vrms3)
set(h,'LineWidth',2)
xlabel('time [s]')
ylabel('voltage magnitude [V]')
title(['Vrms3: ',num2str(icycle),'-cycle window'])
grid on
axis('tight')
%-----

```



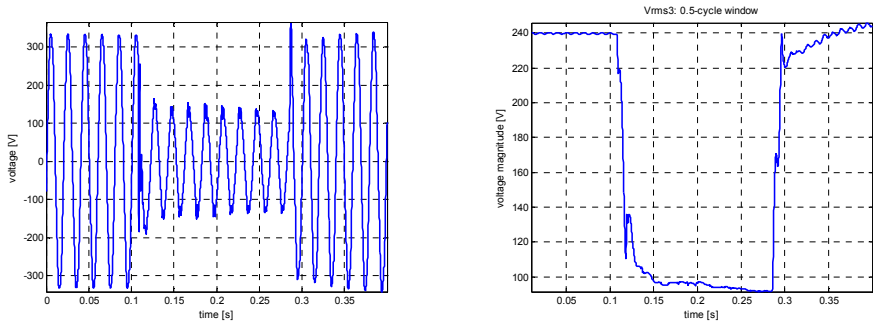


Fig. 8.7. Investigated one-phase signal and its rms trend characteristic using half-cycle "fundamental voltage component" method

### 8.3. Comparison of the methods

The comparison of the methods used in process of the rms calculation can be performed on the basis of dynamism of obtained characteristic and computational power and time consumed for calculation. Fig. 8.8 indicates the “peak value” method as a rough estimation of rms changes. This method is the fastest for calculation. The algorithm based on classical rms calculation is comparable with “fundamental component”, however a classical operation does not involve frequency domain calculation and thereby is more attractive in the point of the fast practical application.

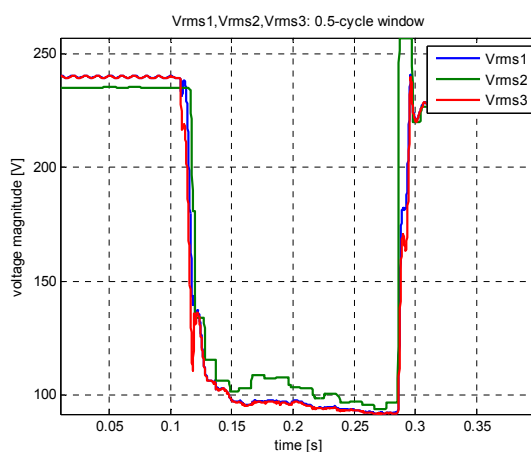


Fig. 8.8. Comparison of the “rms voltage” method (Vrms1), “peak-voltage” method (Vrms2) and “fundamental component” method (Vrms3) for given half-cycle window

The window width, usually defined as a number of cycles of fundamental component, has a crucial meaning for dynamism of rms characteristic, no matter what kind of method is applied. Fig. 8.9, Fig. 8.10, Fig. 8.11 depict a common effect of smearing and reduction of the dynamism of the characteristic when windows longer than one period of fundamental component is applied. Thus, according to the standards, a recommended base of the algorithm is half or one-period of fundamental component.

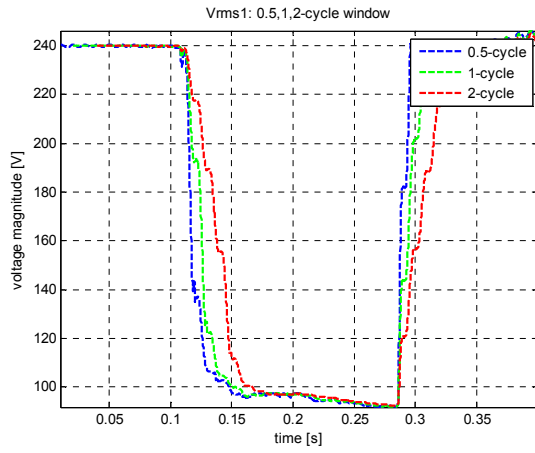


Fig. 8.9. Influence of the window width on “rms voltage” method

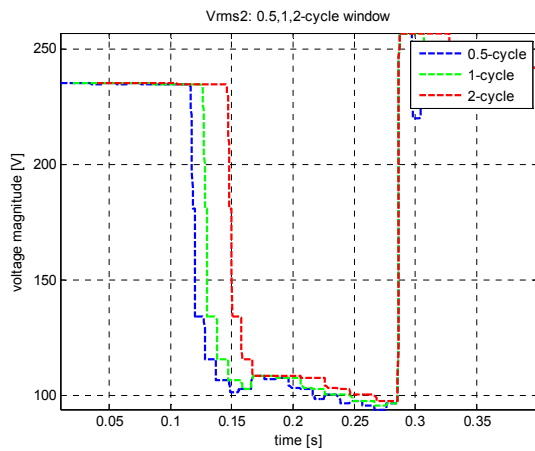


Fig. 8.10. Influence of the window width on “peak voltage” method

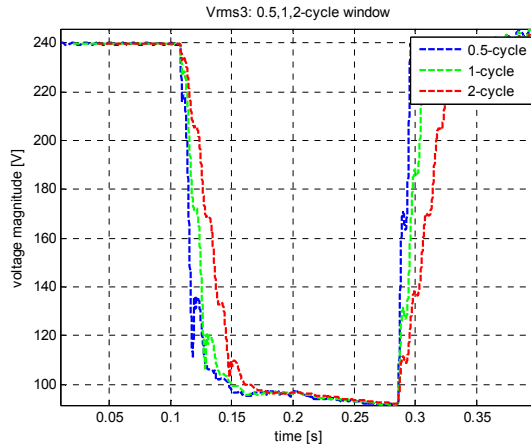


Fig. 8.11. Influence of the window width on “fundamental component” method

#### 8.4.Dip duration

Previous section was concentrated on voltage magnitude estimation during the event. The dip duration is strongly associated with the magnitude variation as a time interval when voltage magnitude is below a given threshold. Referring to the Standards, the threshold initiating dip recognition is 90% of a reference value. Having the detailed information about the recorded phenomena, its origin and voltage condition, we can select nominal value as the reference. However, there are the opinions that allow adapting measured voltage in steady state, before the event, as a reference value. From practical point of view suggested approach uses nominal voltage as reference value in order to set up the threshold.

An example of dip duration identification on the basis of one-cycle “rms voltage” algorithm is shown in Fig. 8.12. The reference value is the nominal voltage in per unit value and the reshould is setup on 90%.

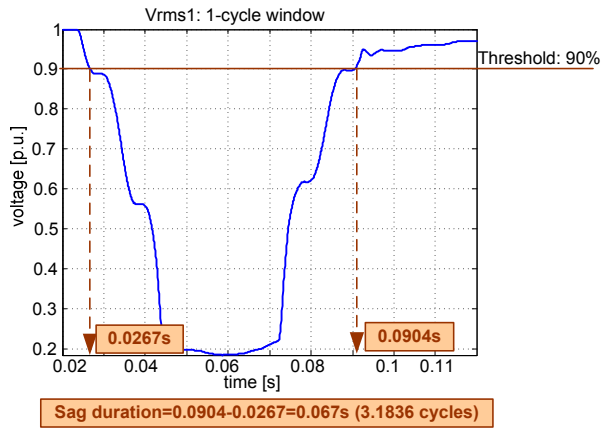


Fig. 8.12. Voltage dip duration identification

Again it must be emphasised that we stay in the high quality mode calculation. It means that estimated voltage magnitude is updated every sample. For a monitoring quality rms value will be calculated once per averaging time on the basis of selected number of half or one-cycle values.

In order to explore the dip duration identification, it is suggested to search automatically the output vectors of rms characteristic in order to indicate values which do not fulfil a given threshold. These values stay in reference to the time axis and indicate dip initiation and voltage recovery. The first activity uncovers influence of the threshold level on dip duration obtained thanks to three applied rms voltage estimation algorithm for given one-cycle window. Second activity aims to compare obtained dip duration for one-cycle window with given threshold 90%. Proposed approach can be treated as an academic off-line calculation in order to uncover the idea of the dip identification using the threshold. Normally, in on-line application, this identification is done automatically, in real time, on the basis of every new sample which does not fulfil requirements for a given threshold. Presented in this section attitude serves as comparison of the threshold level on detected duration time of the dip. Table 8-4 gives a proposition of demonstration algorithm in Matlab dedicated to an influence of a threshold on dip duration. The effects of comparison is presented in Fig. 8.13.

**Table 8-4. Demonstration algorithm applying discussed method and comparison of threshold level on dip duration**

```

%-----SIGNAL-----
clear all, close all
load sag_gd;
% sag_gd.mat contain uL1 uL2 uL3 4096 samples
% fs=10240Hz
% it covers 20 cycles (period of fundamental component)
% 4096 total number of samples
% 2048 samples/ 10cycle
% 204.8 samples/ 1cycle, round 204 sample/cycle
x=uL1;
h=plot(t,x)
set(h,'LineWidth',2);
xlabel('time [s]')
ylabel('voltage [V]')
grid on
axis('tight')
%-----INITIAL PARAMETERS-----
icyle=1/2; % icyle- executive window width in cycles of fundamental component
fo=50; % fundamental component 50Hz
To=1/fo; % one cycle of the fundamental component in [s]
tN=icyle*To; % executive window width in [s]
N=round(icyle*To/dt) % executive window width in [samples]
%-----
%-----
%TIME ANALYSIS - Vrms1- rms voltage: 1-phase, high quality
%-----
%Vrms1 - vector of local rms voltage
%calculated on the basis of N samples of the signal
%High quality mode - every next Vrms1 are obtained
%by shifting the window along signal sample by sample.
%Note - first value of Vrms1 can be obtained after recording of
%assumed N samples of executive window (tN in seconds).
%Thus we should rescale time axis in Figure representing rms voltage
%starting from tN and finish with end of the signal ->t1
%For high quality mode we preserve time step in t1 as dt
for k=1:length(x)-N
    k
    n=[k:k+N-1]; %identification of windowed samples
    xN=x(n); %windowed signal samples taken for calculation of local rms
    Vrms1(k)=sqrt(1/N*sum(xN.^2));
end
t1=t(N+1:length(x));
figure
h=plot(t1,Vrms1)
set(h,'LineWidth',2)
xlabel('time [s]')
ylabel('voltage magnitude [V]')
title(['Vrms1: ',num2str(icyle),'-cycle window'])
grid on
axis('tight')
%-----
%TIME ANALYSIS - Vrms2 - peak voltage: 1-phase, high quality
%-----
%Vrms2 - vector of local rms voltage
%calculated on the basis of N samples of the signal
%High quality mode - every next Vrms2 are obtained
%by shifting the window along signal sample by sample.
%Note - first value of Vrms2 can be obtained after recording of
%assumed N samples of executive window (tN in seconds).
%Thus we should rescale time axis in Figure representing rms voltage
%starting from tN and finish with end of the signal ->t1
%For high quality mode we preserve time step in t1 as dt
for k=1:length(x)-N
    k
    n=[k:k+N-1]; %identification of windowed samples
    xN=x(n); %windowed signal samples taken for calculation of local rms
    Vrms2(k)=1/sqrt(2).* (max(abs(x(n))));
end
t2=t(N+1:length(x));
figure
h=plot(t2,Vrms2)
set(h,'LineWidth',2)
xlabel('time [s]')
ylabel('voltage magnitude [V]')
title(['Vrms2: ',num2str(icyle),'-cycle window'])
grid on
axis('tight')

```

```

%-----
%FREQUENCY ANALYSIS - fundamental voltage component
%-----
switch icycle
case 0.5
p=To/dt; %p-delta phase shift
n=[0:N*2-1]; %frequency axis in [bin number]
fanalysis=(fs*m)/(N*2); %frequency axis in [Hz]
m50=50*(N*2)/fs+1; %bin of 50Hz
for k=1:(length(x)-N);
k
n=[k:k+N-1]; %identification of windowed samples
xN=x(n); %special series windowed signal samples taken for FFT
localspectrum=fft(xN,N*2);
%local complex rms voltage of fundamental component
fundamental50uc=localspectrum(m50)*exp(-j*(2*pi/p)*(k-1))./(sqrt(2));
s1=2/(N); %scale factor for magnitude
real50u(k)=real(fundamental50uc).*s1; %real part of local rms voltage of fundamental component
img50u(k)=imag(fundamental50uc).*s1; %imaginary part of local rms voltage of fundamental component
s2=180/pi;%scale factor for phase in angle
phase50u(k)=(angle(fundamental50uc)+pi/2)*s2; %local phase of fundamental component
end
Vrms3=sqrt((real50u).^2+(img50u).^2);
t3=t(N+1:length(x));
otherwise
p=To/dt; %p-delta phase shift
n=[0:N-1]; %frequency axis in [bin number]
fanalysis=(fs*m)/(N); %frequency axis in [Hz]
m50=50*(N)/fs+1; %bin of 50Hz
for k=1:(length(x)-N);
k
n=[k:k+N-1]; %identification of windowed samples
xN=x(n); %windowed signal samples taken for FFT
localspectrum=fft(xN,N);
%local complex rms voltage of fundamental component
fundamental50uc=localspectrum(m50)*exp(-j*(2*pi/p)*(k-1))./(sqrt(2));
s1=2/(N); %scale factor for magnitude
real50u(k)=real(fundamental50uc).*s1; %real part of local rms voltage of fundamental component
img50u(k)=imag(fundamental50uc).*s1; %imaginary part of local rms voltage of fundamental component
s2=180/pi;%scale factor for phase in angle
phase50u(k)=(angle(fundamental50uc)+pi/2)*s2; %local phase of fundamental component
end
Vrms3=sqrt((real50u).^2+(img50u).^2);
t3=t(N+1:length(x));
end
figure
h=plot(t3,Vrms3)
set(h,'LineWidth',2)
xlabel('time [s]')
ylabel('voltage magnitude [V]')
title(['Vrms3: ',num2str(icycle),'-cycle window'])
grid on
axis('tight')
%-----
%-----
vartreshold=[0.95 0.9 0.85 0.8]; %various threshold level for given icycle
%-----
for m=1:4
threshold=vartreshold(m)
durationVrms1samples=find(Vrms1<=threshold*Vrms1(1));
beginVrms1=t1(durationVrms1samples(1))
endVrms1=t1(durationVrms1samples(length(durationVrms1samples)))
durationVrms1seconds(m)=endVrms1-beginVrms1
durationVrms1cycles(m)=durationVrms1seconds(m)/To

durationVrms2samples=find(Vrms2<=threshold*Vrms2(1));
beginVrms2=t2(durationVrms2samples(1))
endVrms2=t2(durationVrms2samples(length(durationVrms2samples)))
durationVrms2seconds(m)=endVrms2-beginVrms2
durationVrms2cycles(m)=durationVrms2seconds(m)/To

durationVrms3samples=find(Vrms3<=threshold*Vrms3(1));
beginVrms3=t3(durationVrms3samples(1))
endVrms3=t3(durationVrms3samples(length(durationVrms3samples)))
durationVrms3seconds(m)=endVrms3-beginVrms3
durationVrms3cycles(m)=durationVrms3seconds(m)/To
end
h=plot(vartreshold,durationVrms1seconds,'--bs','MarkerEdgeColor','k','MarkerFaceColor','b','MarkerSize',8)
set(h,'LineWidth',2)
hold on
h=plot(vartreshold,durationVrms2seconds,'--gv','MarkerEdgeColor','k','MarkerFaceColor','g','MarkerSize',8)
set(h,'LineWidth',2)
hold on
h=plot(vartreshold,durationVrms3seconds,'--rd','MarkerEdgeColor','k','MarkerFaceColor','r','MarkerSize',8)
set(h,'LineWidth',2)
hold off
xlabel('voltage threshold')
ylabel('dip duration [s]')
title(['Vrms1,Vrms2,Vrms3: ',num2str(icycle),'-cycle window'])
legend('Vrms1','Vrms2','Vrms3')
grid on
axis('tight')
%-----

```

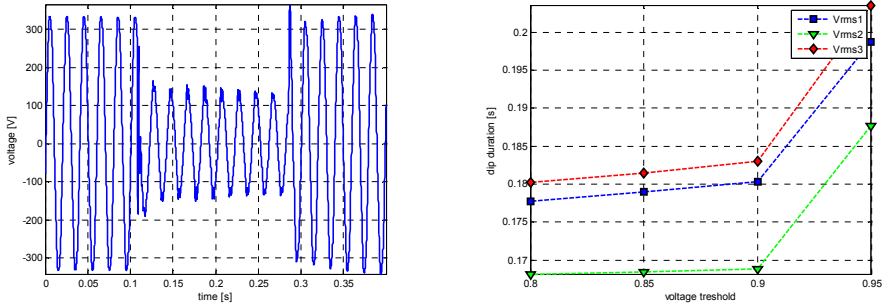


Fig. 8.13. Investigated one-phase signal and comparison of threshold level on dip duration

### 8.5. Phase-angle jump

In power systems voltage and current is a complex quantity (phasor) which has magnitude and phase. The description of such event as dips is not limited to magnitude variation but includes also phase changes. It has a meaning when we work with sensitive equipment as power converters which use phase-angle information for their firing instant. The phase-angle jump manifests itself as shift in zero-crossing of the instantaneous voltage. In order to define a phase-angle jump, we need to track a difference between a phase-angle before the event (steady state) and a phase-angle during the event. The instantaneous value of the voltage can be calculated using voltage zero-crossing method (time analysis) or from the phase of fundamental component (frequency analysis).

As it was mentioned in the previous section, the voltage “fundamental component” method introduced frequency analysis using FFT application. In a frequency domain, particular components are the complex value represented by magnitude and phase.

In a digital application, we have to consider one additional issue. In a continuous time-domain the instantaneous voltage waveform of fundamental component is considered as a rotating phasor. The rotation is described by rotation operator and consists two components: time operator  $\exp(-j\omega_0 t)$  and phase operator  $\exp(-j\psi)$ :

$$v_0(t) = V_{max} \cdot \sin(\omega_0 t + \psi) \Rightarrow \underline{V}(t) = V \cdot e^{j(\omega_0 t + \psi)} = V \cdot e^{j\omega_0 t} \cdot e^{j\psi} \quad (8.6)$$

In the point of phase tracking the most important is the phase operator. However, in the digital application using the shifting window, we introduce a rotation operator as complex



mechanism. Thus, in order to identify desirable phase operator we have to “move back” the phasor by correction  $\exp(-j\omega_0 t)$ . In a digital notice, it means  $\exp(-j*(2*\pi/p)*(k-1))$  where  $p=T_0/dt$ ,  $dt$  – sampling rate,  $T_0$  – period of fundamental component.

Table 8-5 contains a demonstration algorithm in Matlab realising a phase-angle jump assessment on the basis of fundamental phasor changes. The transition of phase-angle changes is presented in Fig. 8.14. Additionally, the influence of window width on discussed characteristic is shown in Fig. 8.15.

**Table 8-5. Demonstration algorithm applying fundamental component method for phase-angle jump calculation**

```

%-----SIGNAL-----
clear all, close all
load sa9_gd;
%sa9_gd.mat contain uL1 uL2 uL3 4096 samples
%fs=10240Hz
%It covers 20 cycles (period of fundamental component)
%4096 total number of samples
%2048 samples/ 10cycle
%204.8 samples/ 1cycle, round 204 sample/cycle
x=uL1;
h=plot(t,x)
set(h,'LineWidth',2);
xlabel('time [s]')
ylabel('voltage [V]')
grid on
axis('tight')
%-----INITIAL PARAMETERS-----
icycle=1/2; %icycle- executive window width in cycles of fundamental component
fo=50; %fundamental component 50Hz
To=1/fo; %one cycle of the fundamental component in [s]
tN=icycle*To; %executive window width in [s]
N=round(icycle*To/dt) %executive window width in [samples]
%-----
%FREQUENCY ANALYSIS - Vrmsfundamental voltage component
%-----
switch icycle
case 0.5
p=To/dt; %p-delta phase shift
m=[0:N*2-1]; %frequency axis in [bin number]
fanalysis=(fs*m)/(N*2); %frequency axis in [Hz]
m50=round(50*(N*2)/fs+1); %bin of 50Hz
for k=1:(length(x)-N);
k
n=[k:k+N-1]; %identification of windowed samples
xN=[x(n),-x(n)]; %special series windowed signal samples taken for FFT
localspectrumu=fft(xN,N*2);
%local complex rms voltage of fundamental component
s1=2/(N*2); %scale factor for magnitude
s2=180/pi;%scale factor for phase in angle
fundamental50uc=localspectrumu(m50)*exp(-j*(2*pi/p)*(k-1))./(sqrt(2)).*s1;
real50u(k)=real(fundamental50uc); %real part of local rms voltage of fundamental component
img50u(k)=imag(fundamental50uc); %imaginary part of local rms voltage of fundamental component
s2=180/pi;%scale factor for phase in angle
phase50u(k)=(angle(fundamental50uc)+pi/2)*s2; %local phase of fundamental component as sin
end
Vrms3=sqrt((real50u).^2+(img50u).^2);
t3=t(N+1:length(x));
otherwise
p=To/dt; %p-delta phase shift
m=[0:N-1]; %frequency axis in [bin number]
fanalysis=(fs*m)/(N); %frequency axis in [Hz]
m50=round(50*(N)/fs+1); %bin of 50Hz
for k=1:(length(x)-N);
k
n=[k:k+N-1]; %identification of windowed samples
xN=[x(n)]; %windowed signal samples taken for FFT
localspectrumu=fft(xN,N);
%local complex rms voltage of fundamental component
s1=2/(N); %scale factor for magnitude
s2=180/pi;%scale factor for phase in angle
fundamental50uc=localspectrumu(m50)*exp(-j*(2*pi/p)*(k-1))./(sqrt(2)).*s1;
real50u(k)=real(fundamental50uc); %real part of local rms voltage of fundamental component
img50u(k)=imag(fundamental50uc); %imaginary part of local rms voltage of fundamental component
phase50u(k)=(angle(fundamental50uc)+pi/2)*s2; %local phase of fundamental component as sin
end
Vrms3=sqrt((real50u).^2+(img50u).^2);
t3=t(N+1:length(x));
end
%-----
figure
h=plot(t3,Vrms3)
set(h,'LineWidth',2)
xlabel('time [s]')
ylabel('voltage magnitude [V]')
title(['Vrms3: ',num2str(icycle),'-cycle window'])
grid on
axis('tight')
figure
h=plot(t3,phase50u)
set(h,'LineWidth',2)
xlabel('time [s]')
ylabel('phase [deg]')
title(['phase: ',num2str(icycle),'-cycle window'])
grid on
axis('tight')
phase50uanglejump=phase50u-phase50u(1);
figure
h=plot(t3,phase50uanglejump)
set(h,'LineWidth',2)
xlabel('time [s]')
ylabel('phase-angle jump [deg]')
title(['phase-angle jump: ',num2str(icycle),'-cycle window'])
grid on
axis('tight')

```

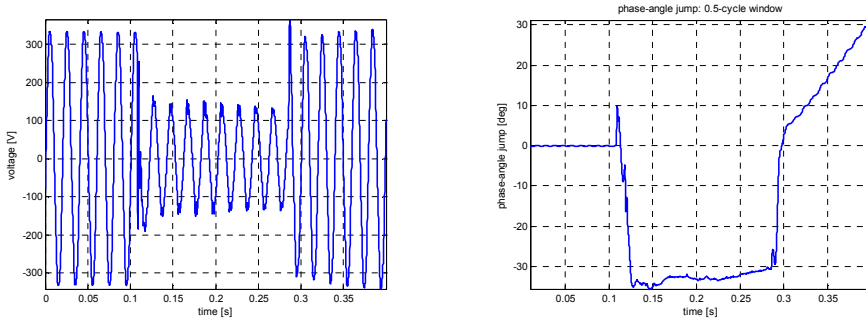


Fig. 8.14. Investigated one-phase signal and its phase-angle jump

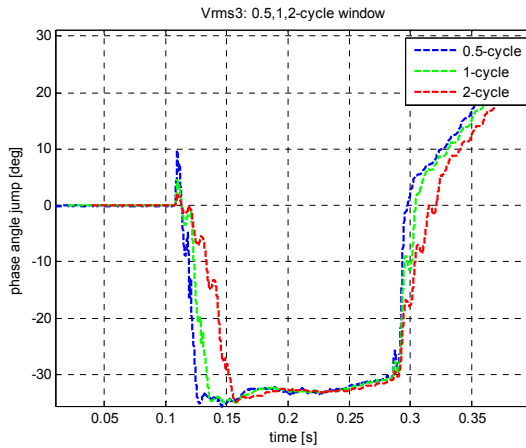


Fig. 8.15. Influence of the window width on on transition of phase-angle jump characteristic

## 8.6. Monitoring mode in voltage dips assessment

The previous sections described three algorithms dedicated to voltage magnitude deterioration: rms voltages and peak voltages, associated with a direct time analysis, and fundamental voltage component using frequency analysis. No matter what kind of method was selected to apply, the mechanism of tracking voltage along the signal, which leads to time characteristic of magnitude or phase variation in time, was the same – shifting an executive window. It means that the main algorithm responsible for magnitude estimation was applied only for a particular portion of samples, designated by the window, many times for its particular location. Finally, we have achieved many half or one-cycle local values of rms voltage associated with a position of the window along time axis. Representation of

these local rms values along the time axis gives desirable characteristic of voltage variation during the event.

Until now, we have applied high quality calculation, where the shift of the window was fine i.e. sample by sample. In a practical adaptation of the rms estimation high quality mode is too time-consuming and requires computational power. Thus, for monitoring mode, we often reintroduce the ideas of rms algorithms as the rms value is calculated once per cycle and can be grouped and averaged in interval of 200ms or 10 minutes [3],[4],[6]. In a monitoring mode the shift is "fat" i.e. window by window with an optional averaging period or not. Please notice that this time, the first value of estimated rms voltage is localized in time moment equals  $N*dt$  where  $dt$  is the sampling rate. The next points of desirable rms voltage characteristic are calculated on the basis of fragments of the recorded data, designated by shifting cycle-by-cycle window. Thus, we need to recalculate the time axis using "fat" time step  $N*dt$ ,  $t=[N*dt, 2*N*dt, ..., k*N*dt...]$ . The description of the idea is depicted in Fig. 8.16. In comparison with Fig. 8.3, we can observe rough estimation, that however saves the computational power for calculation.

Additionally, the averaging time is introduced concerning one value for selected numbers of cycles (half-cycles) i.e. 200ms averaging time means that we achieve one value of rms from 10 one-cycle values or 20 half-cycles values [3],[4],[6].

In order to close the idea, Table 8-6 and Fig. 8.17 show demonstration algorithm or classical rms calculation working in a monitoring mode without additional averaging. To understand the difference between high-quality and monitoring mode, we recommend comparing Fig. 8.17 and Fig. 8.5.

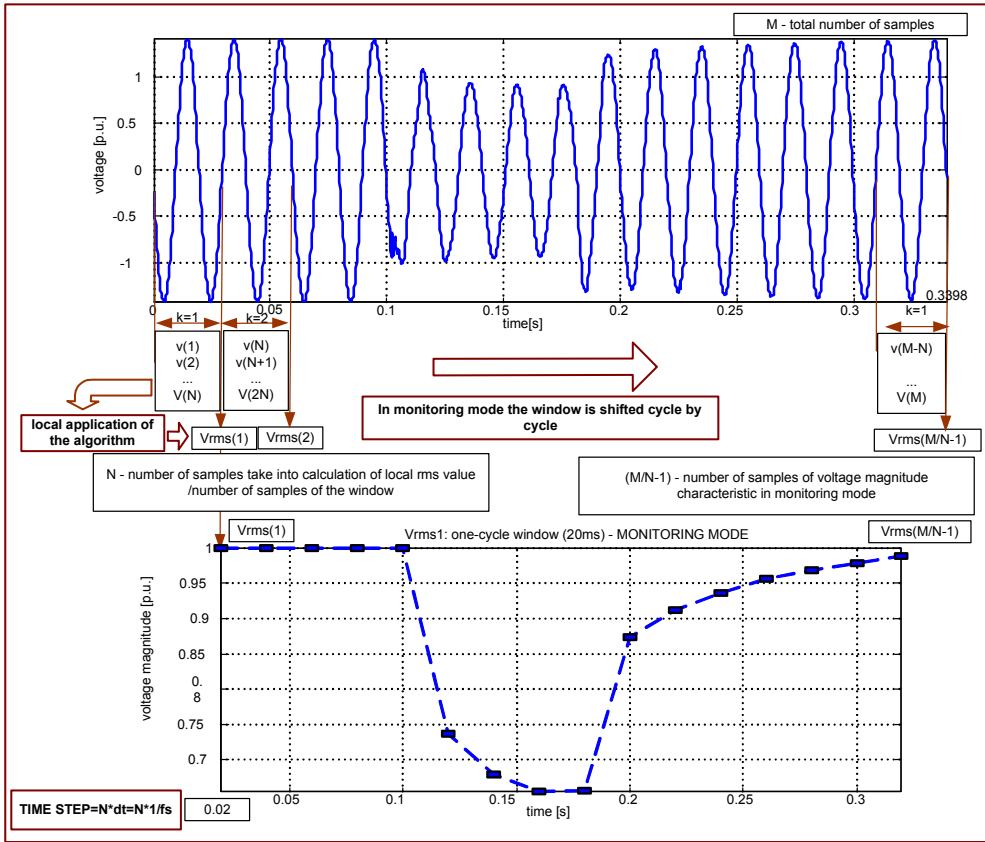


Fig. 8.16. Mechanism of rms voltage characteristic in monitoring mode without averaging

**Table 8-6. Demonstration algorithm applying classical rms calculation method in monitoring mode without additional averaging**

```

%-----SIGNAL-----
clear all, close all
load sa9_gd;
%sa9_gd.mat contain uL1 uL2 uL3 4096 samples
%fs=10240Hz
%It covers 20 cycles (period of fundamental component)
%4096 total number of samples
%2048 samples/ 10cycle
%204.8 samples/ 1cycle, round 204 sample/cycle
x=uL1;
h=plot(t,x)
set(h,'LineWidth',2);
xlabel('time [s]')
ylabel('voltage [V]')
grid on
axis('tight')
%-----INITIAL PARAMETERS-----
icycle=1; %icycle- executive window width in cycles of fundamental component
fo=50; %fundamental component 50Hz
To=1/fo; %one cycle of the fundamental component in [s]
tN=icycle*To; %executive window width in [s]
N=round(icycle*To/dt) %executive window width in [samples]
%-----
%TIME ANALYSIS - Vrms1- rms voltage: 1-phase, monitor mode
%-----
%Vrms1 - vector of local rms voltage
%calculated on the basis of N samples of the signal
%High quality mode - every next Vrms1 are obtained
%by shifting the window along signal sample by sample.
%Note - first value of Vrms1 can be obtained after recording of
%assumed N samples of executive window (tN in seconds).
%Thus we should rescale time axis in Figure representing rms voltage
%starting from tN and finish with end of the signal ->t1
%For high quality mode we preserve time step in t1 as dt
%For monitoring mode time step equals number of cycles -> window by widnow
l=1; %monitoring mode storage initial
for k=1:N:length(x)-N
    k
    n=[k:k+N-1]; %identification of windowed samples
    xn=x(n); %windowed signal samples taken for calculation of local rms
    Vrms1(l)=sqrt(1/N*sum(x(n).^2));
    l=l+1;
end
t1=t(N+1:N:length(x));
figure
h=plot(t1,Vrms1,'--bs','MarkerEdgeColor','k','MarkerFaceColor','b','MarkerSize',8)
set(h,'LineWidth',2)
xlabel('time [s]')
ylabel('voltage magnitude [p.u.]')
title(['Vrms1: ',num2str(icycle),'-cycle window'])
grid on
axis('tight')
%-----

```

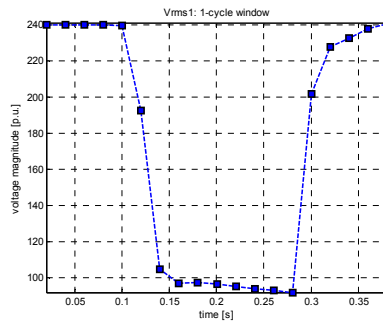
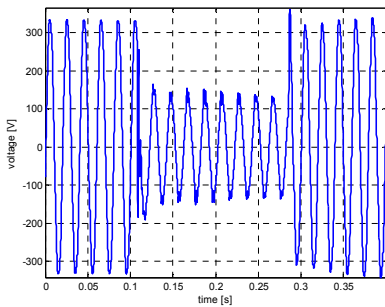


**Fig. 8.17. Investigated one-phase signal and its rms trend using one-cycle classical rms algorithm in monitoring mode without additional averaging**

## 8.7. Dip transfer in power systems

The prominent number of dips in power systems comes from short-circuit faults which can appear in a different level of the system structure: transmission system faults, remote distribution systems faults, local distribution system faults. Other origins of the dips may have their sources in a starting process of large motors, short interruption and fuses [1],[2],[3],[4].

According to the standards, dips can be entirely defined by the magnitude and duration. Considering the duration of dips, we can distinguish self-decaying events and events determined by fault-clearing equipments. Generally speaking, the faults in transmission systems are cleared faster than faults in distribution systems. In transmission systems, the critical fault-clearing time is rather small. Thus, fast protection and fast circuit breaker are essential. Also transmission and subtransmission systems are normally operated as a grid, requiring a distance protection or a differential protection, both of which are rather fast. The principal form of a protection in distribution systems are overcurrent protection. This often requires some time-grading which increases the fault –clearing time. An exception constitutes systems in which current-limiting fuses are used that have the ability to clear a fault within one half-cycle [1],[2],[3],[4].

The drop of rms voltage during the dips depends on a few conditions. One of the crucial issue is relation between the location of the fault and the location of observation in the system structure i.e. point of common coupling (PCC). A general rule indicates significant influence of the dips on the customers grouped at the same level of voltage as appearing fault. Further distribution of the dip depends on the location of the fault in the system structure and the presence of the impedance of the transformer. Thus, a short-circuit fault in local distribution networks (medium or low voltage) typically leads to deep dips whpse injury every customer grouped in near regions. This is due to small impedance taken into consideration which comes only from impedance of distribution feeders often with limited length. These dips will not cause much voltage drop for the customers fed at the sub-transmission and transmission level. The impedance of the transformers between the distribution and subtransmission, and further, between the sub-transmission and transmission level are large enough to considerably limit the voltage drop at the high voltage side of the transformer. However, the fault in the sub-transmission system will cause a deep dip in the subtransmission substation and for all customers fed from this substation. The

dips will be visible at every lower voltage side of the substation. Customers working on the transmission voltage level will experience a shallow dip, again due to the transformer impedance. Finally, the fault in the transmission system will cause a serious dip for fed substations bordering the faulted line. This dip is then transferred down to all customer fed from these substations [1],[2],[3],[4].

In order to emphasize mentioned general rules of the dips transfer in the power systems, we have attached an example of the power network with possible fault position Fig. 8.18 and the table of scenarios dedicated to dips influence Table 4-1. It must be mentioned that given characterization has a general nature and does not include some specific situations as distributed generation.

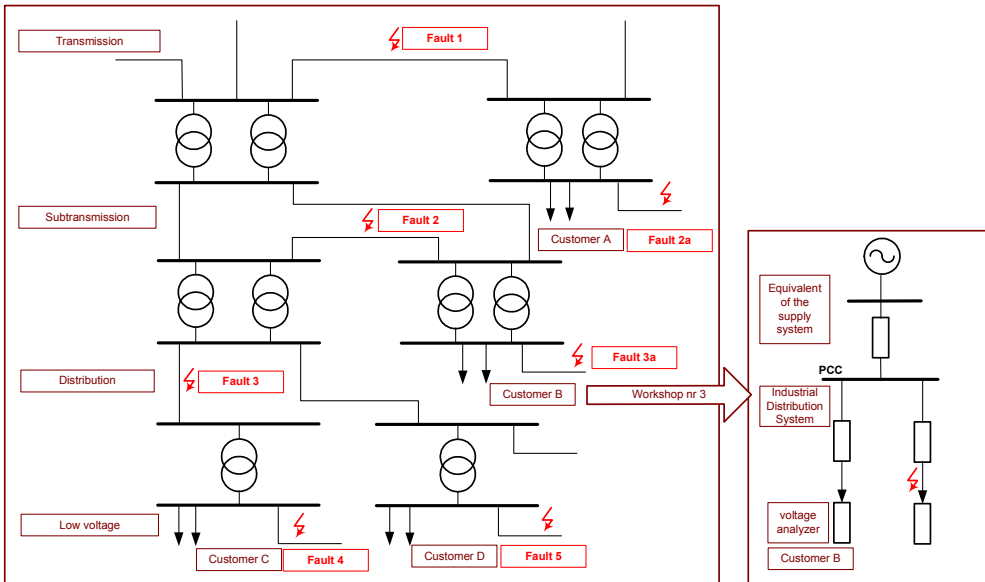


Fig. 8.18. Example of power network with possible fault position scenarios dedicated to general dips transfer



Table 8-7 Possible scenarios of dips transfer in power systems from Fig. 8.18 referring to fault position

	Label 8.18	Fig.	Customer A	Customer B	Customer C	Customer D
Transmission	Fault 1		deep dip	deep dip	deep dip	deep dip
Subtransmission	Fault 2		not much	deep dip	deep dip	deep dip
Subtransmission/ industrial network	Fault 2a		deep dip	not much	not much	not much
Distribution	Fault 3		not much	not much	deep dip	deep dip
Distribution/ industrial network	Fault 3a		not much	deep dip	not much	not much
Distribution utility network	Fault 4		rather notice	not rather notice	not deep dip	shallow dip
Distribution utility network	Fault 5		rather notice	not rather notice	shallow dip	deep dip

As an example, we would like to consider an often met scenario – a fault in a local distribution network. Range of the investigation is scoped around influence on “neighbour” customer. It corresponds to scenario **Fault 3a** from Fig. 8.18 and Table 4-1, where measurements are localized at customer, fed by a feeder without the fault. Considering the mentioned scenario, we can scope on some details as influence of the local parameters on character of the dips observed by the customer, especially relation between the dips and length of the faulted feeder as well as relation between the dips and kind of fault. The aim of the activities is to familiarize with a selected origin of the dips. In order to perform the investigations we have prepared the model of the simplified diagram of the network illustrated in Fig. 8.19. Presented here diagram was modelled in Matlab (R13 6.5) Simulink environment using SimPowerSystem Blockset [7] ,[8]. The model is available at <http://eportal.eny.pwr.wroc.pl/> .

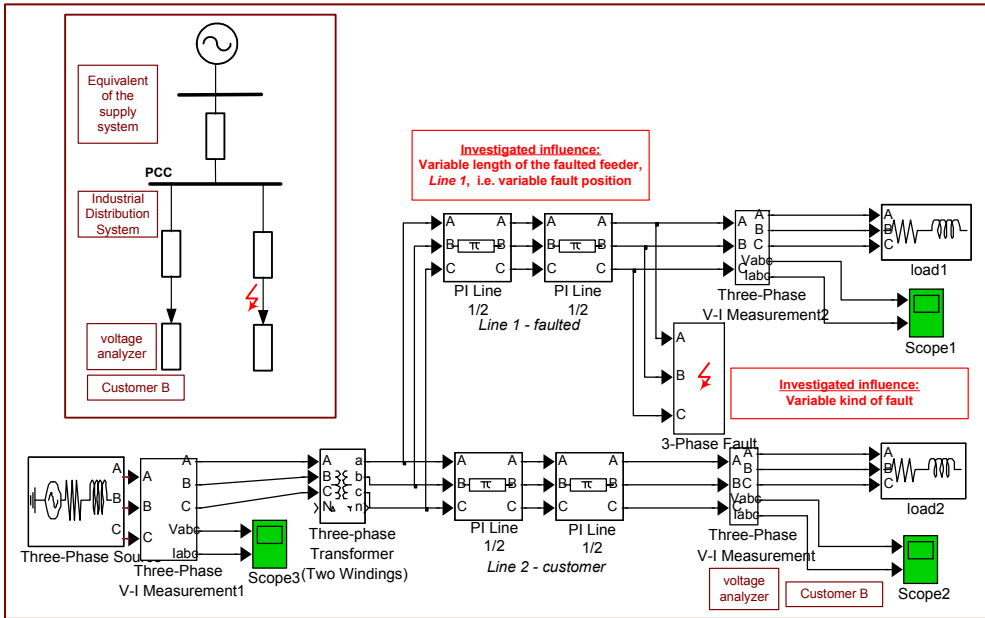


Fig. 8.19. Simplified diagram of the investigated network and its model in Simulink SimPowerSystem Blockset

The system is described by an initial short-circuit apparent power 3GVA and a voltage level of 110 kV. The transformer is a two-winding (delta-wye-isolated) 110/15-kV distribution transformer with a nominal power 10MVA. L1 and L2 are typical overhead lines. Both lines supply the RL loads. The line 2 has a 5km length and fed observed industrial customer. In a point of numerical reasons, the lines are modeled as two Pi-line components. The short circuit occurs at the end of the line L1.

The investigation is aimed at:

- the influence of the length of **Line 1 (faulted line)** on the dips injured Customer B: suggested range  $L1=1\text{km}$ ,  $L1=5\text{km}$ ,
- the influence of the **kind of fault** on the dips injured Customer B: suggested range – A-GND one-phase fault with ground, A-B two-phase fault.

The investigated signals comes from the observation made by Customer B. In model it is realized by *Scope 2*. Setup of the Scope considers sample time  $2e-4\text{s}$  (0.2ms). For a digital calculation, it is very important information which allows defining sampling frequency  $f_s=1/(0.2\text{ms})=5\text{kHz}$ . The time axis is automatically saved in workspace. Selected range of the observation is (0-0.6s).

As an example Fig. 8.20 represents the character of the dip for the same kind of a fault, A-GND, but for different fault location  $L_1=1\text{km}$  vs  $L_1=5\text{km}$ . Estimation method utilizes classical rms definition in high-quality mode.

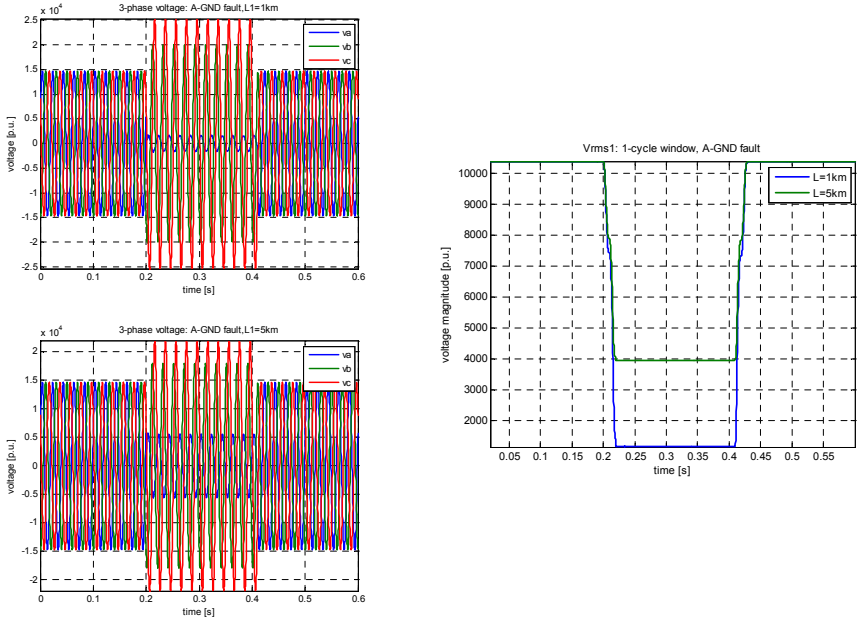


Fig. 8.20. Influence of distance of faulted line on observed dip in grid point in neighbour line

Fig. 8.21 depicts the influence of the kind of fault in faulted line on observed dip in grid point in neighbour line for the same length of faulted line which equals 1km. Estimation method utilizes classical rms definition in high quality mode.

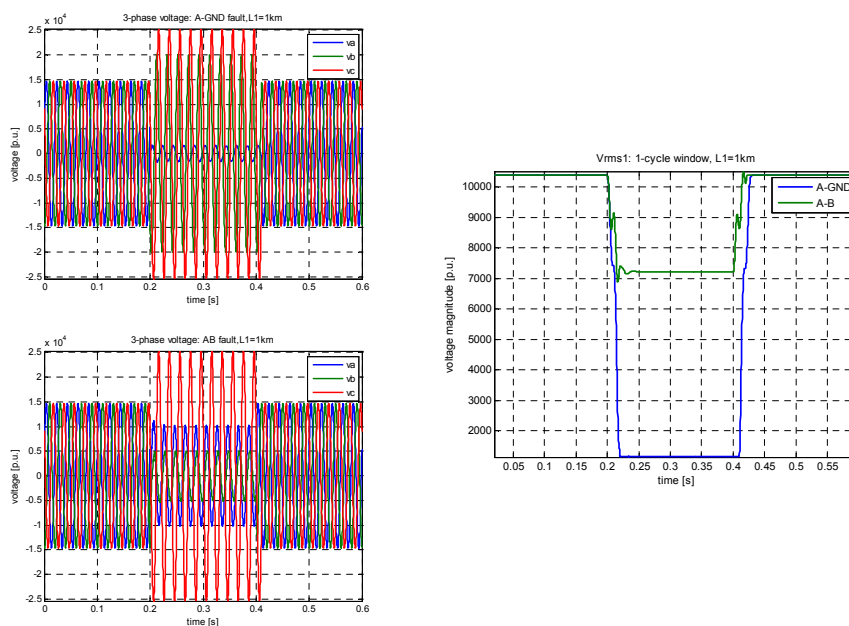


Fig. 8.21. Influence of kind of fault in faulted line on observed dip in grid point in neighbour line

## 8.8.Literature

- [1] Bollen M.H.J., *Understanding Power Quality Problems. Voltage sags and interruptions*, IEE Press Series on Power Engineering, 2000.
- [2] Dugan R. C. et al, *Electrical Power Systems Quality*, McGraw-Hill, 2004.
- [3] Sankaran C., *Power Quality*, CRC Press, 2002.
- [4] *Power Quality Application Guide. Chapter 5. Voltage Disturbances*. The European Copper Institute, Leonardo da Vinci European Program on Power Quality Assessment.
- [5] Łobos T., Sikorski T., Amaris H., Alonso M., Florez D., *Classical and alternative methods to voltage quality monitoring*, Computer Application in Electrical Engineering, Poznan, 2009.

- [6] IEC 61000-4-30:2008, *Electromagnetic compatibility (EMC): Testing and measurement techniques -Power quality measurement method*.
- [7] *SimPowerSystems User's Guide*. The Math Works Inc., 2006.
- [8] P. Janik, *Charakterystyka zakłóceń jakości energii elektrycznej za pomocą zaawansowanych metod analizy sygnałów*, in Polish, Ph.D. Thesis, 2005.

## 9. Computational application of power quality assessment: harmonics

The previous chapter was dedicated to dips assessment, as the representative of events. It is worth emphasising that main division of power quality disturbances includes events as well as variations. Events are sudden disturbances with a beginning and an ending. To measure the events, triggering process must be involved, usually using a threshold. Variations are steady-state or quasi-steady-state disturbances that require continuous measurements.

With reference to more classical power engineering, the measurement of variations is similar to metering of the energy consumption (i.e., continuous), whereas the measurement of events is similar to the functioning of a protection relay (i.e., triggered). Neglecting the purpose of the measurements, every process of quantification starts from devices responsible for voltage and current measurements. The difference is in the further processing and application of the measured signals. The results of power quality monitoring are not used for any automatic intervention in the system. Exceptions are the measurements as part of power quality mitigation equipment, but such equipment is more appropriately classified as protection or control equipment. Fig. 9.1 depicts a general scheme of power quality measurements with distinction between variation and event .

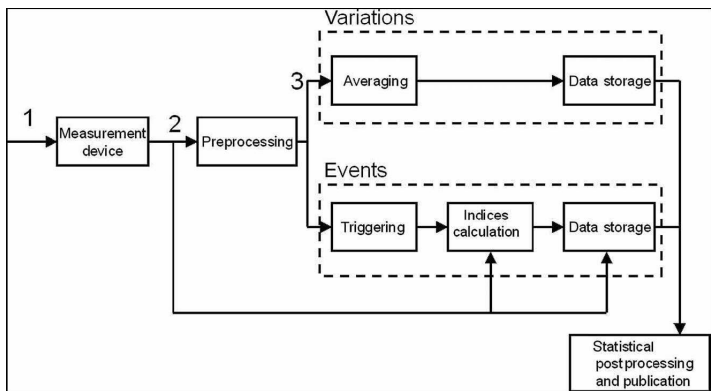


Fig. 9.1. General scheme of power quality measurements: (1) voltage or current in system; (2) sampled and digitized voltage or current; (3) quantity for further processing [2]

This chapter is dedicated to variations. The process of variations assessment requires calculation of appropriate characteristics. This may be the rms voltage trend, the frequency trend or the

spectrum. Due to a continuous character of measurement some averaging conditions over a certain interval must be introduced. The calculation of rms-voltage, the frequency or the spectrum in high-quality mode would generate huge number of data with high requirements for data storage and computational power. Thus, for variations much more practical approach consider monitoring-mode with additional parameter called averaging time. For example, if averaging time equals 200ms i.e. 10 periods of fundamental 50Hz component, we achieve one averaged value of rms from ten one-cycles values, or one estimated frequency value from 10-cycle, or at least one spectrum obtained on the basis of 10-cycle [1],[2].

The standard document IEC 61000-4-30 [4] prescribes the following intervals: 10 or 12 cycles, 150 or 180 cycles, 10 min, and 2 h. Some monitors use different window lengths. Some monitors also give maximum and minimum values obtained during each interval. Some monitors do not take the average of the characteristic over the whole interval but a sample of the characteristic at regular intervals, for example, the spectrum obtained from one cycle of the waveform once every 5 min. Further postprocessing consists of the calculation of representative statistical values (e.g., the average or the 95 percentile) over longer periods (e.g., one week) and over all monitor locations. The resulting values are referred to as site indices and system indices, respectively [2].

### **9.1.Harmonics distortion and Fourier series parameterization**

Waveform distortion includes all deviations of the voltage or current waveform from the ideal sine wave. But variations in magnitude and frequency are not considered as waveform distortion although a complete distinction between the different types of variations is not possible. A number of different forms of waveform distortion can be distinguished:

- harmonic,
- interharmonic,
- nonperiodic distortion.

In most studies, only the harmonic distortion is considered. Nonharmonic distortion (interharmonics and nonperiodic distortion) is much harder to quantify through suitable parameters and it is regularly neglected. Another reason for neglecting nonharmonic distortion is that harmonic distortion dominates in most cases. Coming back to the harmonics we can distinguish odd-harmonics and even-harmonics. The odd-harmonics manifests itself symmetrically for the positive and negative half of sine wave. Odd-harmonic distortion is typically dominant in supply voltage and load current. The result of even-harmonic distortion is that positive and

negative half-cycles of the signal are no longer symmetrical. Even-harmonic distortion of voltage or current is normally rather small.

The measurement of harmonic distortion is defined in two IEC standards: IEC 61000-4-7 [5] and IEC-61000-4-30 [4]. The first one defines the way in which harmonic current distortion shall be measured when comparing equipment emission with the emission limit. The latter document defines the way in which voltage quality shall be measured.

According to the IEC standards, the Fourier series shall be obtained over a rectangular window with a length equal to 10 cycles in a 50-Hz system and equal to 12 cycles in a 60-Hz system. However we have to realize that the measurement systems may use different sampling rate. Thus, given 10-cycle interval would contain different number of samples, more for high sampling rate, and less for low sampling rate. Here it is worth noticing that in pair with condition given by IEC runs IEEE document IEEE Standard Common Format for Transient Data Exchange (COMTRADE) for Power Systems [6]. This document gives some hints for sampling rate and number of samples in one-cycle of basic components, that can be easily recalculate for 10 cycles, Fig. 9.2.

Samples/cycle	$f$ for 60 Hz	$f$ for 50 Hz
384	23040	19200
192	11520	9600
128	7680	6400
96	5760	4800
64	3840	3200
48	2880	2400
32	1920	1600
24	1440	1200
16	960	800
12	720	600
8	480	400
6	360	300
4	240	200

Samples/cycle	$f$ for 60 Hz	$f$ for 50 Hz
3200	192000	160000
1600	96000	80000
800	48000	40000
640	38400	32000
400	24000	20000
320	19200	16000
200	12000	10000
160	9600	8000
128	7680	6400
100	6000	5000
80	4800	4000
64	3840	3200
50	3000	2500
40	2400	2000
32	1920	1600
20	1200	1000
16	960	800
10	600	500
8	480	400
4	240	200

Fig. 9.2. Sampling rates for 50Hz system and 60Hz system with its relations to number of samples in one-cycle of fundamental component [6]

The assessment of the harmonic and interharmonic distortion is based on the discrete Fourier spectrum. The output of the discrete Fourier transform consists of a number of frequency



components, both harmonics and interharmonics. The efficient assessment of the spectrum requires some initial calculation and preparation in order to associate the output of Fourier series with signal parameters. Main activities are scoped around frequency bin specification. An undermentioned example shows a required initial calculation so that performed Fourier series might have a physical meaning.

Example: initial calculation for Fourier series parameterization

**Given:** sampling rate  $f_s=4kHz$ , system  $f_0=50Hz$ , interval 10-cycle

**Searched:** a number of samples in the interval and a total number of frequency bins  $N=?$ , frequency resolution of DFT algorithm  $dfF=?$ , frequency axis  $f=[...]$ , maximum order of harmonics  $H=?$ , frequencies of particular harmonics  $hf$ , index of the harmonics at the frequency axis  $nfch=[...]$ .

Answer:

Referring to Fig. 9.2 for given sampling rate  $f_s=4kHz$  we have 80 samples per fundamental component 50Hz.

The interval includes 10 cycles, thus for a calculation of DFT we take  $N=10 \times 80=800$  samples.

Frequency resolution is then  $dfF=f_s/N=4000/800=5Hz$ .

According to “Nyquist theory” frequency observation range is limited to  $1/2 f_s=2kHz$ . Thus, we can generate the frequency bins for the frequency axis  $f=[0:dfF: 1/2 f_s]=[0:5:2000]$  – length of frequency axis is 401 bins.

Please notice that total number of frequency bins is  $N=800$  and the length of frequency observation is limited to 401 bins. Remember that performing the DFT, you achieve the information about positive and negative part of frequency axis. **For the real signal the spectrum is symmetrical and desirable information of the spectrum can be reached from the positive part of frequency axis – in case of DFT algorithm it is first  $N/2+1$  elements.**

Maximum order of harmonics can be calculated as  $H=(1/2f_s)/f_0=2000/50=40$ .

Frequencies of particular harmonics  $hf=[1:1:H]*f_0=[50,100,150....2000]$  in Hz.

Index of the harmonics in the linear spectrum  $nfch=([1:1:H]*f_0/dfF)+1=[11,21, ..., 401]$

Finally, frequency bin is characterised which depicts Fig. 9.3.

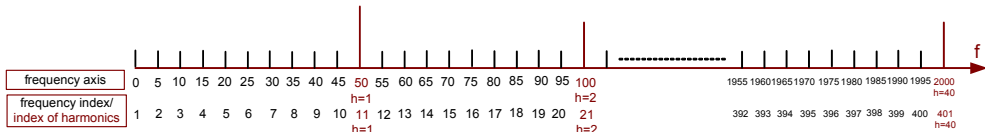


Fig. 9.3. Example of frequency bins characterisation

Some additional comments:

The result of applying the DFT is a spectrum with 5-Hz spacing between frequency components. The spectrum thus contains both harmonics and interharmonics.

We can distinguish the spectrum estimation for voltage and current. The voltage quality is how the network affects the customer or the load; the current quality is how the customer or load affects the network. A similar distinction holds for waveform distortion: the distorted voltages affect the customer equipment; distorted currents affect the network components.

## **9.2. Investigated phenomena**

Main activities in this chapter are concentrated on the investigation of waveform distortion caused by very specific non-linear load which is dc-arc furnace. An electric arc furnace (EAF) is a furnace that heats charged material by means of an electric arc. Arc furnaces range in size from small units of approximately one ton capacity (used in foundries for producing cast iron products) up to about 400 ton units used for secondary steelmaking. Arc furnaces used in research laboratories and by dentists may have a capacity of only a few dozen grams. Electric arc furnace temperatures can be up to 1,800 degrees Celsius. Arc furnaces differ from induction furnaces in that the charge material is directly exposed to the electric arc, and the current in the furnace terminals passes through the charged material. A typical dc arc furnace plant and an example of practical realization is shown in Fig. 9.4.

From the electrical point of view, a furnace plant consists of dc arc furnace connected to a medium voltage ac busbar with two parallel thyristor rectifiers that are fed by transformer secondary winding with  $\Delta$  and Y connection, respectively. The medium voltage busbar is connected to the high voltage busbar with a HV/MV transformer whose windings are Y- $\Delta$  connected. The power of the furnace is 80 MW. The other parameters are: transformer  $T_1$ -80 MVA, 220kV/21kV; transformer  $T_2$ - 87 MVA, 21kV/0.638kV/0.638kV. Some filters are provided in the plants.

In the dc arc furnace, the presence of the ac/dc static converter and the random motion of the electric arc, whose non linear and time-varying nature is known, are responsible for dangerous perturbations, in particular waveform distortions and voltage fluctuations. In particular, the behaviour of the DC arc furnace can lead to the aperiodicity of AC electrical quantities, namely voltage and current at MV busbar. The phenomena correlated to the arc behavior are very complex. In [7],[8] it has been shown that the DC arc voltage waveform has the aperiodic and

irregular behaviour that characterizes every chaotic phenomenon. As an example, Fig. 9.5 shows an example of current waveform and voltage waveform at MV busbar.

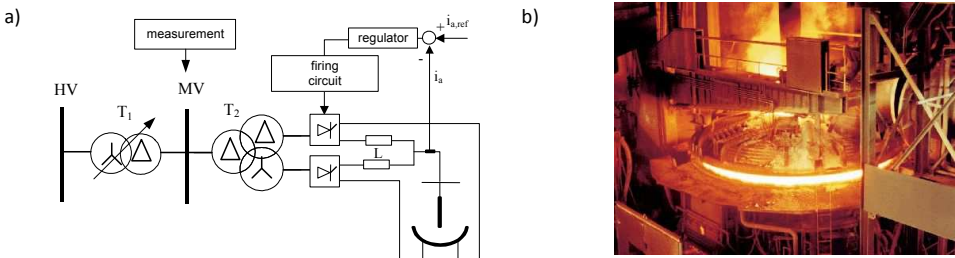


Fig. 9.4. Dc-arc furnace plant (a) and an example of practical realization of arc furnace (b)

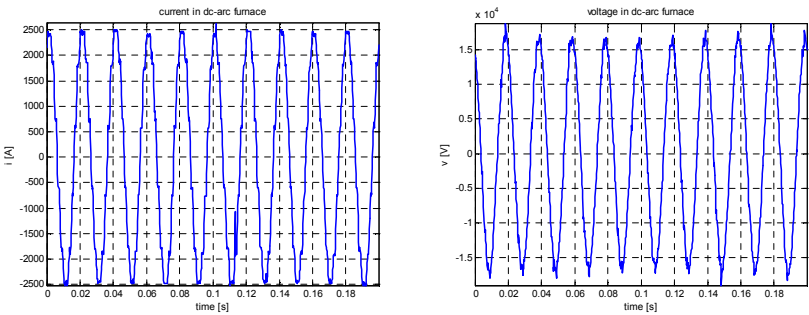


Fig. 9.5. Fragments of current and voltages at MV busbar of dc-arc furnace plant [7],[8]

10-cycle interval of one-phase current ( $i$ ) and voltage ( $u$ ) at MV busbar, with sampling rate equals 5kHz is stored in `DCArcFurnacemeasure0_02.mat`. This file contains also some additional utilizing parameters as: time vector ( $t$ ), sampling rate  $f_s=5kHz$ , and time step (time resolution) ( $dt=1/f_s$ ). The file is available at <http://eportal.eny.pwr.wroc.pl/>

### 9.3. “Linear” spectrum estimation using FFT:

Spectrum estimation is considered as a digital representative of continuous “linear” spectrum, which includes whole spectrum components, including harmonics and interharmonics. Table 9-1 consists of demonstration algorithm applying FFT in Matlab in order to calculate the spectrum of the voltage in example of investigated dc-arc furnace plant.

**Table 9-1. Demonstration algorithm applying FFT in order to reveal “linear” spectrum**

```

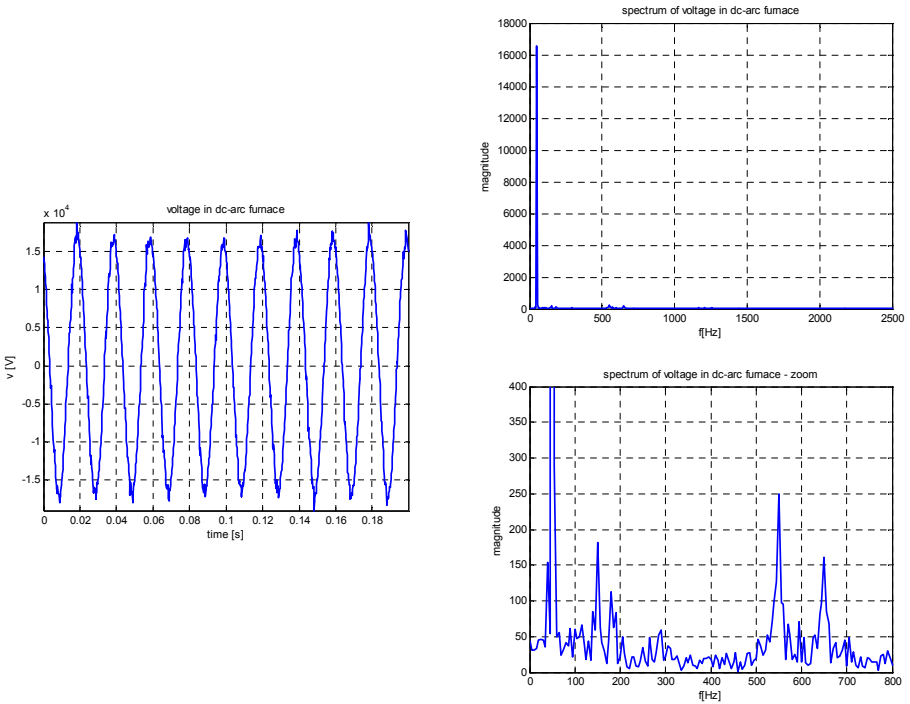
%-----SIGNAL-----
clear all, close all
cd ..
cd Data
load DCArcFurnacemeasure0_02.mat;
cd ..
cd Programs
%file contains 10-cycles 50Hz of dc-arc furnace measured signals:
%sampling rate fs=5KHz;
%Thus we have 100 samples per cycle
% and 1000 total number of samples in 10 cycles
%i - current,
%u - voltage,
%Additionally:
%fs=5000; [Hz] - sampling rate
%dt=1/fs; [s] - sampling interval
%t-time vector [0:dt:0.2-dt];

x=u;
disp('-----ANALYSED SIGNAL-----')
disp(' ')
disp('CONFIRMATION OF SAMPLED DATA:')
disp(['Sampling frequency fs=',num2str(fs),' Hz'])
disp(['Time step dt=',num2str(dt),' s'])
disp(['End of signal in samples:',num2str(length(x)),''])
disp(['End of signal in seconds:',num2str(length(x)*dt),' s'])
figure
h=plot(t,x);
set(h,'LineWidth',2);
xlabel('time [s]')
ylabel('u [V]')
title('voltage in dc-arc furnace')
grid on
axis('tight')

%-----
%-----INITIAL PARAMETERS-----
f0=50; %[Hz]; %fundamental component
N=length(x); %number of frequency bins
dfF=fs/(N); %frequency resolution
%-----
%-----FREQUENCY ANALYSIS-----
X=fft(x,N); %Fourier spectrum (positive and negative frequencies)
X_amp=abs(X)*(2/N); %magnitude spectrum with scaling factor
X_amp_positive=X_amp(1:1:N/2+1); %magnitude spectrum only for positive f
f_positive=dfF*(0:1:N/2); %positive f
%full range of frequency observation 0-fs/2Hz
fc1=0;
fc2=fs/2;
nfc1=round(fc1/dfF)+1;
nfc2=round(fc2/dfF)+1;
figure
h=plot(f_positive(nfc1:nfc2),X_amp_positive(nfc1:nfc2));
set(h,'LineWidth',2);
xlabel('f [Hz]')
ylabel('magnitude');
%title('spectrum of current in dc-arc furnace')
title('spectrum of voltage in dc-arc furnace')
grid on;
%zoom in frequency 0-800Hz
fc1=0;
fc2=800;
nfc1=round(fc1/dfF)+1;
nfc2=round(fc2/dfF)+1;
%zoom in magnitud 0-400
Ampc1=0;
Ampc2=400;
figure
h=plot(f_positive(nfc1:nfc2),X_amp_positive(nfc1:nfc2));
set(h,'LineWidth',2);
xlabel('f [Hz]')
ylabel('magnitude');
%title('spectrum of current in dc-arc furnace - zoom')
title('spectrum of voltage in dc-arc furnace - zoom')
axis([fc1, fc2, Ampc1, Ampc2])
grid on;
%-----

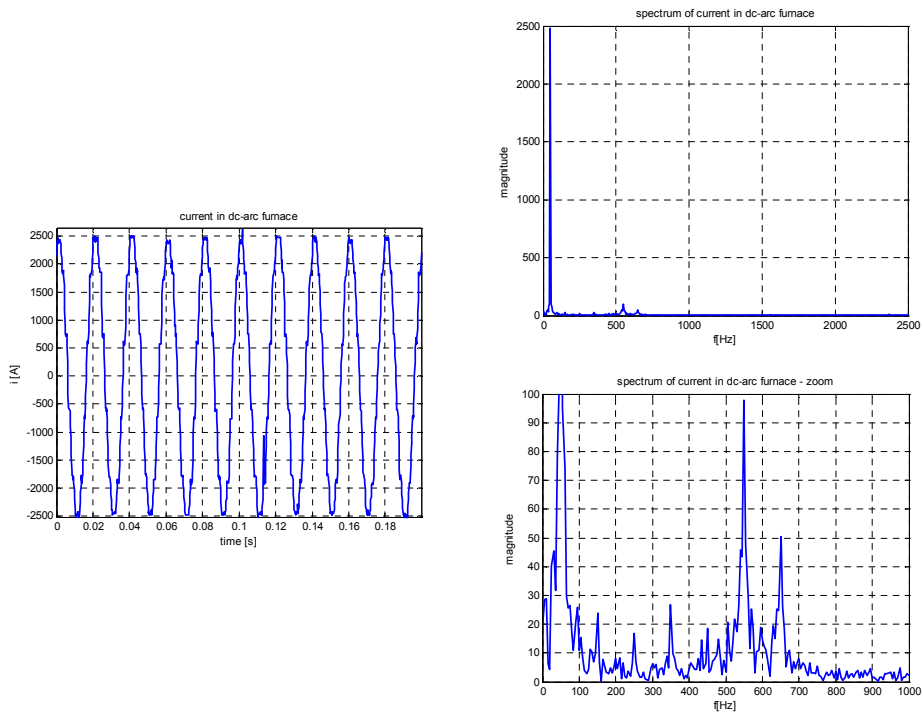
```

After calculation of FFT we obtain a set of the frequency component concentrated on every 5Hz frequency bin including its magnitude and phase. Fig. 9.6 and Fig. 9.7 shows magnitude spectrum of voltage and current, respectively. The next activities in assessment of the frequency component is separation of harmonics and interharmonics.



zoom:(0-400)V – (0-800)Hz

Fig. 9.6. Investigated one-phase voltage signal in dc-arc furnace plant and its “linear” spectrum using FFT



zoom:(0-100)A – (0-800)Hz

Fig. 9.7. Investigated one-phase current signal in dc-arc furnace plant and its “linear” spectrum using FFT

#### 9.4. Harmonics and subdivision into even and odd harmonics

The output of the discrete Fourier transform consists of a number of frequency components, both harmonics and interharmonics. However, the harmonics are only the integral multiplication of fundamental component: 1-st harmonic is 1\*50Hz, 2-nd harmonic is 2\*50Hz, 3-rd harmonic is 3\*50Hz etc. Additionally, the harmonics can be subdivided into even and odd harmonics. Even-harmonic distortion of voltage or current is normally rather small. In many cases odd-harmonics have significant meaning.

Literature provides an additional index in order to depict and summarize a harmonics distortion effect [1],[2],[3],[4],[5]. It is called total harmonic distortion index **THD** define as:

$$THD = \frac{\sqrt{\sum_{h=2}^H C_h^2}}{C_1} * 100\% \quad (9.1)$$

where  $C_h$  – magnitude of  $h$  harmonic (can be voltage or current),  $C_1$  – magnitude of fundamental (*first* harmonic)

The harmonic spectrum can be further subdivided into even harmonics and odd harmonics with their corresponding THD definitions. The total even-harmonic distortion **THDeven** may be defined as:

$$THDeven = \frac{\sqrt{\sum_{h=2}^H C_{2*h}^2}}{C_1} * 100\% \quad (9.2)$$

where  $C_{2h}$  – magnitude of even harmonic,  $C_1$  – magnitude of fundamental (*first* harmonic)

The total odd-harmonic distortion **THDodd** may be defined as:

$$THDodd = \frac{\sqrt{\sum_{h=2}^H C_{2*h-1}^2}}{C_1} * 100\% \quad (9.3)$$

where  $C_{2h-1}$  – magnitude of odd harmonic,  $C_1$  – magnitude of fundamental (*first* harmonic)

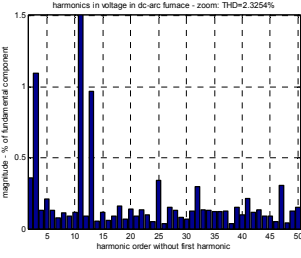
The confirmation of the proper calculation can use below relations:

$$THD^2 = THDodd^2 + THDeven^2 ; THD \approx THDodd \quad (9.4)$$





a) Harmonics relative to fundamental  
zoom – without fundamental

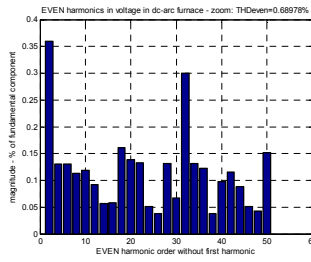


THD =  
2.3254

Checking:  $THD^2 = THD_{odd}^2 + THD_{even}^2$  ;  $THD \approx THD_{odd}$

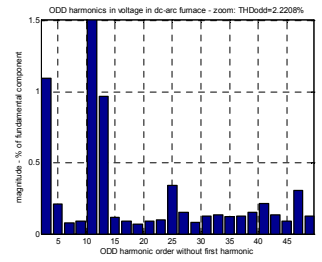
$$2.3254^2 = 2.2208^2 + 0.6898^2 ; 2.3254 \approx 2.2208$$

b) Even harmonics relative to fundamental  
zoom – without fundamental:



THDeven =  
0.6898

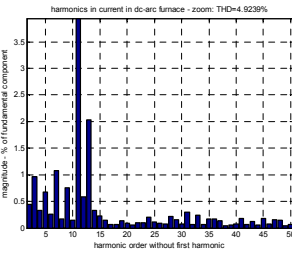
c) Odd harmonics relative to fundamental  
zoom – without fundamental:



THDodd =  
2.2208

Fig. 9.9. Harmonics analysis of voltage in dc-arc furnace plant: presentation of harmonics, THD indices calculation

a) Harmonics relative to fundamental  
zoom – without fundamental

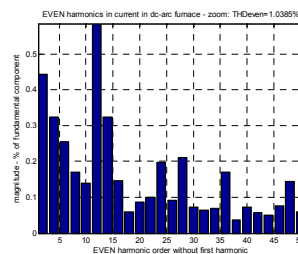


THD:  
4.9239

Checking:  $THD^2 = THD_{odd}^2 + THD_{even}^2$  ;  $THD \approx THD_{odd}$

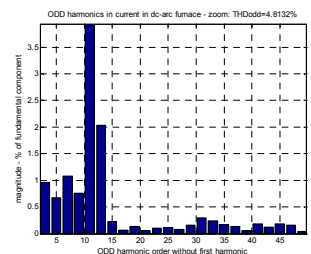
$$4.9239^2 = 4.8132^2 + 1.0385^2 ; 4.9239 \approx 4.8132$$

b) Even harmonics relative to fundamental  
zoom – without fundamental:



THDeven =  
1.0385

c) Odd harmonics relative to fundamental  
zoom – without fundamental:



THDodd =  
4.8132

Fig. 9.10. Harmonics analysis of current in dc-arc furnace plant: presentation of harmonics, THD indices calculation

## 9.5.Groups of harmonics, interharmonic and suharmonic

To deal with the new characteristics of the frequency spectra in voltage and current waveforms, the International Electrotechnical Commission (IEC) in the 2nd edition of its standard 61000-4-7 [5] has proposed the use of harmonic groups instead of the individual harmonic frequencies in order

to obtain a better estimation of harmonic distortion in modern power supply systems. The harmonic groups are defined as the grouping of the spectral bins obtained applying the Discrete Fourier Transform to the samples of voltage or current waveforms taken in rectangular sampling windows of 10 periods of the fundamental frequency in a 50-Hz system (12 periods in 60-Hz systems) and using synchronous sampling [2],[3],[4],[5].

**Harmonic Group  $C_{hg}$**  : in a 50-Hz system there are 9 frequency components between two harmonic orders  $h$  and  $h + 1$ . The lowest four are added to group  $h$ , the highest four to group  $h + 1$ , and the middle one is divided equally between the two groups. The harmonic group  $C_{hg}$  is defined by formula:

$$C_{hg}^2 = \frac{1}{2}C_{nfch(h)-5}^2 + \sum_{i=-4}^{i=4} C_{nfch(h)-k}^2 + \frac{1}{2}C_{nfch(h)+5}^2 \tag{9.5}$$

where  $nfch(h)$  means an index of harmonic order  $h$  in linear spectrum.

Hint: according to our previous initial calculation, **nfch** includes indices associated with particular harmonics in linear spectrum. e.g.  $nfch(1)=11$   $nfch(2)=21$  ...

**Interharmonic Group  $C_{ihg}$**  : All frequency components between harmonic orders  $h$  and  $h+1$  are combined in an interharmonic group:

$$C_{ihg}^2 = \sum_{i=1}^{i=9} C_{nfch(h)+k}^2 \tag{9.6}$$

A specified interharmonic group is associated with frequencies lower than fundamental. Is is called **subharmonic group  $C_{sub1g}$**

$$C_{sub1g}^2 = \sum_{i=-9}^{i=-1} C_{nfch(1)+k}^2 \tag{9.7}$$

Using the previous example of Fourier series parameterization for sampling rate 4kHz and frequency 5-Hz resolution, we can introduce the definition of the harmonic group order  $h$  and interharmonic group as well as a subharmonic group as it was illustrated in Fig. 9.11.

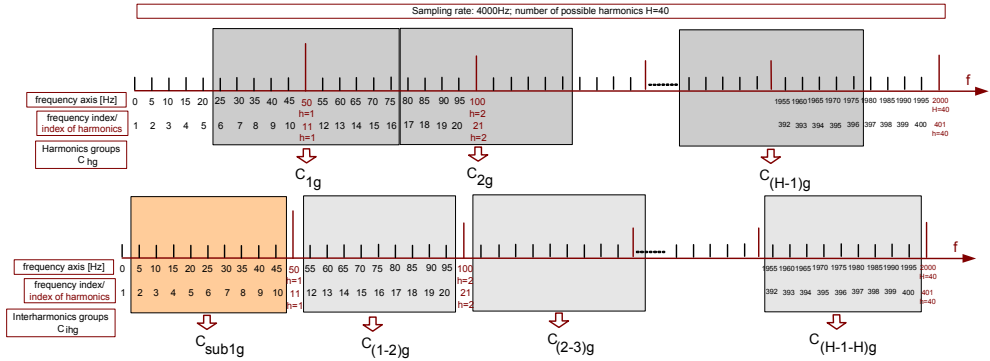


Fig. 9.11. Illustration of harmonic, interharmonic and subharmonic group definition in 50Hz system with sampling rate  $f_s=4\text{kHz}$

In order to practice an idea of grouping the harmonics, we now encourage to define a harmonic, interharmonic and subharmonic group in case of investigated voltage in current in the dc-arc furnace plant.

**Activities: Perform initial calculation to reveal frequency bins to grouping process of the harmonics.**

**Given:** sampling rate  $f_s=5\text{kHz}$ , system  $f_0=50\text{Hz}$ , interval 10-cycle

**Aim:** Selection of frequency bins in order to create a group of harmonics

**Answer:** An expected answer is included in the figure below, Fig. 9.12.

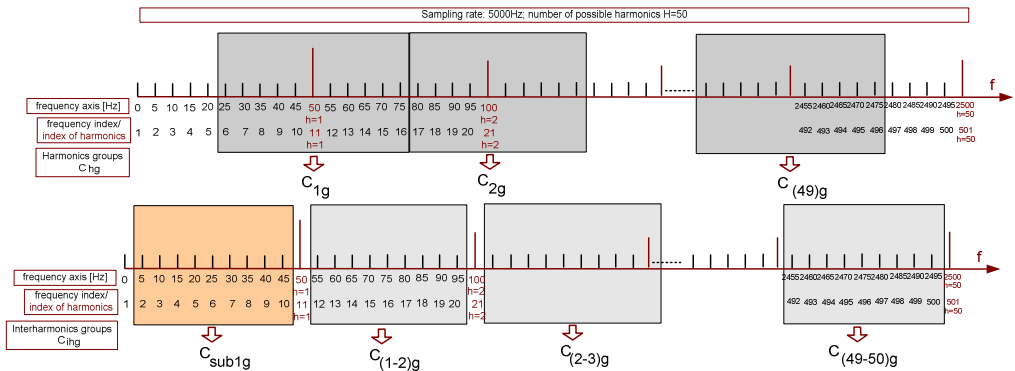


Fig. 9.12. Harmonic, interharmonic and subharmonic group definition of investigated voltage and current in example of dc-arc

The results concerning investigation of groups of harmonics in voltage in the dc-arc furnace plant is presented in Fig. 9.13. If we compare the assessment of the distortion in voltage based only on the harmonics, Fig. 9.9, we can reveal smaller values of particular components in the process of the assessment in comparison with its grouping counterpart. Discussed here an approach can have

a crucial meaning especially in presence of high value of interharmonics which in classical calculation, based strictly on harmonics, is neglected.

Fig. 9.14 represents the contribution of particular harmonics and interharmonics groups. Predominant values are concentrated around the harmonics, however, total neglecting of interharmonics, as in case of classical harmonics assessment, has a right to stay under the discussion.

- a) Harmonic groups relative to fundamental zoom – without fundamental
- b) Interharmonic groups relative to fundamental zoom – without fundamental:
- c) Subharmonic group relative to fundamental zoom – without fundamental:

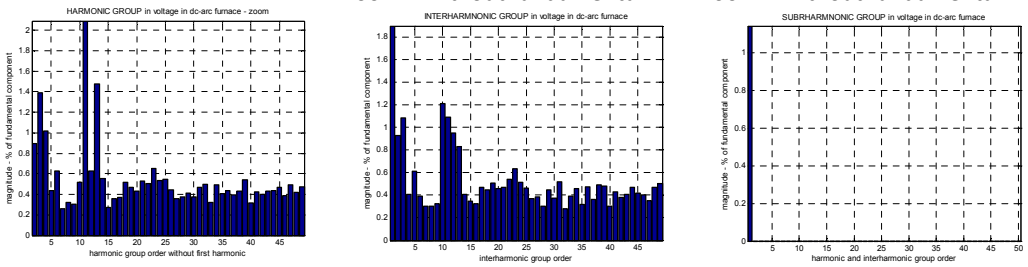


Fig. 9.13. Group of harmonics, interharmonics and subharmonic of voltage in dc-arc furnace plant

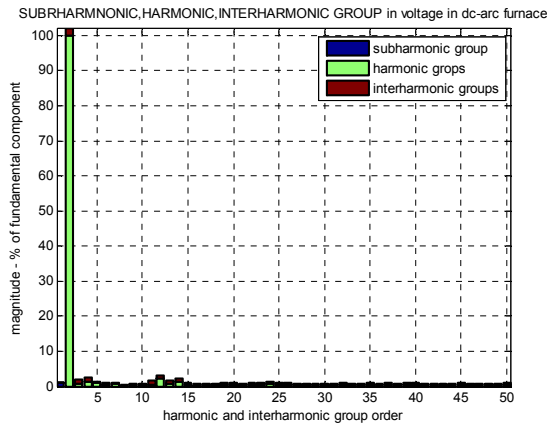


Fig. 9.14. Contribution of particular groups of harmonics, interharmonics and subharmonic of voltage in dc-arc furnace plant

Mentioned above discussion under contribution of interharmonics in assessment of the harmonic distortion has a more significant meaning in case of current, which can be much more affected by the harmonics than voltage. The level of harmonics defined as a group and as selected one frequency bin can be recognized comparing Fig. 9.15 and Fig. 9.10. Additionally, contribution of particular harmonics and interharmonics groups are presented in Fig. 9.16.

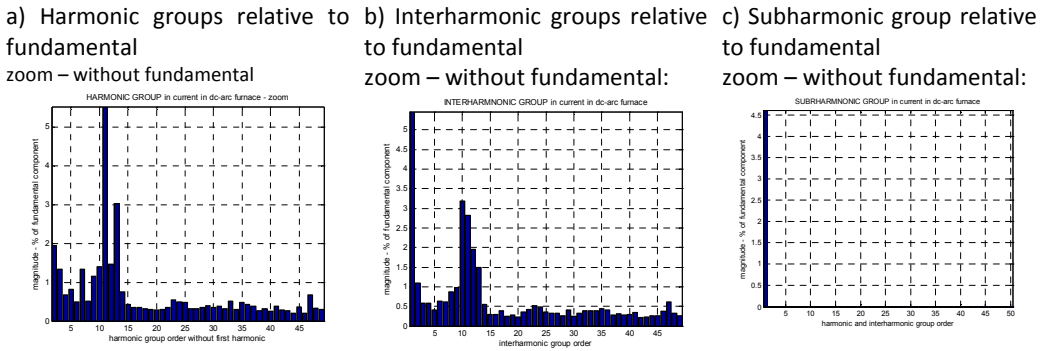


Fig. 9.15. Group of harmonics, interharmonics and subharmonic of current in dc-arc furnace plant

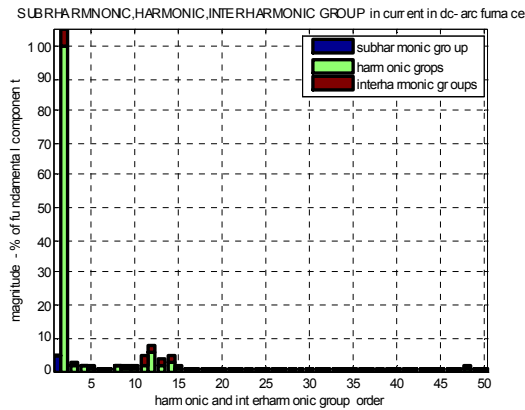


Fig. 9.16. Contribution of particular groups of harmonics, interharmonics and subharmonic of current in dc-arc furnace plant

## 9.6.Literature

- [1] Bollen M.H.J., *Understanding Power Quality Problems. Voltage dips and interruptions*, IEE Press Series on Power Engineering, 2000.
- [2] Bollen M.H.J, Irene Yu-Hua Gu, *Signal Processing of Power Quality Disturbances*, 2006 The Institute of Electronics and Electrical Engineers, Inc.
- [3] *Power Quality Application Guide. Chapter 3. Harmonics*. The European Copper Institute, Leonardo da Vinci European Program on Power Quality Assessment.
- [4] Electromagnetic compatibility (EMC), Part 4, Section 30: Power quality measurement methods, IEC 61000-4-30.
- [5] Electromagnetic compatibility (EMC), Part 4, Section 7: General guide on harmonics and interharmonics measurements and instrumentation, for power supply systems and equipment connected thereto, IEC 61000-4-7.
- [6] IEEE C37.111-1991 - IEEE Standard Common Format for Transient Data Exchange (COMTRADE) for Power Systems
- [7] Bracale A., Carpinelli G., Lauria D., Leonowicz T., Lobos T., Rezmer J., *On Some Spectrum Estimation Methods for Analysis of Non-Stationary Signals in Power Systems. Part I: Theoretical Aspects, Part II – Numerical applications*, 11-th International Conference on Harmonics and Quality of Power, Lake Placid, New York 2004, Session: Harmonic Propagation, paper no. - "f" and "g.
- [8] Łobos Tadeusz, Sikorski Tomasz, Schegner Peter: Joint time-frequency representation of non-stationary signals in electrical power engineering. 15th Power Systems Computation Conference - PSCC. CD-ROM Proceedings, 2005.

## 10. Elements of power quality report

The construction of a power quality report contains the assessment of set of many parameters discussed in this book. Recorded values are compared with recommended values. Standard contents of power quality report includes assessment of :

- power frequency
- -slow voltage variation
- fast voltage variation or flicker severity
- unbalance
- harmonics
- recorded power quality events and transients

Methodology of preparing the data base for assessment of power quality is based usually on one week assessment period. However requirements for aggregation rules, including averaging intervals, for different parameters are different [1],[2],[3].

An Algorithm for frequency estimation is based on ten-cycle series. In 50Hz systems, for every 200ms new value of frequency is stored in monitoring mode. However for assessment aggregation of 10s averaging interval is introduced, giving set of 60480 per week.

**Set of frequency values in one week based on 10s aggregation:**

$$1_{10s} * 6 |_{1min} * 60 |_{1h} * 24 |_{1day} * 7 |_{1week} = 60480$$

In case of rms calculation monitoring the algorithm is based on half or one-cycle series. In the next step, 10 cycle intervals are aggregated and next averaged referring 10 min interval. The trend of voltage variation is finally based on a set of 10 min values that gives 1008 values per week:

**Set of rms in one week based on 10 min aggregation:**

$$1_{10min} * 6 |_{1h} * 24 |_{1day} * 7 |_{1week} = 1008$$

The calculation of unbalance coefficient and harmonics use 10-cycle interval according to requirements for Fourier series. For the assessment of 10-cycle values are averaged in 10 min as in case of rms trend. Thus, similar to slow voltage variation, a set of unbalance and harmonics is based on 1008 values per week.

**Set of unbalance and harmonics in one week based on 10 min aggregation:**

$$I_{10\text{min}} * 6 |_{1\text{h}} * 24 |_{1\text{day}} * 7 |_{1\text{week}} = 1008$$

Short-term flicker coefficient is stored with 10 min aggregation interval. Evaluation of voltage mitigation is defined by long-term flicker coefficient which is based on two hours averaging of 10 min short-term flicker coefficient. Thus, evaluation of flicker severity uses 84 values of long-term flicker coefficient for one-week assessment period.

**Set of long-term flicker coefficient in one week based on 2h aggregation:**

$$I_{2\text{h}} * 12 |_{1\text{day}} * 7 |_{1\text{week}} = 84$$

The mentioned rules of aggregations allows to prepare set of values in the assessment period and perform the evaluation with comparison to referring values [3].

The aim of this chapter is to present an example of power quality report including the assessment of mentioned crucial parameters. Measurements were done in the main point of the supply of the factory which has an electronic assembly line including robots and power electronics. Localisation of the power quality recorder in the distribution station of the factory presents Fig. 10.1.

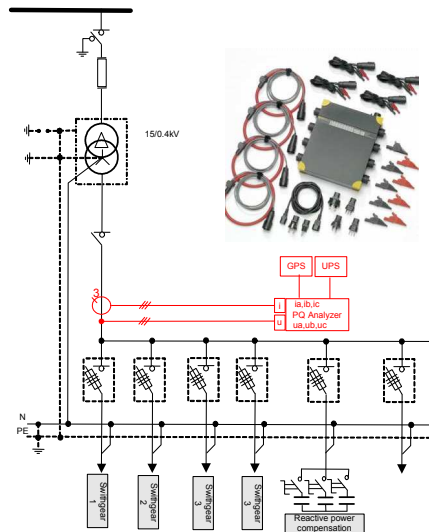


Fig. 10.1. Localisation of the power quality measurements in distribution station



## 10.1. Power frequency assessment

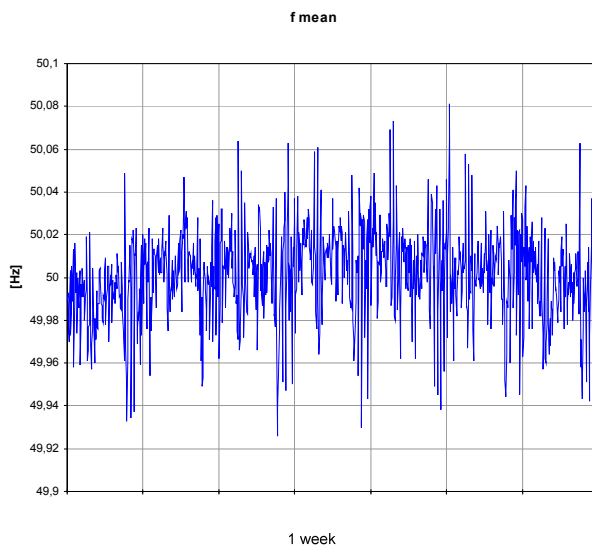


Fig. 10.2. Visualisation of power frequency variation

**Table 10-1. Assessment of power frequency variation**

Frequency assessment		f
		[Hz]
$f_{10s}$	<i>min</i>	<b>49,886</b>
$f_{10s}$	<b>Percentile 99.5%</b>	<b>50.055</b>
$f_{10s}$	max	50,131

Visualization of the recorded set of frequency values is shown in Fig. 10.2. The standard EN 50160 indicates that the nominal frequency of the supply voltage shall be 50 Hz. Under normal operating conditions, the mean value of the fundamental frequency measured over 10 s shall be within a range of

– for systems with synchronous connection to an interconnected system:

50 Hz  $\pm$  1 % (i.e. 49,5 Hz... 50,5 Hz) during 99,5 % of a year;

50 Hz + 4 % / - 6 % (i.e. 47 Hz... 52 Hz) during 100 % of the time;

Table 10-1 contains some statistical parameters which have confirmed that in the investigated case, requirements for frequency standards are fulfilled. During 100% of the assessment, period frequency values hold in range from 49,886 to 50,131 Hz.

## 10.2. Supply voltage variation

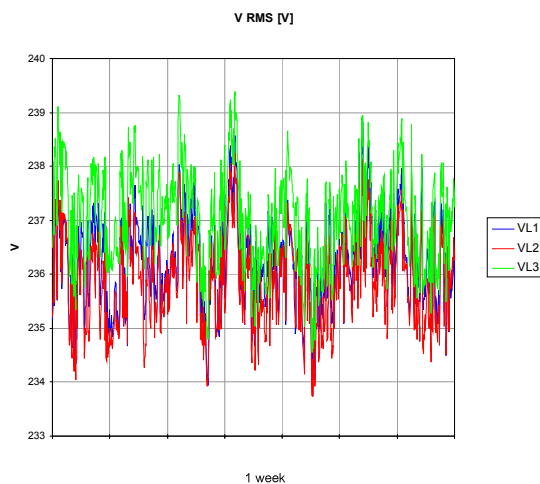


Fig. 10.3. Visualisation of supply voltage variation

**Table 10-2. Assessment of supply voltage variation**

Voltage assesment		VL1	VL2	VL3
		[V]	[V]	[V]
U <sub>10min</sub>	<i>min</i>	<b>233,94</b>	<b>233,43</b>	<b>234,55</b>
	<i>Percentile 95%</i>	<b>237,87</b>	<b>237,51</b>	<b>238,73</b>
	<i>max</i>	238,83	238,24	239,40

Visualization of the recorded set of supply voltage values is shown in Fig. 10.3. The standard EN 50160 indicates that under normal operating conditions:

- during each period of one week 95 % of the 10 min mean r.m.s. values of the supply voltage shall be within the range of  $U_n \pm 10 \%$ ,
- all 10 min mean r.m.s. values of the supply voltage shall be within the range of  $U_n + 10 \%$  /  $- 15 \%$ .

Table 10-2 contains some statistical parameters which have confirmed that in the investigated case requirements for rms supply voltage standards are fulfilled. 95% of the recorded rms values hold in range from 233,43V to 237,87V. Moreover, 100% of the recorded values met standard expectation.

### 10.3. Flicker severity

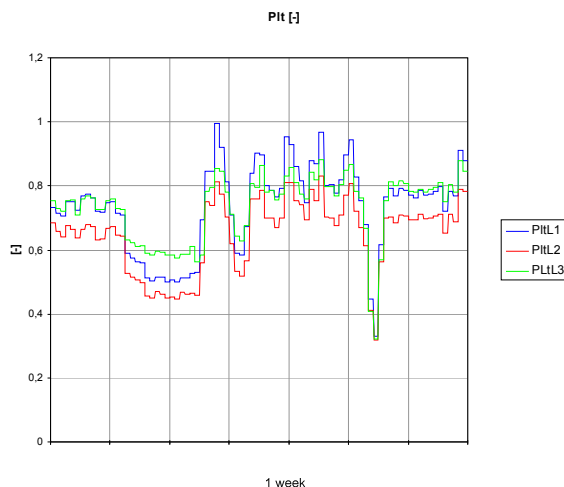


Fig. 10.4. Visualisation of long-term flicker severity

**Table 10-3. Assessment of long-term flicker severity**

Flicker assessment		L1	L2	L3
		[-]	[-]	[-]
Plt <sub>2h</sub>	min	<b>0,33</b>	<b>0,32</b>	<b>0,32</b>
	Percentile 95%	<b>0,93</b>	<b>0,81</b>	<b>0,86</b>
	max	0,99	0,83	0,88

Visualization of the recorded set of long-term flicker coefficient values is shown in Fig. 10.4. The standard EN 50160 indicates that under normal operating conditions, in any period of one week the long term flicker severity caused by voltage fluctuation should be  $Plt \leq 1$  for 95 % of the time.

Table 10-3 contains some statistical parameters which have confirmed that in the investigated case requirements for flicker severity are fulfilled. 95% of the recorded long-term flicker values hold in range from 0,32 to 0,93. Moreover, 100% of the recorded values met standard expectation.

## 10.4. Voltage unbalance assessment

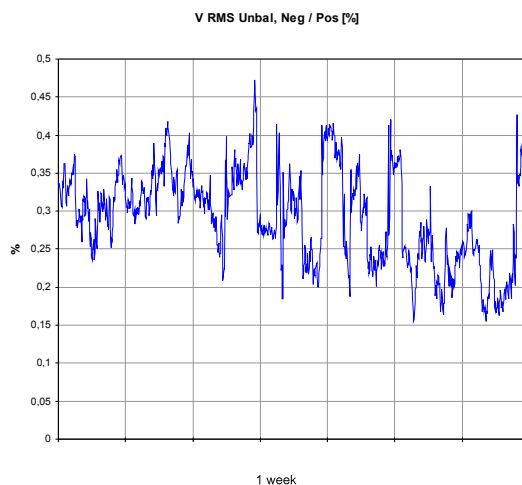


Fig. 10.5. Visualisation of unbalance variation

**Table 10-4. Assessment of unbalance variation**

Unbalance assesment		„Neg/Pos“
		[%]
„Neg/Pos“ <sub>10min</sub>	<i>min</i>	0,15
	<b>Percentile95%</b>	<b>0,40</b>
	<i>max</i>	0,47

Visualization of the recorded set of unbalance values is shown in Fig. 10.5. The standard EN 50160 indicates that Under normal operating conditions, during each period of one week, 95 % of the 10 min mean r.m.s. values of the negative phase sequence component (fundamental) of the supply voltage shall be within the range 0 % to 2 % of the positive phase sequence component (fundamental). In some areas with a partly single phase or two phase connected network users' installations, unbalances up to about 3 % at three-phase supply terminals occur.

Table 10-4 contains some statistical parameters which have confirmed that in the investigated case requirements for unbalance standards are fulfilled. 95% of the recorded unbalance coefficient hold in range from 0,15 to 0,40. Moreover, 100% of the recorded met standard expectation.

## 10.5. Harmonics assessment

Table 10-5. Assessment of harmonic variations

Harmonic assessment							
Order	Limits	Percentile95%			Max		
		L1	L2	L3	L1	L2	L3
Nr.	[ % ]	[ % ]	[ % ]	[ % ]	[ % ]	[ % ]	[ % ]
2	0.00 - 2.00	0.12	0.21	0.17	0.13	0.22	0.17
3	0.00 - 5.00	0.36	0.40	0.35	0.38	0.44	0.38
4	0.00 - 1.00	0.26	0.36	0.24	0.27	0.39	0.26
5	0.00 - 6.00	1.07	1.55	1.03	1.21	1.73	1.24
6	0.00 - 0.50	0.31	0.52	0.35	0.34	0.57	0.38
7	0.00 - 5.00	1.30	1.67	1.46	1.69	2.05	1.80
8	0.00 - 0.50	0.37	0.49	0.62	0.46	0.54	0.70
9	0.00 - 1.50	0.49	0.66	0.79	0.69	0.76	0.96
10	0.00 - 0.50	0.44	0.42	0.56	0.54	0.45	0.63
11	0.00 - 3.50	1.46	1.23	1.45	2.02	1.68	1.91
12	0.00 - 0.50	0.61	0.36	0.51	0.76	0.51	0.67
13	0.00 - 3.00	0.85	0.73	0.63	1.02	0.83	0.68
14	0.00 - 0.50	0.56	0.62	0.53	0.63	0.73	0.58
15	0.00 - 0.50	0.43	0.53	0.43	0.49	0.69	0.55
16	0.00 - 0.50	0.49	0.45	0.35	0.67	0.78	0.59
17	0.00 - 2.00	0.51	0.38	0.43	0.79	0.69	0.59
18	0.00 - 0.50	0.36	0.20	0.33	0.66	0.38	0.50
19	0.00 - 1.50	0.27	0.24	0.31	0.54	0.39	0.65
20	0.00 - 0.50	0.22	0.12	0.23	0.52	0.23	0.55
21	0.00 - 0.50	0.22	0.12	0.17	0.45	0.29	0.42
22	0.00 - 0.50	0.17	0.10	0.12	0.37	0.22	0.27
23	0.00 - 1.50	0.14	0.07	0.11	0.30	0.17	0.21
24	0.00 - 0.50	0.10	0.06	0.07	0.20	0.11	0.12
25	0.00 - 1.50	0.09	0.07	0.06	0.18	0.12	0.09

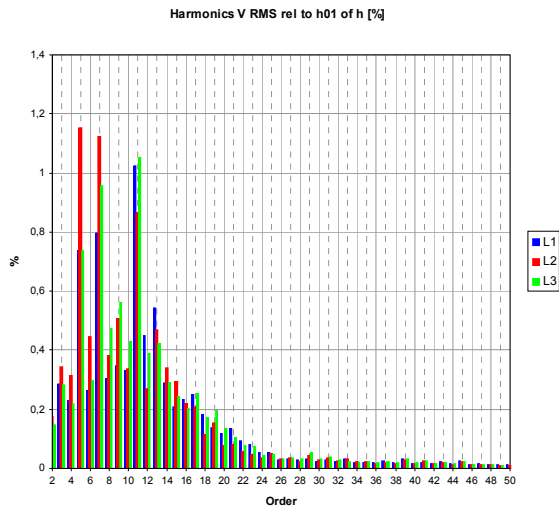


Fig. 10.6. Visualisation of harmonic spectrum averaged in one week

Table 10-5 contains limits for particular harmonics defined in EN 50160 and some statistical parameters of recorded data. Distribution of the harmonics is also visible in Fig. 10.6. Classical for LV supply network contribution of odd harmonics, especially 3-rd, 5-th, 7-th, 11-th is confirmed. There are dominated components. Performed measurements have detected values over the limits in case of even harmonics as 6-th, 8-th, 10-th, 12-th, 14-th. The conclusion concerning harmonics assessment is that the requirements for harmonics contribution is not fulfilled in the investigated case. Further tests shown that exceeded values appear temporary and come from resonance effects in the supply in companion with capacitor banks under process of reactive power compensation.

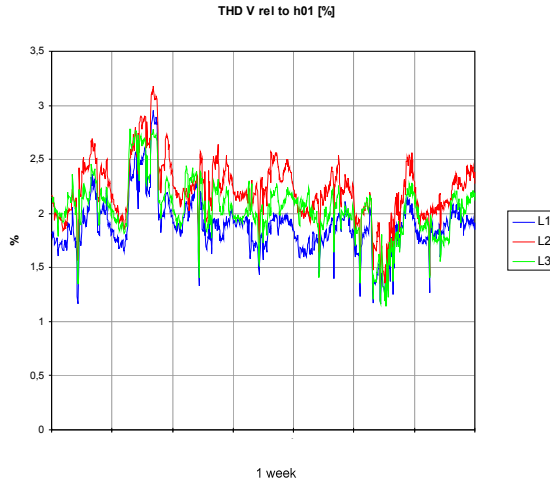


Fig. 10.7. Visualisation of THDV variation

**Table 10-6. Assessment of THDV variation**

THDV assesment		THDVL1	THDVL2	THDVL3
		[%]	[%]	[%]
THDV 10min	<i>min</i>	<b>1,16</b>	<b>1,34</b>	<b>1,14</b>
	<i>Percentile95%</i>	<b>2,36</b>	<b>2,68</b>	<b>2,59</b>
	max	2,95	3,18	2,78

Visualization of the recorded set of total harmonics distortion in voltage is shown in Fig. 10.7. The standard EN 50160 indicates THD of the supply voltage (including all harmonics up to the order 40) shall be less than or equal to 8 %.

Table 10-6 contains some statistical parameters of THDV which have confirmed that in the investigated case requirements are fulfilled. 95% of the recorded THDV coefficient hold in range from 1,14 to 2,68. Moreover, 100% of the recorded values met standard expectation.

## 10.6. Summary of the report

Presented in the previous section, the assessment of crucial power quality parameters indicates that:

- in case of power frequency, requirements are fulfilled
- in case of voltage supply, requirements are fulfilled
- in case of flicker severity, requirements are fulfilled
- in case of voltage unbalance, requirements are fulfilled
- in case of THD of the supply voltage, requirements are fulfilled
- in case of harmonics requirements are not fulfilled

Performed measurements have detected values over the limits in case of even harmonics as 6-th, 8-th, 10-th,12-th,14-th. It is recommended to make the test of the cooperation the capacitor banks with the supply during the regulation process of reactive power consumption.

During the assessment period no voltage events were detected.

## 10.7. Literature

- [1] IEC 61000-4-30:2008, *Electromagnetic compatibility (EMC): Testing and measurement techniques -Power quality measurement method.*
- [2] Bollen M.H.J, Irene Yu-Hua Gu, *Signal Processing of Power Quality Disturbances*, 2006  
The Institute of Electronics and Electrical Engineers, Inc
- [3] EN 50160: *Voltage characteristics of electricity supplied by public distribution networks*